8 Bond Strength Determination

8.1 Introduction

The response of a layered composite asphalt pavement depends on the interlayer bond. Shahin, et al [35] have shown that even minor loss of bond between layers can cause stresses in the overlays to increase dramatically. The results are amplified at intersections where vehicles accelerate and brake resulting in application of large horizontal forces. The loss of bond will cause higher tensile strains at the bottom of the overlay and increased vertical compressive strains on the subgrade. Both of these deformations will cause a reduction in life of the pavement. The horizontal surface shear forces will cause crescent shaped cracks (Figure 1-4) in the top layer. The development of such cracks will reduce the strength further as well as cause penetration of surface water resulting in an accelerated decline of pavement performance. To eliminate such distresses, either the interfacial shear stresses can be reduced by using a thicker overlay or using a tack coat with higher bond strength. This chapter examines bond strengths of various materials. The following tests were conducted:

- Shear ramp tests
    - AC bonded to AC (AC-AC) – 20, 40, and 60 °C
    - AC bonded to PCC (AC-PCC) – 20, 40 and 60 °C
    - AC bonded to CTB (AC-CTB or CTB-AC) – 40 and 60 °C
- Axial ramp tests
    - AC bonded to AC (AC-AC) – 40 and 60 °C

8.1.1 Shear Test Description

A simple shear test at constant height was conducted to determine the bond strength between various types of materials. The test was conducted in a controlled strain mode in which the composite sample was sheared at a constant rate (1.0 and 2.5 mm/min). The rates were based on a study conducted by Uzan et al [48] in which rectangular AC samples were sheared using a direct shear test. The test was conducted at temperatures of 40 and 60 °C, and in some cases at 20 °C. The composite samples were glued to metal platens and were sheared at constant height in the SST. The peak shear load per unit area was the failure shear strength. Axial load and displacement were monitored during the test. The specimens were sheared to a displacement of 5mm.

8.2 Bond Strength using Metal Platens

Metal platens (anodized aluminum) were used to determine the bond strength of tack and prime coat emulsions. Tack coat was applied to the one of the platens at the standard rate of 0.06 gallons per square yard. Using the gluing jig for SST specimens, the two platens were aligned and a minimal axial pressure of 10 psi was applied to keep them in contact. After 8 hours, the platens were removed from the jig and left in a draft oven at 40 °C to break the emulsions. Twenty four hours after gluing; the platens were sheared using the SST machine at strain rates of 1.0 and 2.5 mm per minute. The test results were highly variable and the entire procedure was error prone due to following reasons:

- At the time of coating, the emulsions were in an unbroken state and, therefore, very fluid. When the two platens were pressed against each other, the liquid emulsion tended to ooze out from the sides. This changed the effective rate of application of tack coat and ultimately the interlayer asphalt film thickness available for bonding.
- When the platens were pressed against each other, the water from the emulsion was trapped in between the two impervious platens. The trapped water could, potentially, adversely affect the bond strength. This is not the case with bonded AC, PCC or CTB specimens as the emulsions are allowed to break.
- When the platens were inserted into the SST and clamped, they tended to separate before testing. This was due to presence of inadequately cured tack coats or due to high forces applied by the SST or extremely low strength of the tack coat.
- An alternative approach would have been to allow the emulsion to break on one of the platens and, after 24 hours, bond it with another platen. But this approach had similar problems. At a pavement interface, the asphalt penetration into adjacent layers provides a stronger bond compared to the bond developed between two impervious platens.

- The relative strength of any tack (or prime) coat, by itself, is small when compared to the interfacial strength of a composite pavement specimen it helps bond together. The use of heavy metal platens and SST to test the strength of tack (or prime) coats yielded erroneous results due to noise and low sensitivity of the equipment. A better alternative would be to use platens comparable to the size of a DSR spindle and a sensitive machine. An alternative is to use ATACKER™[3] device that uses a light weight aluminum spindle (sizes – 1, 2, and 4 inch in diameter) and a dial gauge that can measure the load to ½ lb accuracy. The set up is similar to DSR. The specimens are sheared or pulled apart in a strain-controlled mode and the load at which the two plates separate is noted as the bond strength.

Overall, the results from these tests did not contribute much to this study due to practical problems encountered in the testing protocol.

8.3 Bond Strength of AC-AC specimens

8.3.1 Axial and Shear Ramp Test

Axial ramp test is similar to the simple shear test, except that the load is applied axially in controlled strain mode. Similarly, for shear ramp test, the samples were sheared at a constant strain rate. The rate of loading used for axial and shear tests was 1 and 2.5 mm/minute. The axial test is used to measure the adhesion of the interfaces glued by a tack coat whereas the shear test measures the interfacial shear resistance. The specimens used were 2 inch thick and 6 inch in diameter with interface between the two layers roughly at mid-height. This test was performed on composite asphalt concrete specimens (AC bonded to AC) to determine the effectiveness of PG64-22 versus CMS-2 as a tack coat. Control specimens were also prepared without using a tack coat. However, during the coring and cutting process, control samples (Figure 8-1) made without any tack coat separated at the interface and, therefore, could not be tested.

[3] ATACKER™ is equipment developed by Instrotek Inc, of Raleigh, NC.

8.3.2 Axial Test Results

The axial test results are presented in Table 8-1 and Table 8-2. It can be seen that low strain rate produces lower peak load values. For CMS-2 at 40 °C, when the strain rate reduces from 2.5 mm/minute to 1.0 mm/minute, the shear strength changes from 221 to 95 psi – a reduction of 57%. Similarly, for CMS-2, the reduction in peak axial strength when tested at a lower rate of 1 mm/minute is 48 percent at 60 °C. Comparing the axial test data for 40 and 60 °C, for CMS-2, (Table 8-1 and Table 8-2) the peak axial stress falls with rise in temperature. When the temperature increases from 40 to 60 °C, the peak axial strength reduces by 85 and 75 percent for 1.0 and 2.5 mm/min strain rates respectively.

For the same axial strain rates, the corresponding peak load values and axial strains are much higher for PG64-22 binder than the CMS-2 emulsion. This suggests that PG64-22 binder has a higher axial strength than CMS-2 emulsion at both temperatures. This is expected because:

1. Amount (wt/sq. yd) of residual asphalt available at the interface is higher for PG64-22 binder than for CMS-2 emulsion (which has about 33% water).
2. In addition, the PG rating of the residual asphalt in CMS-2 is PG52 (Table 4-2).

The failure of CMS-2 tacked specimens in axial testing mode was observed to be at the interface as shown in Figure 8-2 and Figure 8-3; however for PG64-22 tacked specimens the failure was not well defined as CMS-2 tacked specimens, as shown in Figure 8-4 and Figure 8-5. This observation confirms that PG64-22 provides better adhesion than CMS-2 emulsion.

8.3.3 Shear Test Results

The results for shear tests are presented in Table 8-3 through Table 8-5. The test was conducted in a constant height mode to simulate the confinement observed in situ. Negative axial stresses shown in the tables indicate compressive load and are due to prevention of dilation of specimens during the shearing process. The pattern for shear failure varies depending on the testing temperature and rate of shear. The test results are graphically presented in Figure 8-6 through Figure 8-8. The failure pattern (Figure 8-9 through Figure 8-12) observed for the shear test at 40 °C is similar to that of a monolithic sample – there was a development of a crack along the principal diagonal, typical of a shear failure for both CMS-2 and PG64-22 tacked specimens. This indicated that the bond was as strong as the mix at 40 °C. From Table 8-3 to Table 8-5 it can be seen that there is very little difference in the bond strength of specimens tacked with CMS-2 and PG64-22, especially at a higher strain rate of 2.5 mm/minute. There is a small difference in bond strength at lower strain rate of 1 mm/minute with the average (across all temperatures) difference being about 14% with PG64-22 tacked specimens showing higher bond strength.

For CMS-2 tacked specimens the interfacial failure was observed regardless of the rate of shear at 20 °C. For PG64-22, at 20 °C, failure at lower strain rate was monolithic (Figure 8-13) but at higher strain rate the failure was interfacial (Figure 8-14). At 20 °C, the peak bond strength of CMS-2 is lower than PG64-22 by 8%

The shear strength values drop drastically at 60 °C, with PG64-22 specimens performing marginally better than CMS-2 specimens. A higher strain rate produces a higher strength as is clear from data in Table 8-5. The difference between the shear strengths of PG64-22 and CMS-2 emulsion is 9% and 45% at strain rates of 1.0 and 2.5 mm/min. Referring to Figure 8-6 and Figure 8-7, it can be seen that failures occur rapidly under higher strain rates than compared to lower strain rates. Further, the occurrence of peak load shifts to the right with increase in temperature and reduction of strain rate – a phenomenon occurring due to mix getting softer. The failure of composite specimens at 60 °C was observed to be at the interface suggesting that the bond was the weakest link at that temperature. Figure 8-8 shows the summary of bond strength as function of temperature. It can be seen from this figure that, in general, the CMS-2 bond strength is not very much different compared to PG64-22.

8.4 Bond Strength of PCC-AC specimens

The composite specimens of PCC and AC were tested in shear using the ramp tests described earlier. The testing was conducted at 20, 40 and 60 °C. In all, three cases were considered: no tack coat, PG64-22 binder as tack coat and CMS-2 emulsion as tack coat. For specimens prepared without tack coat, immediately after curing and drying the slab, the surface of PCC slab was cleaned and an asphalt layer was paved on the PCC slab. While dismantling the mold and coring the slab, the two layers of AC and PCC tended to separate (Figure 8-15 and Figure 8-16). The black slab is the asphalt concrete slab paved on top of the white PCC slab. This occurred on two attempts and it was evident that bond formation did not occur between these two layers.

For composite specimens tacked with PG64-22 binder and CMS-2 emulsion, the shear results are listed in Table 8-6 through Table 8-8, and Figure 8-17 through Figure 8-19. The behavior of PCC-AC interface bond is the property of tack coat as well as the asphalt mix; PCC only serves as a rigid layer to which the AC is tacked as the PCC stiffness is much higher than the AC mix. The properties of PCC do not change significantly with temperature or rate of shear. It can be seen that with increasing temperature, the bond strength continues to reduce.

For PCC-AC specimens, PG64-22 composite specimens have slightly lower shear strengths at a strain rate of 1.0 mm/min compared to CMS-2. However, the trend at higher strain rates reflects PG64-22 as a stronger tack coat. It can be argued that the bond strength of PG64-22 is very close to the actual mix strength at lower strain rates and, therefore, CMS-2, PG64-22 rate equally well in shear strength. The CMS-2 bond strength, however, is lower than PG64-22 by 2.5%, 17.9%, and 31.8% (strain rate of 2.5mm/min) at 20, 40, and 60 °C respectively. The difference in the shear strengths progressively widens with increasing temperature, between PG64-22 and CMS-2 at higher temperatures. With increasing temperatures, the development of peak shear stress (Figure 8-17 and Figure 8-18) gets less clearly defined. At 20 °C the peaks for CMS-2 and PG64-22 are clearly defined; at 40 °C the peaks are not as clearly defined and at 60 °C they cannot be identified at all. This is due to progressive weakening of the bond strength between PCC and AC. Further, the failure (signified by occurrence of peak) is instantaneous at lower temperatures whereas at higher temperatures it is gradual. Most of the specimens, regardless of the tack coat, show a clear-cut slipping at the interface. While the PCC layer has been minimally affected, cracks developed in the AC layer for interfaces tacked with PG64-22 as is evident in Figure 8-20. It suggests that the strength of PG64-22 bond is at least as strong as the mix. In case of CMS-2 specimens, the failure was at the interface for all the specimens. Figure 8-21 shows a failed

PCC-AC composite tacked with CMS-2. The deformation in AC was negligible with all slippage occurring at the interface suggesting bond strength as the weakest link.

The bond strengths of PCC-AC composite specimens are lower than the corresponding values for AC-AC except at 60 °C. Thus, keeping everything else equal, dissimilar surfaces (like PCC and AC) produce a weaker bond compared to bond between similar surfaces (AC-AC). The difference between the dynamic moduli of PCC and AC could be a contributory factor to the lower strength of the interface. Further, the PCC layer being relatively impervious, the tack coat does not penetrate into it potentially affecting the bond strength. In case of AC-AC interfaces, the elevated temperature of the overlay mix during the paving process could cause the underlying layer to soften up causing them to fuse and thereby enhancing the bond strength. Overall, based on the data it can be concluded that PG64-22 performs marginally better than CMS-2 emulsion when used to bond PCC and AC. Figure 8-19 summarizes the bond strength as a function of temperature.

8.5 Bond Strength of CTB-AC specimens

This section deals with the shear strength of composite specimens (Figure 8-22) made of CTB and AC. The testing was carried out at 40 and 60 °C at strain rates of 1.0 and 2.5 mm per minute at constant height. Three types of emulsions – CSS-1h, EA-P and EPR-1 – were used as prime coats. In addition, composite CTB-AC samples without any prime coat were manufactured to be used as a control case. The performance of unprimed CTB-AC samples was similar to non-tacked composite (AC-AC and PCC-AC) specimens. The bond formation between CTB and AC was not strong enough to withstand the handling stresses. After extruding the samples from gyratory molds, AC and PCC layers could be easily pulled apart by hand. The results from the tests for primed samples are summarized in Table 8-9 and Table 8-10, and Figure 8-23 through Figure 8-26.

It should be noted that unlike AC-AC and PCC-AC, the CTB-AC specimens show decreasing shear bond strength with increasing applied shear strain rate. The CTB has very low strength and brittle behavior. During the shearing process it is possible that aggregates from the CTB, at the interface, must be loosened and reoriented causing dilation in the specimen. As the test was carried out at constant height, the loosening of aggregates and subsequent dilation could cause a jump in axial stresses. These increased axial stresses lead to an increase in the shear resistance of the interface. The behavior (Figure 8-23 through Figure 8-25) of CTB-AC interface when subjected to a shear strain (at constant height) shows substantially higher shear strengths compared to AC-AC and PCC-AC composite specimens.

At 40 °C, CSS-1h performs better than the other two prime coats, EA-P and EPR-1. The strengths of EA-P and EPR-1, at 40 °C, are 30.9% and 17.2% lower than CSS-1h at a strain rate of 1.0 mm per minute. At a higher strain rate (2.5 mm per minute) and at 40 °C, the shear strengths of EA-P and EPR-1 are 41.6% and 2.8% lower than CSS-1h. Based on shear strengths at 40 °C, the prime coats with decreasing order of shear strengths can be rated as CSS-1h, EPR-1, and EA-P. Another observation is that, at 40 °C, the reduction in strength with increasing rate of shear (from 1.0 to 2.5 mm per minute) is 25.6%, 37.1% and 12.7% for CSS-1h, EA-P, and EPR-1 respectively. The reason, perhaps, would be due to inadequate time for development of aggregate interlock owing to faster interlayer movement. Observation of tested CSS-1h (at 40 °C) samples indicated a failure pattern consistent with a monolithic specimen. No debonding or layer separation was observed and diagonal cracks were seen in AC and CTB (Figure 8-27). For EA-P specimens (at 40 °C), diagonal cracking in AC as well as a shear failure at interface was observed but for EPR-1 only interfacial shear with minor cracking in the AC layer was observed.

At 60 °C, the EA-P primed specimens show a high degree of variability. Indeed the strength was so low that the specimens could be de-bonded by hand (Figure 8-29). Therefore, these results were discarded. At 60 °C, CSS-1h bond strength is higher than EPR-1 at 2.5 mm per minute rate of shear. The failure pattern observed for CSS-1h specimens at 60 °C was similar to the pattern observed at 40 °C. For EA-P and EPR-1 specimens the failure was due to interlayer debonding (Figure 8-28, Figure 8-29). The shear strengths at 60 °C are comparable to shear strengths at 40 °C for CSS-1h and EA-P. That means it is possible that the rough CTB surface plays a greater role compared to the bonding agent, especially under axial confinement.

Based on the test results, it can be concluded that priming does increase the bond between the CTB and the AC layer; however temperature plays only a minor role. The mobilization of bond strength appears to be primarily due to a combination of prime coat adhesion and more importantly aggregate interlock. Figure 8-26 summarizes the results for bond strength versus temperature.

8.6 Summary and Conclusions

The objective of this task was to evaluate the performance of composite samples made by bonding AC-AC, AC-PCC and AC-CTB. Of particular interest was the effect of type of tack coat and test temperatures. The observations and conclusions from the bond strength determination tests are summarized below:

1. The shear and axial ramp tests clearly differentiate between the bond strengths of various tack and prime coats. The numbers from these tests are consistent with the visually observed failure pattern of the test specimens.

2. The problems encountered in testing the bond strength of the tack (or prime) coat using SST metal platens were due to size effects, loss of asphalt from sides, and problems in curing the emulsions. The heavy weight of platens and low sensitivity of SST, vis-à-vis low strength of asphalt, posed hurdles to getting meaningful results. A better alternative would be to use a device like Atacker™ to measure the adhesion properties where the size of equipment is small and the accuracy higher.

3. The absence of tack or prime coat would severely hinder development of bond between two layers causing undue slippage. This is evident from the debonding that occurred between non-tacked AC-AC, AC-PCC and AC-CTB interfaces.

4. For AC-AC composites the strength of PG64-22 binder, when used as a tack coat, provides comparable adhesion to CMS-2 emulsion. This is supported by similar axial and shear strengths of PG64-22 tacked specimens compared to CMS-2 tacked specimens.

5. For PCC-AC composites, the results confirm the earlier observation that CMS-2 provides comparable adhesion to PG64-22.

6. The bond between two similar surfaces (AC-AC vis-à-vis PCC-AC) is stronger than the bond between two dissimilar surfaces. Further the absorption of emulsion into underlying AC layer could potentially contribute to the higher strength of AC-AC interface compared to that of PCC-AC interface.
7. CSS-1h performs better than EA-P and EPR-1 as prime coats. The apparent strength of CTB-AC bond is higher due to the dilation of composite specimens. The strength of CTB-AC composites appears to be influenced significantly by the aggregate interlock.

Overall, the relative performance of various tack and prime coats could be determined based on SST tests. Emulsions, though easy to use, could pose problems if improperly applied or cured prior to paving AC layer. The use of PG64-22 binder as a tack coat could not only eliminate these problems but provide better bonding as well.

Table 8-1 Results for AC-AC axial ramp tests (tensile), 40 °C

Specimen ID	Height (mm)	Air voids (%)	Strain rate (mm/min)	Tack Coat	Peak Axial Stress (kPa)	Average Peak Axial Stress (kPa)
10c4 6-16-2	49.96	3.7	1.0	CMS-2	113.74	95.19
10x 6-16-2	50.48	3.6	1.0	CMS-2	76.64	
25c4 6-3-2	51.36	3.9	2.5	CMS-2	307.80	221.28
25m2 6-16-2	50.93	3.8	2.5	CMS-2	134.78	
10c4 4-15-2	52.65	3.6	1.0	PG64-22	145.17	149.40
10x 5-16-2	51.55	3.8	1.0	PG64-22	153.62	
25m1 5-16-2	50.17	4.3	2.5	PG64-22	240.07	285.53
25m2 5-16-2	51.20	4.3	2.5	PG64-22	330.99	

Table 8-2 Results for AC-AC axial ramp tests (tensile), 60 °C

Specimen ID	Height (mm)	Air voids (%)	Strain rate (mm/min)	Tack Coat	Peak Axial Stress (kPa)	Average Peak Axial Stress (kPa)
10m1 7-20-2	50.39	4.4	1.0	CMS-2	9.10	14.75
10m3 6-16-2	49.20	4.5	1.0	CMS-2	20.40	
25c3 7-20-2	49.88	4.3	2.5	CMS-2	62.35	57.19
25x 7-20-2	50.95	4.5	2.5	CMS-2	52.03	
10c2 4-15-2	48.47	4.5	1.0	PG64-22	19.16	20.87
10m4 5-16-2	50.83	4.5	1.0	PG64-22	22.58	
25c2 5-16-2	49.56	4.2	2.5	PG64-22	59.06	70.29
25m3 9-3-2	49.05	4.3	2.5	PG64-22	81.52	

Table 8-3 Results for AC-AC shear ramp tests, 20 °C

Specimen ID	Height (mm)	Air voids (%)	Strain rate (mm/min)	Tack Coat	Axial Stress (kPa)	Peak Shear Stress (kPa)	Average Peak Shear Stress (kPa)
1mmc2	49.91	4.3	1.0	CMS-2	-923.32	1098.39	1077.94
1mmc3	50.73	4.4	1.0	CMS-2	-986.23	1057.48	
25mmm1	50.87	4.2	2.5	CMS-2	-967.73	1232.25	1096.87
25mmm2	50.17	4.1	2.5	CMS-2	-729.49	961.49	
1mmc2	53.09	3.8	1.0	PG64-22	-894.55	1076.37	1177.01
1mmc21	50.41	4.2	1.0	PG64-22	-1010.72	1277.65	
25mmm3	48.70	4.1	2.5	PG64-22	-53.67	617.61	625.94
25mmx	49.69	4.3	2.5	PG64-22	-58.47	634.26	

Table 8-4 Results for AC-AC shear ramp tests, 40 °C

Specimen ID	Height (mm)	Air voids (%)	Strain rate (mm/min)	Tack Coat	Axial Stress (kPa)	Peak Shear Stress (kPa)	Average Peak Shear Stress (kPa)
10m1 6-16-2	49.58	4.2	1.0	CMS-2	-485.37	384.94	448.57
10m3 6-3-2	47.81	4.1	1.0	CMS-2	-652.51	512.20	
25c1 6-3-2	51.58	4.1	2.5	CMS-2	-641.14	521.53	479.16
25c1_1 6-16-2	52.27	4.3	2.5	CMS-2	-560.57	436.78	
10c3 4-15-2	51.05	3.9	1.0	PG64-22	-653.78	492.93	451.02
10m1 4-15-2	52.38	3.8	1.0	PG64-22	-504.93	409.11	
25m1 5-7-2	51.91	3.7	2.5	PG64-22	-686.60	568.26	554.03
25m2 5-7-2	51.14	3.7	2.5	PG64-22	-662.86	539.79	

Table 8-5 Results for AC-AC shear ramp tests, 60 °C

Specimen ID	Height (mm)	Air voids (%)	Strain rate (mm/min)	Tack Coat	Peak Shear Stress (kPa)	Average Peak Shear Stress (kPa)
10m1 6-3-2	51.74	3.6	1.0	CMS-2	0.84	2.96
10m4 6-16-2	50.29	3.5	1.0	CMS-2	5.08	
25m2 7-20-2	51.07	3.7	2.5	CMS-2	4.62	7.02
25c2 7-20-2	49.83	4.2	2.5	CMS-2	9.42	
10c3 5-7-2	50.04	3.5	1.0	PG64-22	5.78	5.34
10x 9-3-2	49.22	4.3	1.0	PG64-22	4.90	
25m1 9-3-2	48.48	3.6	2.5	PG64-22	7.93	7.71
25c1 5-16-2	50.55	4.2	2.5	PG64-22	7.49	

Table 8-6 Results for PCC-AC shear ramp tests, 20 °C

Specimen ID	Height (mm)	Strain rate (mm/min)	Tack Coat	Axial Stress (kPa)	Peak Shear Stress (kPa)	Average Peak Shear Stress (kPa)
1mm7	51.21	1.0	CMS-2	58.13	235.05	332.16
1mm8	49.54	1.0	CMS-2	-22.84	429.26	
25mm6	50.87	2.5	CMS-2	-40.62	109.51	360.18
25mm9	53.58	2.5	CMS-2	-110.03	611.86	
1mm6	50.91	1.0	PG64-22	-53.12	446.89	224.11
1mm16	48.01	1.0	PG64-22	-85.46	102.03	
1mm18	47.40	1.0	PG64-22	-140.10	123.42	
25mm14	50.07	2.5	PG64-22	-132.47	226.04	363.96
25mm8	50.18	2.5	PG64-22	-70.23	501.88	

Table 8-7 Results for PCC-AC shear ramp tests, 40 °C

Specimen ID	Height (mm)	Strain rate (mm/min)	Tack Coat	Axial Stress (kPa)	Peak Shear Stress (kPa)	Average Peak Shear Stress (kPa)
1mm12	48.95	1.0	CMS-2	-108.48	78.11	63.47
1mm13	50.35	1.0	CMS-2	-27.92	48.82	
25mm11	46.87	2.5	CMS-2	-38.19	121.31	106.35
25mm14	49.90	2.5	CMS-2	-115.57	91.38	
1mm04	52.54	1.0	PG64-22	-73.38	78.32	62.05
1mm13	49.72	1.0	PG64-22	-49.39	45.78	
25mm02	52.46	2.5	PG64-22	-9.13	99.03	129.57
25mm10	49.74	2.5	PG64-22	-114.73	160.11	

Table 8-8 Results for PCC-AC shear ramp tests, 60 °C

Specimen ID	Height (mm)	Strain rate (mm/min)	Tack Coat	Axial Stress (kPa)	Peak Shear Stress (kPa)	Average Peak Shear Stress (kPa)
1mm04	50.07	1.0	CMS-2	-17.18	21.64	25.13
1mm10	51.80	1.0	CMS-2	-29.01	28.61	
25mm01	50.74	2.5	CMS-2	-17.853	19.15	20.38
25mm02	49.84	2.5	CMS-2	-14.92	21.60	
1mm07	49.80	1.0	PG64-22	-8.58	13.74	20.93
1mm15	44.69	1.0	PG64-22	-25.02	28.11	
25mm01	49.91	2.5	PG64-22	-9.63	18.13	29.86
25mm12	50.63	2.5	PG64-22	-54.42	41.59	

Table 8-9 Results for CTB-AC shear ramp tests, 40 °C

Specimen ID	Height (mm)	Strain rate (mm/min)	Tack Coat	Axial Stress (kPa)	Peak Shear Stress (kPa)	Average Peak Shear Stress (kPa)
1mm06	50.34	1.0	CSS-1h	-433.95	353.52	367.49
1mm10	50.42	1.0	CSS-1h	-454.80	381.46	
25mm07	51.01	2.5	CSS-1h	-384.17	328.16	273.23
25mm09	50.27	2.5	CSS-1h	-252.53	218.31	
1mm12	52.87	1.0	EA-P	-262.10	201.83	253.82
1mm02	52.01	1.0	EA-P	-421.71	305.80	
25mm03	54.56	2.5	EA-P	-237.98	155.92	159.62
25mm13	51.15	2.5	EA-P	-244.48	163.32	
1mm02	51.12	1.0	EPR-1	-305.84	225.03	304.38
1mm04	50.22	1.0	EPR-1	-465.11	351.91	
1mm05	51.37	1.0	EPR-1	-429.51	336.19	
25mm03	52.51	2.5	EPR-1	-397.30	280.99	265.65
25mm99	52.54	2.5	EPR-1	-336.37	250.31	

Table 8-10 Results for CTB-AC shear ramp tests, 60 °C

Specimen ID	Height (mm)	Strain rate (mm/min)	Tack Coat	Axial Stress (kPa)	Peak Shear Stress (kPa)	Average Peak Shear Stress (kPa)
1mm01	50.27	1.0	CSS-1h	-464.15	343.00	327.60
1mm05	51.51	1.0	CSS-1h	-414.71	312.19	
25mm02	50.54	2.5	CSS-1h	-439.87	308.00	288.58
25mm08	53.78	2.5	CSS-1h	-368.20	269.16	
1mm10	50.75	1.0	EA-P	-548.90	390.34	408.94
1mm11	54.85	1.0	EA-P	-653.41	427.53	
25mm08	50.84	2.5	EA-P	-73.04	66.93	153.95
25mm11	54.85	2.5	EA-P	-338.59	240.37	
1mmOA	50.39	1.0	EPR-1	-256.48	177.18	218.27
1mmOI	51.39	1.0	EPR-1	-389.84	259.35	
25mmOQ	52.65	2.5	EPR-1	-209.00	134.49	176.12
25mm01	53.12	2.5	EPR-1	-312.59	258.29	
25XOC	51.46	2.5	EPR-1	-197.55	135.59	

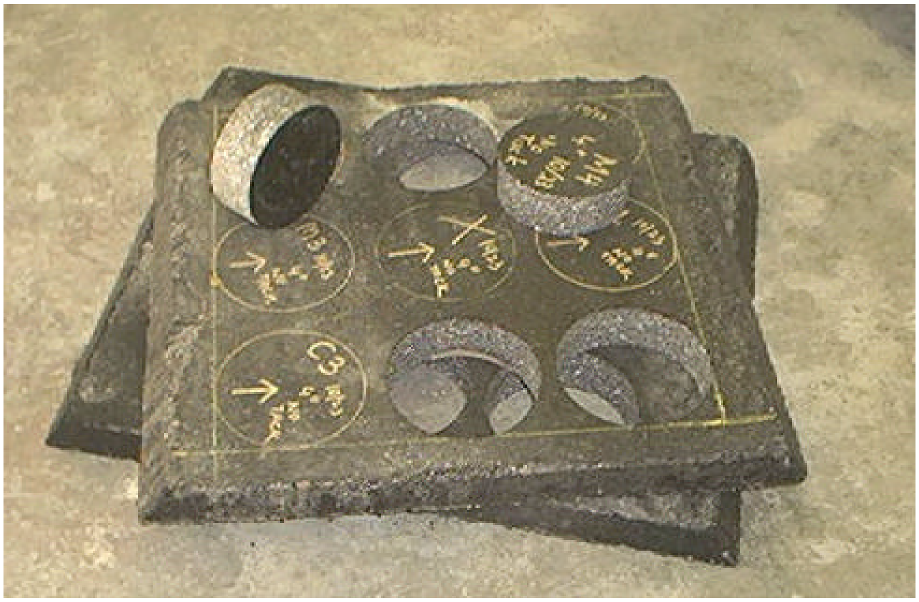

Figure 8-1 Debonded composite AC-AC slab without tack coat

Figure 8-2 Axial failure of CMS-2 specimen (C4 6-3-2) at 2.5 mm/min, 40 °C

Figure 8-3 Axial failure of CMS-2 specimen (C4 6-3-2) at 2.5 mm/min, 40 °C

Figure 8-4 Axial failure of PG64-22 specimen (M1 5-16-2) at 2.5 mm/min, 40 °C

Figure 8-5 Axial failure of PG64-22 specimen (M1 5-16-2) at 2.5 mm/min, 40 °C

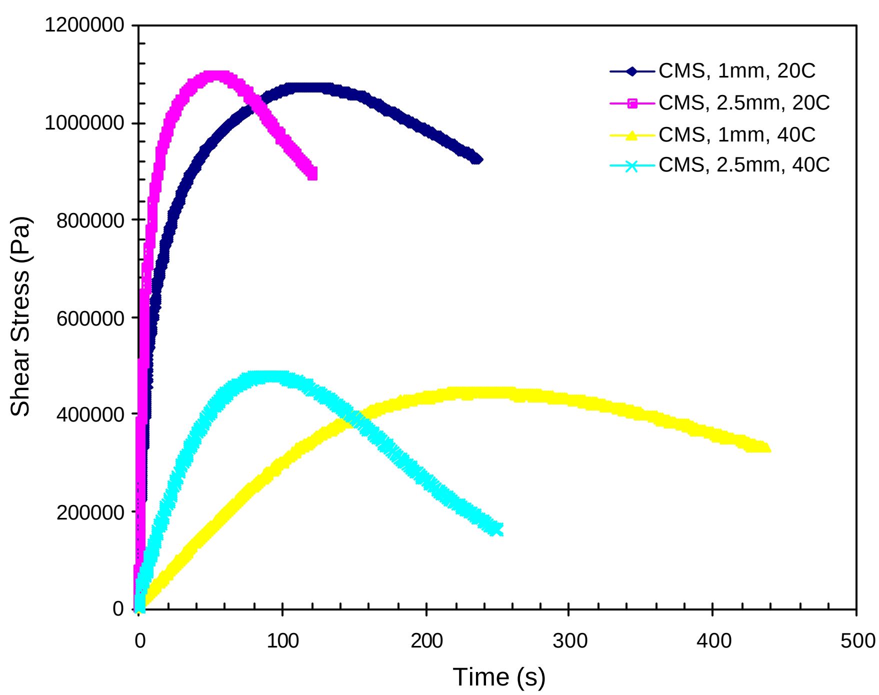

Figure 8-6 Average shear stress vs. time for AC-AC interface tacked with CMS-2

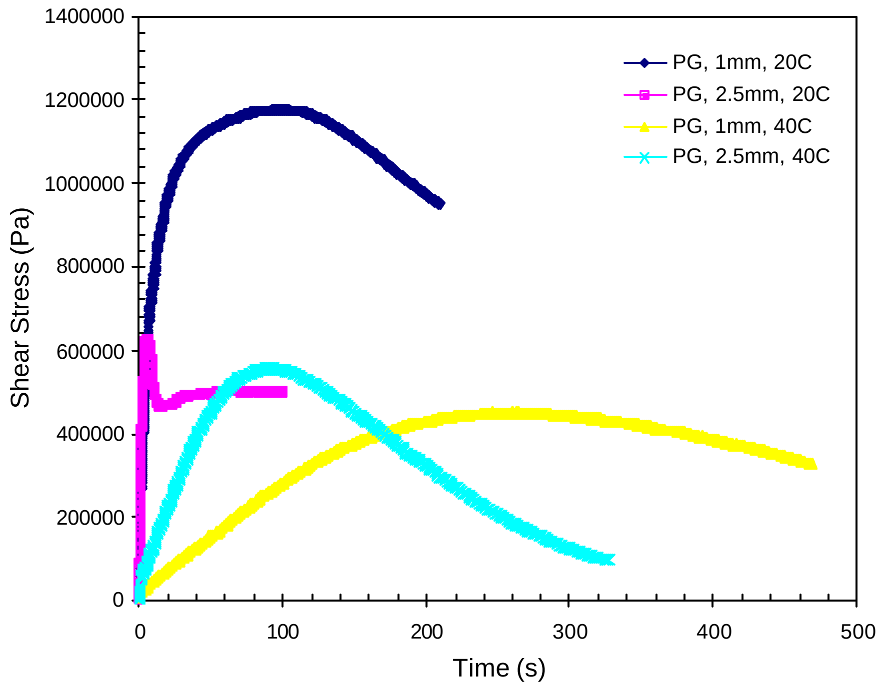

Figure 8-7 Average shear stress vs. time for AC-AC interface tacked with PG64-22

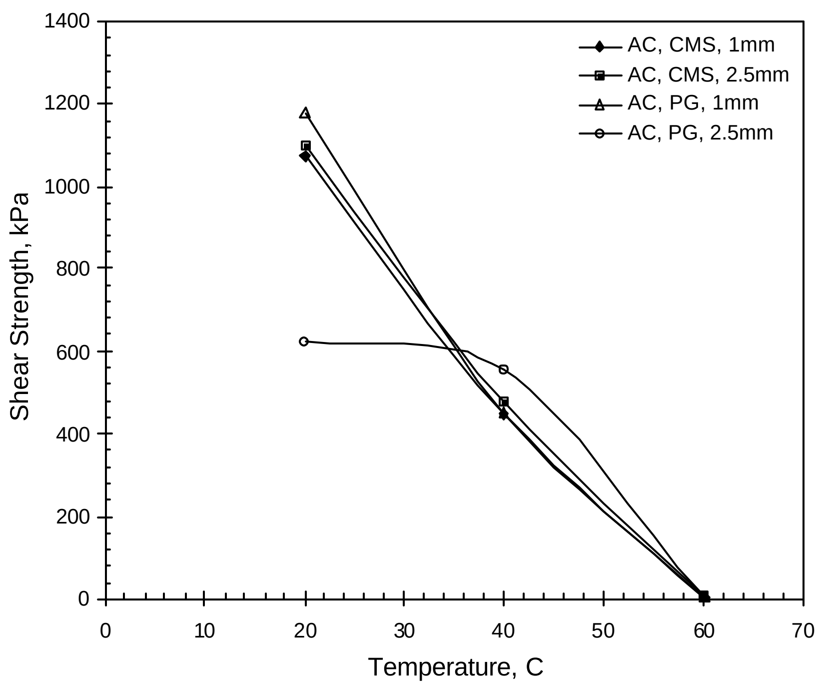

Figure 8-8 Summary of bond strengths for AC-AC interface

Figure 8-9 Shear failure of CMS-2 specimen (m1 6-16-2) at 1.0mm/min, 40 C

Figure 8-10 Shear failure of CMS-2 specimen (m3 6-3-2) at 1.0mm/min, 40 C

Figure 8-11 Shear failure of CMS-2 specimen (c1 6-3-2) at 2.5mm/min, 40 C

Figure 8-12 Shear failure of PG64-22 specimen (m1 5-7-2) at 2.5 mm/min, 40 C

Figure 8-13 Shear failure of PG64-22 specimen (1mmc2_1) at 1.0 mm/min, 20 C

Figure 8-14 Shear failure of PG64-22 specimen (25mmm3) at 2.5 mm/min, 20 C

Figure 8-15 Debonding of composite PCC-AC specimen without tack coat

Figure 8-16 Debonded composite PCC-AC slabs without tack coat

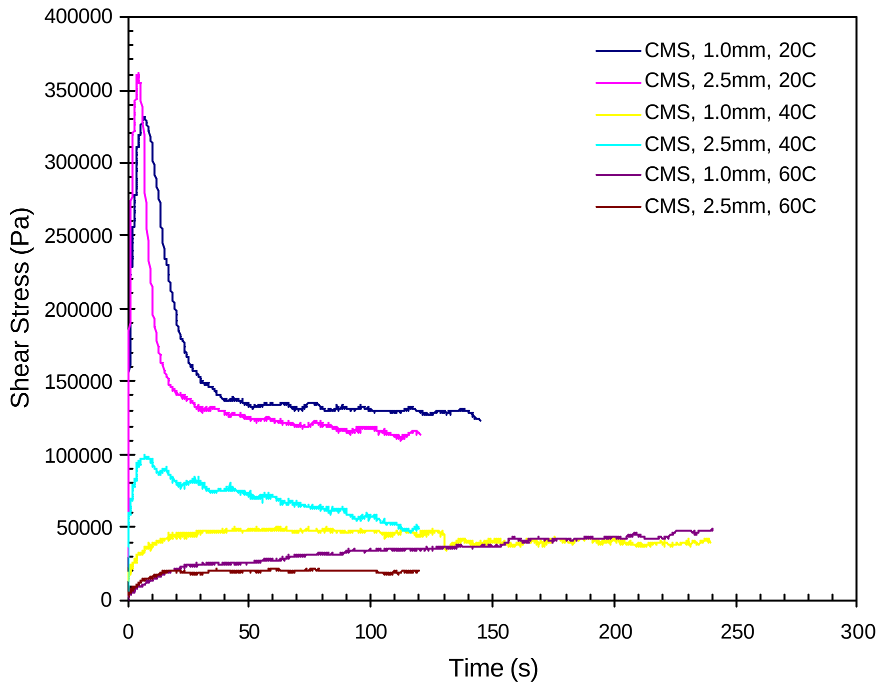

Figure 8-17 Average shear stress vs. time for PCC-AC interface tacked with CMS-2

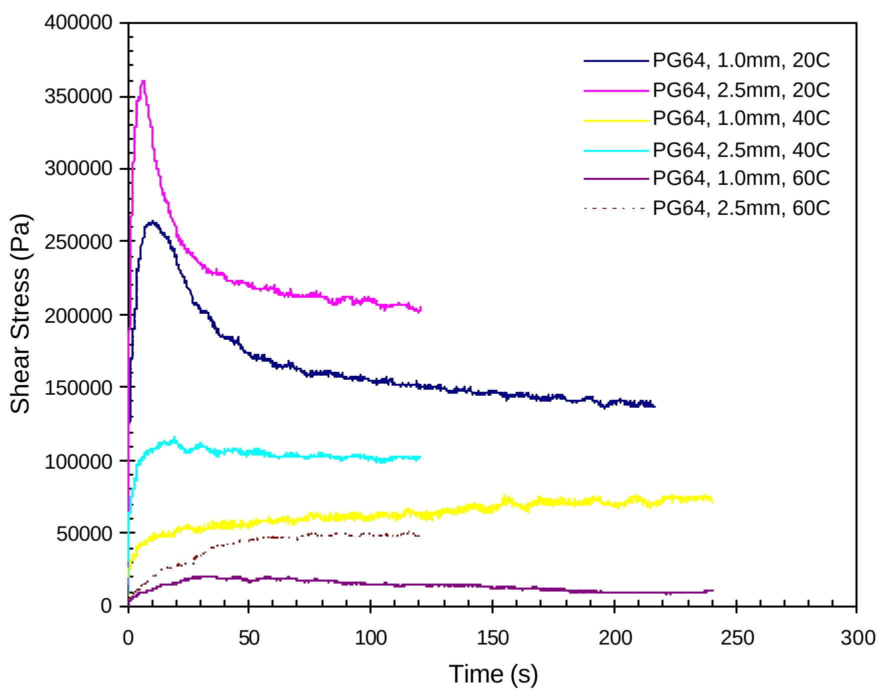

Figure 8-18 Average shear stress vs. time for PCC-AC interface tacked with PG64-22

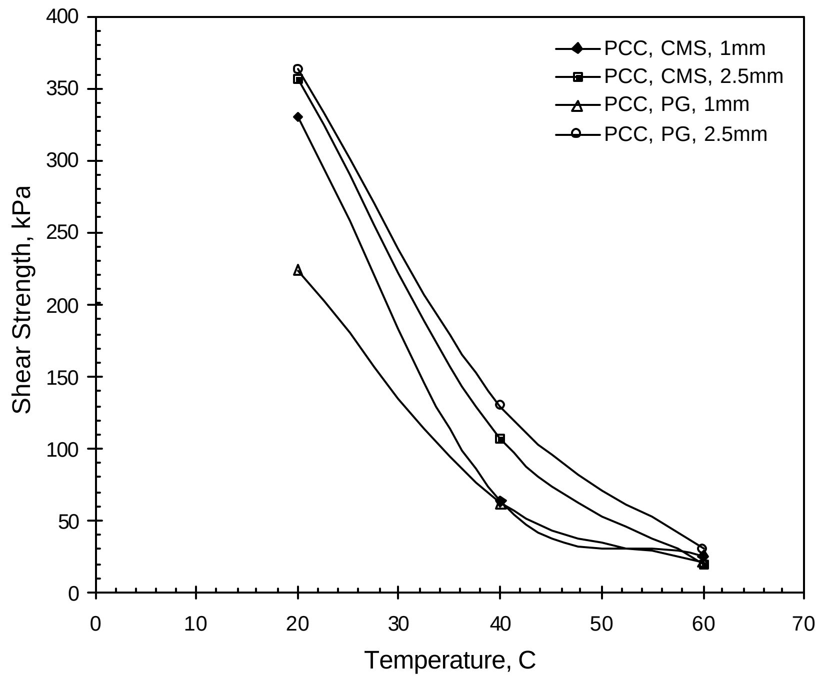

Figure 8-19 Summary of bond strengths for PCC-AC interface

Figure 8-20 PCC-AC specimen tacked with PG64-22 (cracks highlighted in white)

Figure 8-21 PCC-AC specimen tacked with CMS-2

Figure 8-22 Composite CTB-AC specimen

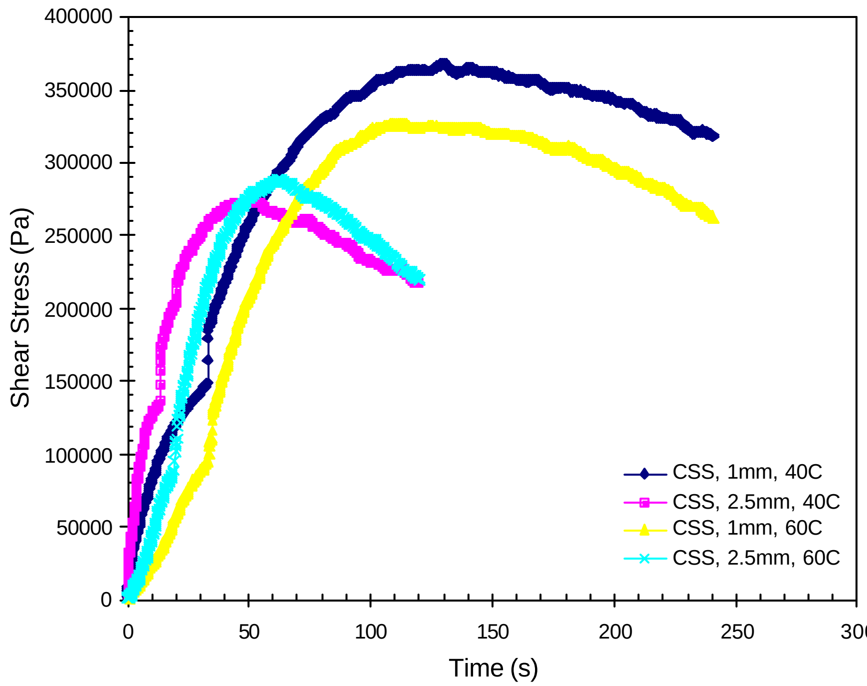

Figure 8-23 Average shear stress vs. time for CTB-AC interface primed with CSS-1h

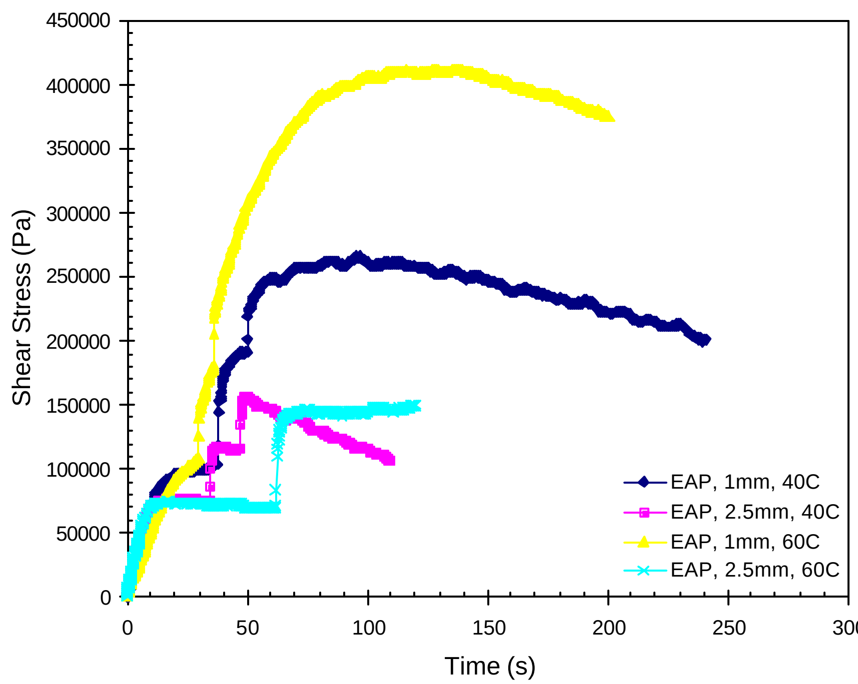

Figure 8-24 Average shear stress vs. time for CTB-AC interface primed with EAP

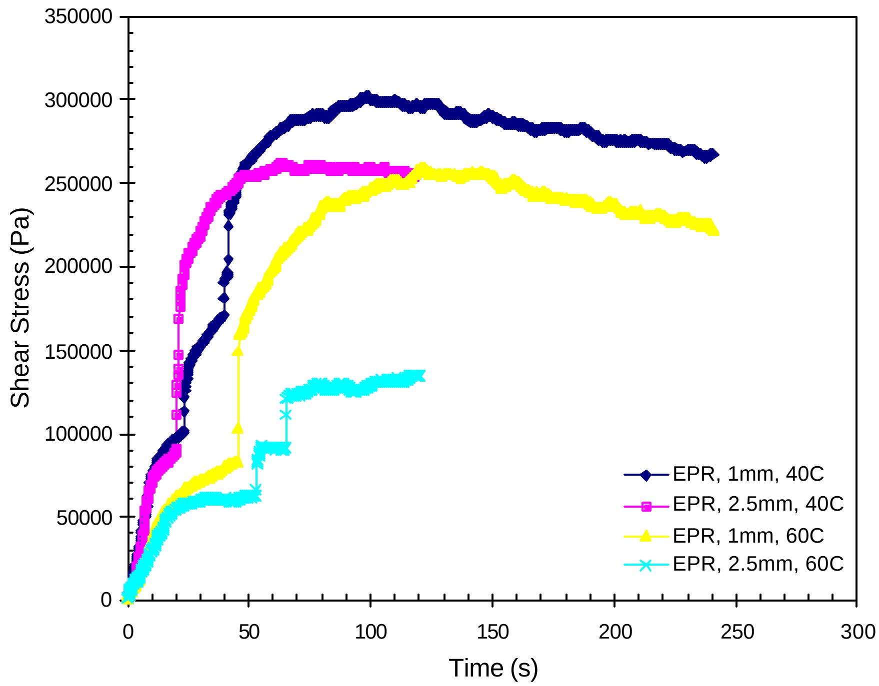

Figure 8-25 Average shear stress vs. time for CTB-AC interface primed with EPR-1

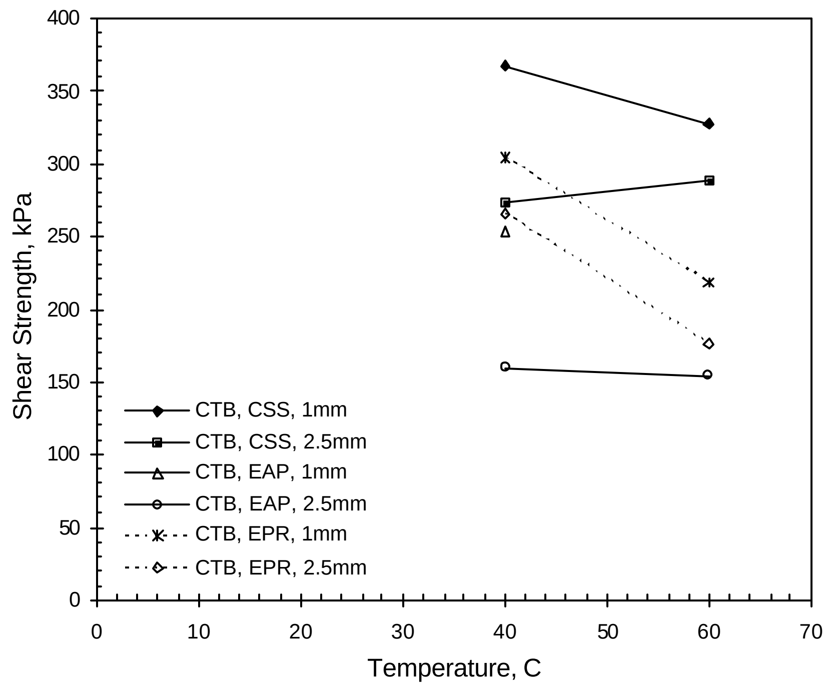

Figure 8-26 Summary of bond strengths for CTB-AC interface

Figure 8-27 CTB-AC specimen primed with CSS-1h, sheared at 1mm/min (40 °C)

Figure 8-28 CTB-AC specimen primed with EPR-1, sheared at 1mm/min (60 °C)

Figure 8-29 Debonded CTB-AC specimen primed with EA-P, 60 °C

9 Development of Design Guidelines for Use of Tack and Prime Coats

9.1 3-D Layered Elastic Program Description

The final objective of the determination of interfacial bond strength is to develop guidelines that can be used to minimize interlayer slippage. A detailed parametric study was conducted to investigate the effect of system parameters including layer thickness and stiffness on the stress-strain-displacement fields induced in the pavement.

Although BISAR (Bitumen Structures Analysis in Roads) developed by Shell Research is a program that considers vertical and horizontal loadings in a multilayered system, its shortcoming is that it can be used only for three layered systems. Another program, ELSYM5, developed at University of California, Berkeley uses a similar approach to analyze a multilayered system but cannot analyze the effect of horizontal loads.

In this investigation, a computer program was developed by Xu, et al [50] as part of this research to study stresses, strains and displacements modeling in various types of pavement sections using a 3-D approach. The following simplifying assumptions, similar to Burmister's theory [14], are made in modeling the pavement:

- The pavement is made up of layered elastic materials that are homogenous, isotropic and follow Hooke's law.
- Each layer is weightless, of uniform thickness and extends infinitely in horizontal directions. (An assumption that contribution of layer weights to delamination is negligible compared to the effect of vehicular loads is made.)
- The bottommost layer is of infinite depth, and the stresses and displacements at infinite depth are zero.
- The layer surfaces are fully bonded and it is reflected by stress and displacement continuity across interfaces.
- The surface shear and normal stresses on the top of the uppermost layer are zero outside loading areas.

- The contact pressure is same as the tire pressure, and the tire contact areas are circular with uniform distribution of shear and normal stresses over area of contact.

The method of calculating the stresses, strains and displacements in the pavement sections is semi-analytic. The model formulation in this method is analytic but the solution is obtained numerically. Using Hankel transforms (Small and Booker, [39, 40]) the three dimensional analytic problem is reduced to two or one dimensions, simplifying the solution process.

9.2 Load Conditions

The loading for analysis is assumed to be a standard, static, 18 kip dual tire assembly. This assembly consists of two tires at each end of the axle. The axle length is 6 ft, and the dual tire separation at each end is 1ft (center-to-center). Only tires at one end of the axle are considered for analysis as the assembly at the other end of axle is considered too far away to have any significant impact on loading under consideration. Figure 9-1 shows the layout of dual tires at end of the axle and the location of axes. The vehicle axle is oriented along Y-axis and the direction of motion is along positive X-axis. For convenience, the origin is assumed to lie midway on the line joining the center of two tire assembly. The vertical load on each tire is 4500 lb, a quarter of the load on the whole assembly. The tires are inflated to a pressure of 100 psi and, therefore, the contact pressure between the tire and the pavement is 100 psi as well. For each tire, the vertical load divided by the contact pressure (100 psi) gives the contact area which is 45 in^2 in this case. Assuming a circular contact area, the radius of contact area is 3.785 in.

The effect of horizontal load (shear) is modeled by considering three cases: (a) pure vertical load with no horizontal load, (b) vertical load with 40% of vertical load as shear load and, (c) vertical load with 70% of vertical load as shear load. The case with pure vertical load represents the situation when the vehicle is stationary or moving at a high speed. Kummer and Meyer [28] have recommended a skid number of at least 37, measured at 40 mph, for main rural highways. Skid number is coefficient of friction multiplied by 100. The case with 40% shear load is equivalent to having 40% horizontal shear at moderate speeds. Barber [11] has shown that the coefficient of friction between the tires and the pavement can be as high as 0.80 when the effect of wind is considered. This type of loading is obtained while traveling on a 75-ft radius curve with no banking at 30 mph. Studies by Kummer and Meyer [28] have recommended a skid number value of 60 at or near 0 mph. Based on these two findings, a maximum value of 0.7 was chosen for coefficient of friction for worst case scenario. For the purpose of this study, the shear loads are considered only in the direction of motion of traffic that simulates the forces while braking. Typical skid number are shown in Table 9-1.

9.3 Temperature Effects

The properties of asphalt mix depend on the binder properties which, in turn, are significantly influenced by temperature. In addition, the bond strength of any interface tacked with asphalt is also dependent on temperature. Thus, the resistance of a pavement to horizontal loads depends on temperature as well. This section deals with incorporation of temperature effects into design of pavements to minimize interfacial shear failure.

Most of delamination and eventual shoving occurs either at high temperature or very high loads or a combination of the two. The pavement temperature considered for analysis in this study is the maximum 7-day high temperature at the selected depth. Using either LTPPBind™ (http://www.tfhrc.gov/) or SHRPBind™ programs, the ambient 7-day maximum air temperature is obtained. For details, please refer to Section 5.3, which deals with the computation of pavement temperatures using the program for a given location. Using the technique outlined in section 5.3, pavement temperatures were calculated for Enka, NC. Enka, NC was chosen as the mix used in this study was from a plant in this area. Figure 9-2 shows the variation of high pavement temperature as a function of depth for Enka, NC. The temperature at mid-height for any asphalt layer was assumed to be the representative temperature for the whole layer. The asphalt mix stiffness was calculated based on the temperature at its mid-height using the data obtained and presented in Chapter 7. Using the dynamic moduli of the AC mix (Table 7-12 and Table 7-14) Figure 9-3 was developed showing the dynamic axial moduli for AC mix at various temperatures. PCC and CTB moduli are assumed to not change with temperature and hence are assumed to be constant. The interfacial temperatures were calculated using Figure 9-2 and the bond strength measured at various temperatures were interpolated at the interface temperature based on data presented in Chapter 8. Table 9-2 and Table 9-3 summarize the bond strengths obtained for various interfaces.

9.4 Analysis of AC-AC Bonding

Using representative pavement section, shown in Figure 9-4, the analysis was conducted using the computer program developed in the study. The properties of aggregate base course (ABC), cement-treated subbase (CT Subbase), and subgrade were typically available values [24] and are shown in the figures. The properties of the overlay (AC) as well as the underlying layer (AC) are assumed to be solely dependent on temperature; although in practice the underlying AC layer could have a different stiffness due to oxidative hardening, and weathering action of traffic and climate. The analysis was conducted at numerous points along Y-axis (vehicle axle) and on a line parallel to X-axis passing through center of one of the tires. Figure F-1 and Figure F-2 in Appendix F summarize the mobilized interfacial shear stresses for AC-AC combination case. The maximum shear stress at the interface was determined at each point using the following equation:

$$t_{\max} = \sqrt{t_{zx}^2 + t_{zy}^2} \qquad \textbf{(Equation 9-1)}$$

Figure 9-5 and Figure 9-6 show the mobilized shear stresses at 20 °C and 7-day maximum average high temperature, respectively. It can be seen from Figure 9-5 that the interfacial shear stress increases with increasing magnitude of horizontal shear load. Further, an increase in layer thickness reduces the interfacial shear stress as would be expected. The higher shear stress produced due to presence of horizontal loading reduces with increasing thickness. Thus, unaccounted horizontal loads are more likely to have an adverse effect on pavements with thin overlays than thicker ones. At 20 °C, the bond strength of AC-AC is much higher (regardless of the tack coat used) than the mobilized shear stresses. This indicates that, at 20 °C, delamination will not occur. The thickness of the overlay at 20 °C should be the minimum required by practical and construction guidelines as debonding is not likely to take place irrespective of the tack coat used.

Figure 9-6 shows the mobilized shear strengths combined with interfacial bond strengths at 7-day maximum average high temperature. The shear stresses decrease with increase in layer thickness whereas the bond strength increases with layer thickness. Increasing layer thickness causes the interfacial temperatures to be lower and lower temperature results in higher bond strength. The intersection of these two sets of curves gives the minimum required thickness for pavement design to prevent delamination. It can be observed that the minimum required thickness for PG64-22 and CMS-2 tack coats based on strain rate of 1.0 mm/min is 2.5 to 3.5 inches depending on magnitude of shear (horizontal) load. For pure vertical loads, the thickness is 2.5 inches, whereas if 70% horizontal shear is taken into account the thickness is 3.5 inches for, both, PG64-22 and CMS-2 based on 1mm/minute strain rate. The difference in performance of PG64-22 and CMS-2 as tack coat at low strain rates is marginal.

At a strain rate of 2.5 mm/min, the PG64-22 binder performs better as a tack coat than CMS-2. The minimum required thickness for 70% horizontal load for PG64-22 is 2.25 inches whereas for CMS-2 it is 3.25 inches. Based on this data it can be concluded that PG64-22 performs better or equal to CMS-2 emulsion. Considering that the residual asphalt has a grading of PG52 for CMS-2, the result of this analysis seems to be reasonable.

9.5 Analysis of PCC-AC Bonding

Figure 9-7 shows the pavement structure used for analysis of a concrete pavement. The pavement consists of an 8 inch thick concrete slab overlaid by a variable thickness of AC overlay. The stiffness of the overlay as well as the interface shear strength was calculated at various temperatures, and the design curves generated. Figure F-3 and Figure F-4 in Appendix F summarizes the mobilized interfacial shear stresses in PCC-AC combination case. Figure 9-8 and Figure 9-9 show the developed shear stresses versus thickness of overlay for various types of loading conditions. It can be observed that the mobilized interfacial shear stresses reduce with increasing temperature. This indicates that with increasing temperature, the shear deformation of the asphalt layer increases. From Figure 9-8 it can be seen that at a strain rate of 2.5 mm/minute, the performance of PG64-22 and CMS-2 as tack coats is almost similar. The minimum required thickness for overlay is 2 inches considering the worst case scenario, and a little more than 1 inch considering a moderate horizontal shear loading.

It can be observed from Figure 9-9 that at 7-day maximum temperature, CMS-2 and PG64-22 generate equal bond strengths. The interpolated bond strength at higher temperatures turns out to be significantly lower for PCC-AC interface compared to AC-AC combination. This implies that debonding would occur for all overlay thicknesses; however this does not happen in practice. The surface roughness of PCC provides sufficient friction to reduce the chances of delamination. The likelihood of debonding occurring for PCC-AC interfaces at higher temperatures is minimized if minimum design thickness requirements can be met.

9.6 Analysis of CTB-AC Bonding

Figure 9-10 shows the pavement structure used for CTB-AC bonding analysis. Figure F-5 and Figure F-6 in Appendix F summarize the mobilized interfacial shear stresses in CTB-AC combination case. The bond strength determination for CTB-AC interface was conducted at 40 and 60 °C, and Figure 9-11 and Figure 9-12 show the development of shear stresses at 40 °C and 7-day maximum average temperature. Analysis conducted at 40 °C at 1.0 mm/minute strain rate, shows a minimum required design thickness of 2.25, 3.0 and 3.75 inches for CSS-1h, EPR-1, and EA-P emulsion as prime coats at 70% horizontal shear. However, at 40 °C and 2.5 mm/minute strain rate, the minimum design thickness increases to 3.75 inches for CSS-1h and EPR-1, and to 6 inches for EA-P. Figure 9-12 shows design curves for 7-day maximum average temperatures. CSS-1h emulsion performs better than EA-P and EPR-1 emulsion as prime coats. The required design thickness for CSS-1h at 70% horizontal shear loads is 2.5 and 4.0 inches at 2.5 and 1.0 mm/minute strain rate. For EA-P, the design thickness is 4.5 inches regardless of the rate of shear at 70% horizontal load. For EPR-1, the required thickness is 4.0 and 4.5 inches at 1.0 and 2.5 mm/min shear rate. Based on the performance, the emulsions can be rated as CSS-1h, EPR-1 and EA-P. Nevertheless, this analysis clearly confirms the practice recommendation by some DOT’s and AI that prime coat should be used for AC overlay thickness smaller than 4-5 inches thick, regardless of its type (cutback versus emulsion).

9.7 Outline of Guideline Development for Use of Tack or Prime Coat

Using the steps outlined below, the procedure described in this chapter can be applied to any pavement section for bond strength analysis. The procedure is following:

1. Select a design pavement structure, e.g. similar to shown in Figure 9-4 or Figure 9-10.
2. For the location under consideration, develop a temperature curve, e.g. similar to Figure 9-2.
3. Determine the dynamic moduli values for the materials used therein. For AC mixes, determine the values at various temperatures (Figure 9-3). The appropriate moduli for AC layers can be computed based on the temperature at its mid height.
4. Determine the interfacial temperatures based on layer thicknesses and interpolate the peak bond strength values available in Table 9-2 and Table 9-3.
5. Using the ASP program compute the interlayer stress ($\sqrt{t_{zx}^2 + t_{zy}^2}$) at various points.

   Generally, the peak stresses will occur at the edge of the wheel. Skid numbers presented in Table 9-1 can be used to compute the minimum horizontal loads at various speed levels. Various loading conditions can be considered, including horizontal loads, and the mobilized interfacial stress curves for different thicknesses can be plotted (similar to Figure 9-12).
6. Superimpose the interpolated bond strength values (Figure 9-12) on these curves to obtain the minimum required thickness. The minimum required thickness would be the intersection of the 'bond strength curve' and the 'mobilized shear stress' curve.

9.8 Summary and Conclusions

This chapter covers the development of design guidelines to reduce interfacial bond failures. Using SHRPBind and LTPPBind programs, the pavement temperature was determined for various depths for Enka, Buncombe County, NC. The dynamic axial moduli for asphalt mixes and the interfacial bond strengths were computed at various depths. The loading conditions considered for analyses were the standard 18-kip axle combined with zero, 40% and 70% horizontal shear loads. For each scenario, complete analysis was performed. Using a layered elastic program stresses, strains and displacements were computed in the pavement at various locations. The program used a 3-D semi-analytic method to compute the stresses and strains but the method of solution was numeric.

Appendix F shows the distribution of mobilized interfacial shear stresses for various combinations. The peak stress occurs, for horizontal load cases, at the front edge of the wheel. At low overlay thicknesses, the stresses are higher and localized, and they dissipate very fast with increasing distance from the center of the wheel. With increasing thickness, the stress distribution become more uniform with stresses dissipating less rapidly with distance from the center of the wheel. The application of horizontal load increases the shear stress at the interfaces in all combinations, AC-AC, AC-PCC and AC-CTB.

For AC-AC interface, CMS-2 performs as good at PG64-22 binder as tack coat. The difference in their bond strengths at high temperatures is marginal. At 20 °C, the chance of debonding at AC-AC interface is negligible. At 7-day maximum average high temperatures expected in-situ, the overlay thickness has to be designed appropriately based on the procedure developed herein to assure that chances of delamination are minimized. For PCC-AC interface, the chances of debonding are significantly lower if minimal thickness design requirements are met. For CTB-AC interface, clearly CSS-1h performs better than EA-P and EPR-1 as prime coats. Furthermore, an overlay thickness of minimum 4-5 inches will ensure that the prime coat bond will not fail or debonding will not occur.

Table 9-1 Recommended minimum skid numbers for rural highways [28]

Mean Traffic Speed, *V*, (mph)	Skid Number	
	SN[4]	SN_{40}[5]
0	60	–
10	50	–
20	40	–
30	36	31
40	33	33
50	32	37
60	31	41
70	31	46
80	31	51

Table 9-2 Interfacial shear bond strength summary for PG64-22 and CMS-2

Interface	Temperature (°C)	Strain rate (mm/min)	CMS-2	PG64-22
			Shear Strength (psi)	Shear Strength (psi)
AC-AC	20	1.0	156.3	170.7
		2.5	159.1	90.8[6]
	40	1.0	65.1	65.4
		2.5	69.5	80.4
	60	1.0	0.43	0.77
		2.5	1.02	1.12
PCC-AC	20	1.0	48.25	32.5
		2.5	52.3	52.8
	40	1.0	9.2	9.0
		2.5	15.4	18.8
	60	1.0	3.6	3.0
		2.5	3.0	4.3

Table 9-3 AC-CTB shear bond strength summary for CSS-1h, EA-P, and EPR-1

Temp. (°C)	Strain rate (mm/min)	CSS-1h	EA-P	EPR-1
		Shear Strength (psi)	Shear Strength (psi)	Shear Strength (psi)
40	1.0	53.3	36.8	44.1
	2.5	39.6	23.2	38.5
60	1.0	47.5	59.3[7]	31.7
	2.5	41.9	22.3	25.5

[4] SN = skid number, measured at mean traffic speeds
[5] SN_{40} = skid number, measured at 40 mph
[6] This value is too low when compared with others.
[7] Value is high compared to other trends.

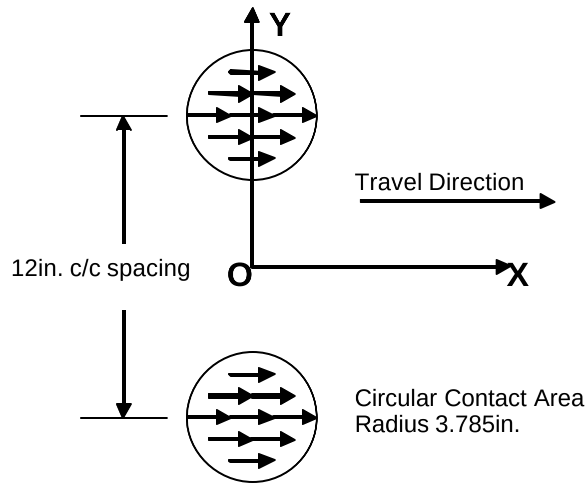

Figure 9-1 Tire layout, travel direction, and axes orientation

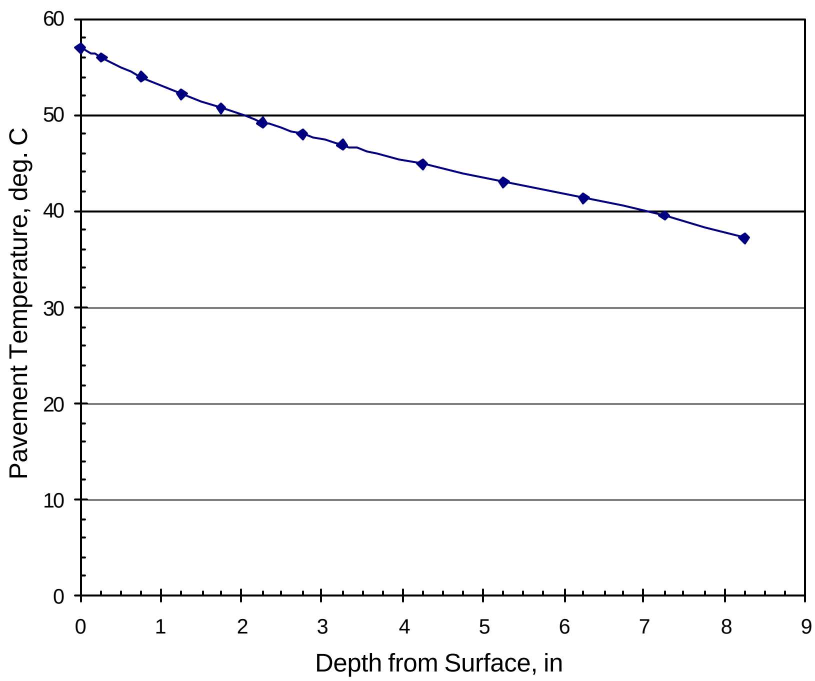

Figure 9-2 AC average 7-day maximum high pavement temp. vs. depth

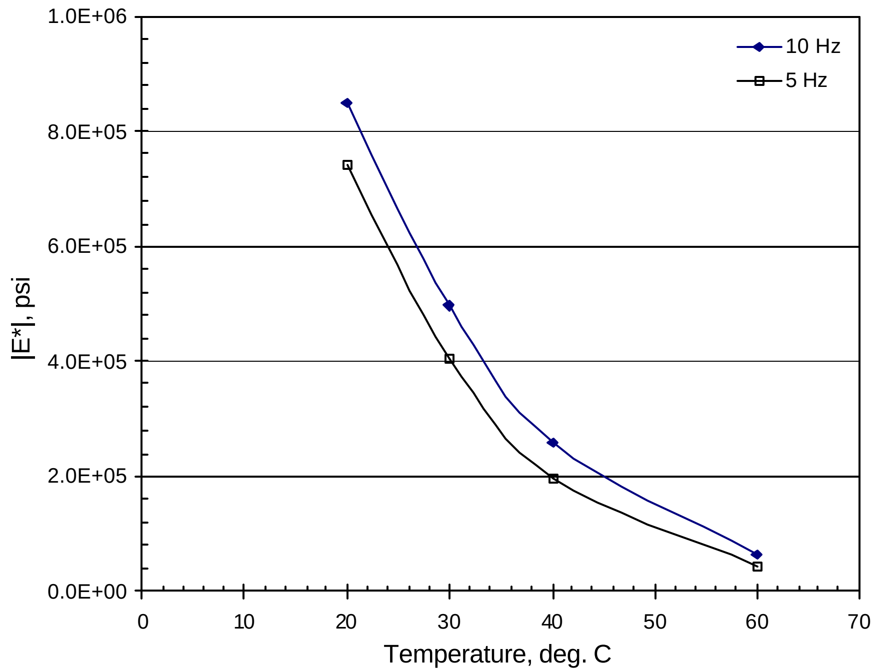

Figure 9-3 Dynamic axial modulus for asphalt mixes vs. temperature

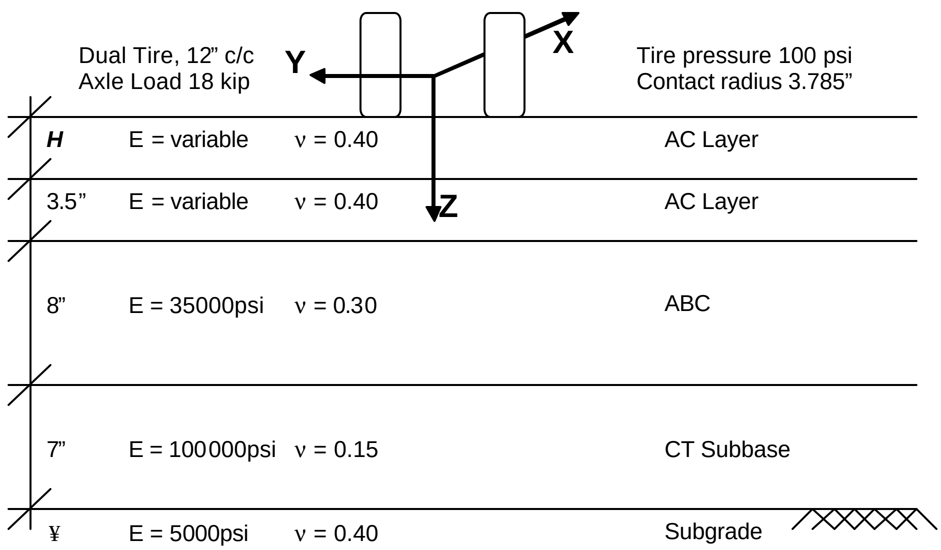

Figure 9-4 Pavement structure and layer properties, AC over AC

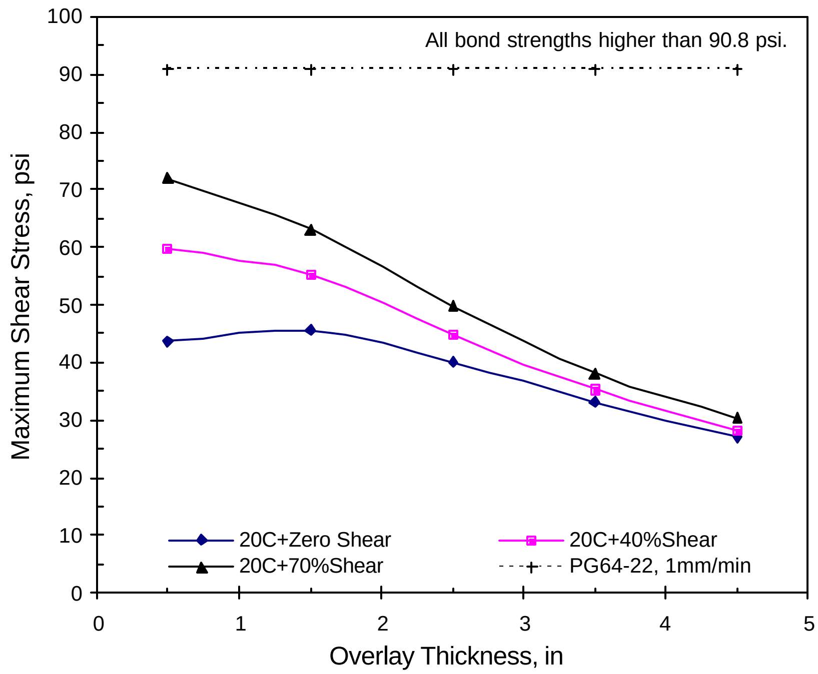

Figure 9-5 Mobilized interfacial shear vs. overlay thickness, AC-AC, 20 °C

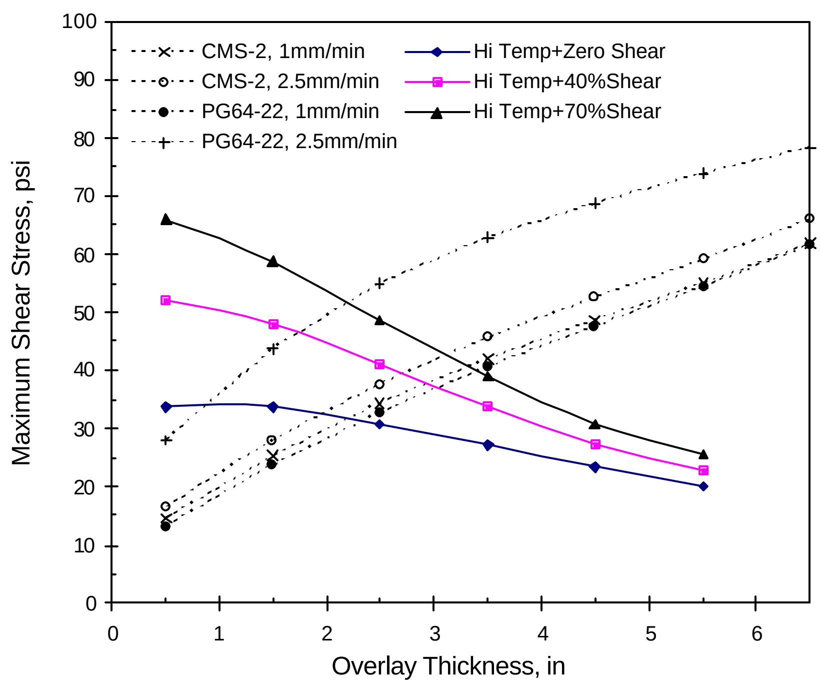

Figure 9-6 Mobilized interfacial shear vs. overlay thickness, AC-AC, 7-d max temp.

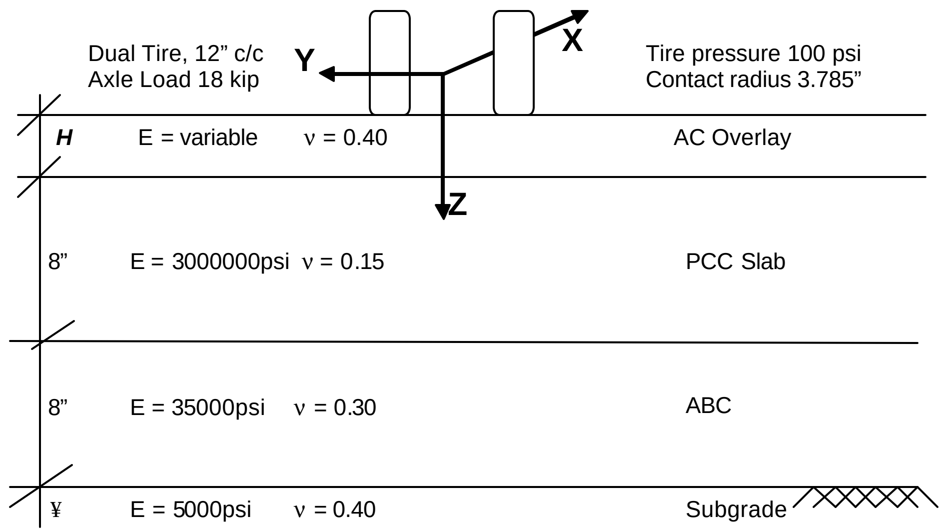

Figure 9-7 Pavement structure and layer properties, AC over PCC

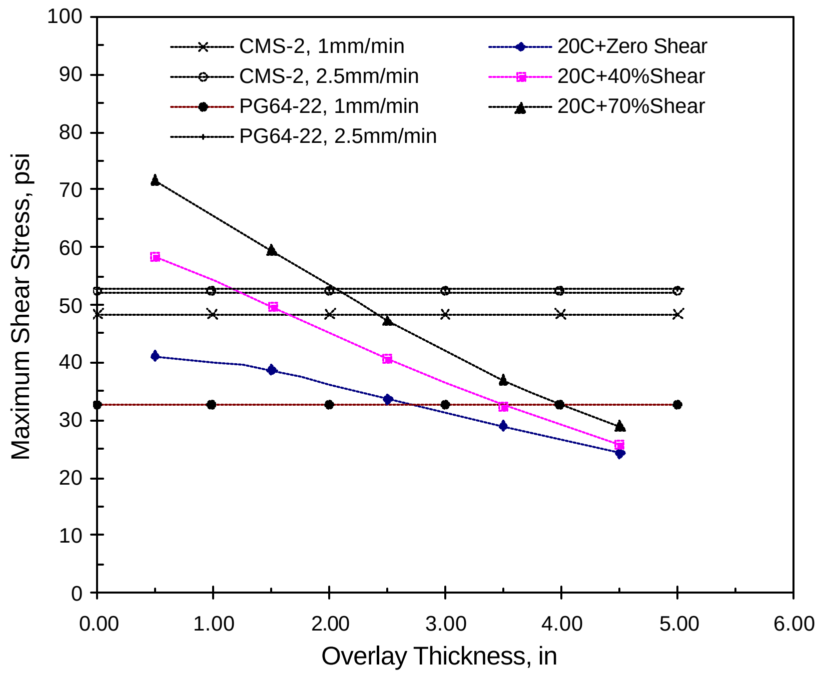

Figure 9-8 Mobilized interfacial shear vs. overlay thickness, PCC-AC, 20 °C

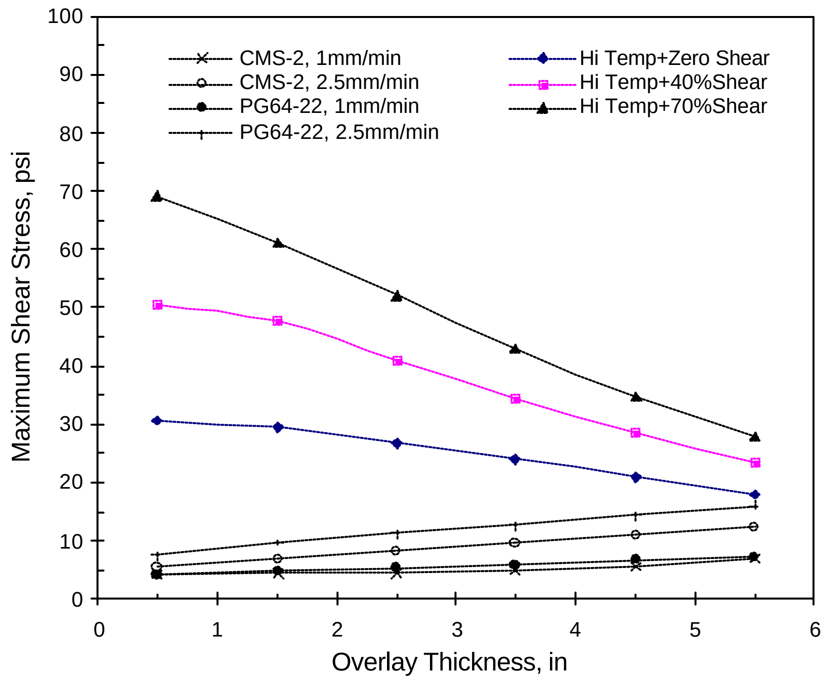

Figure 9-9 Mobilized interfacial shear vs. overlay thickness, PCC-AC, 7-d max temp.

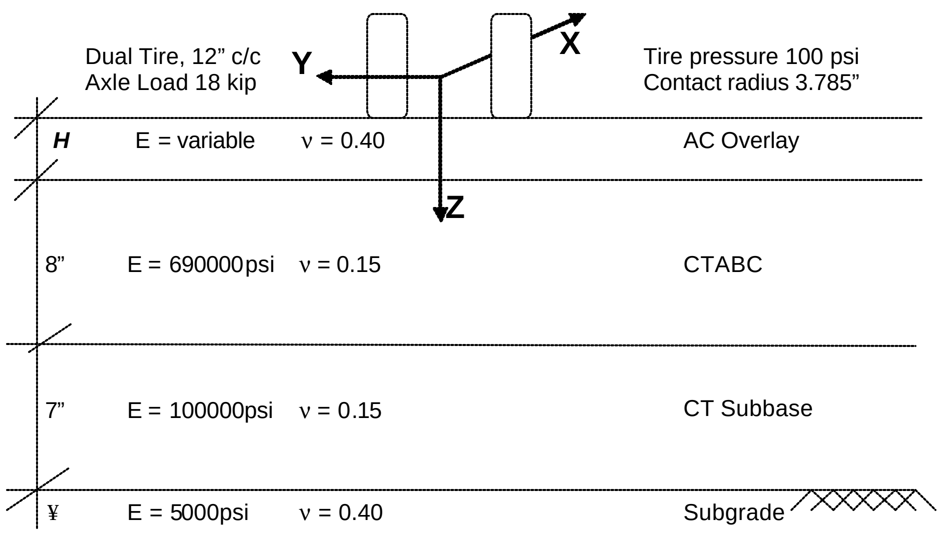

Figure 9-10 Pavement structure and layer properties, AC over CTB

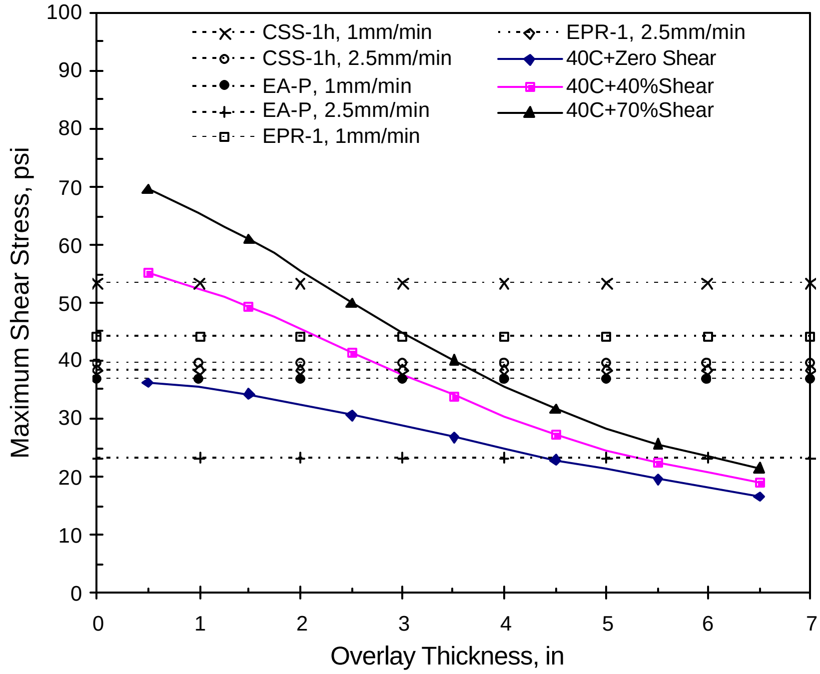

Figure 9-11 Mobilized interfacial shear vs. overlay thickness, CTB-AC, 40 °C

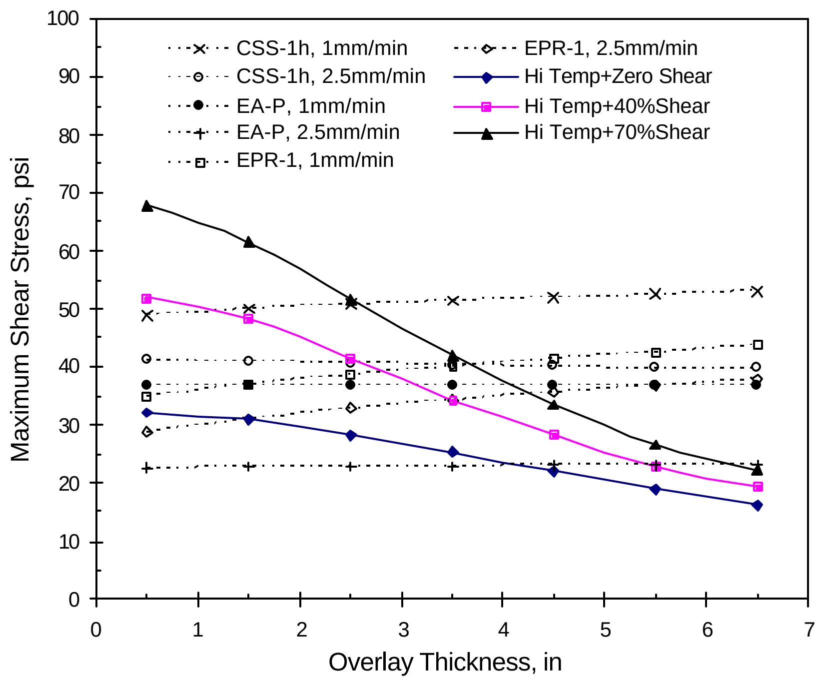

Figure 9-12 Mobilized interfacial shear vs. overlay thickness, CTB-AC, 7-d max temp.

10 Summary, Conclusions and Recommendations

This study investigated the cause of excessive delamination and shoving distress observed in NCDOT Division 13. Two potential causes of these distresses were identified to be: (a) Unstable mixtures caused due to intermittent purging of baghouse fines, and, (b) Improper choice and/or application of tack coat.

Work conducted by Tayebali et al [43] evaluated the field cores and their compliance with NCDOT specifications. The field cores were obtained based on a survey conducted in Division 13 of NCDOT. Field cores from two counties, Buncombe and Rutherford, were selected for evaluation. The results of gradation, volumetric, and stability analysis indicated that the in-situ asphalt mixes used in Buncombe and Rutherford counties were generally within the NCDOT design specifications, and should have performed well under normal traffic conditions. Buncombe County sections, however, had excessive delamination and shoving distresses whereas Rutherford County sections did not show an occurrence of any of such distresses. It was originally hypothesized that one of the contributory factors to the delamination and shoving was the intermittent purging of baghouse fines in the field asphalt mixtures and, therefore, additional laboratory tests were conducted to verify the claim.

Gradation analysis using particle analyzer, however, showed comparable gradations for baghouse fines and regular mineral fillers for both counties. The dynamic mechanical analysis of mastics using DSR suggested that baghouse fines might lead to stiffening of the binders, and consequently increased rut resistance of AC mixes. Further, there was no significant difference in $|G^*|$ values of mastics prepared with baghouse fines versus regular filler. Laboratory FSCH and RSCH tests conducted on mixes with baghouse fines showed that:

- Baghouse fines have a stiffening on mixes from both counties;
- Mixes containing baghouse fines are more resistant to rutting compared to mixtures without baghouse fines; and
- Mixes from both counties show similar dynamic shear stiffness and rutting characteristics.

Mixtures containing regular mineral filler and baghouse fines were subjected to APA testing at NCDOT Materials and Tests Unit. Test results showed that the accumulated rut depths for mixtures from Buncombe and Rutherford counties were approximately 6.15-mm (1/4-inch) and 12.5-mm (1/2-inch) respectively for both mixtures with and without baghouse fines. Although these rut depths suggest excessive rutting susceptibility for mixes based on the NCDOT specification, it confirms findings based on other tests that indicated that the performance of mixtures with and without baghouse fines are very similar. However the modified AASHTO T283 test clearly indicated that the mixtures containing baghouse fines were more moisture sensitive as compared to the mixtures containing regular mineral filler, even though an anti-strip additive was used for both mixtures. The TSR ratios for the Buncombe County mixtures were 78 and 85-percent for mixtures with and without baghouse fines respectively. The TSR ratios for Rutherford County mixtures were 83 and 92-percent for mixtures with and without baghouse fines, respectively.

Based on the results of this investigation, it is concluded that the intermittent purging of baghouse fines could be the contributory factor in the delamination and shoving distress observed in NCDOT Division 13. It appears that the mechanism by which this distress is manifested is the following:

- Some in-situ mixtures may contain very high proportion of baghouse fines in relation to regular fines due to intermittent purging of the baghouse fines. Although the NCDOT JMF requires use of an anti-strip additive, the dosage does not appear to be sufficient to counteract moisture damage leading to in-situ mixture deterioration and, consequently, loss of strength and stability. Once the moisture damaged mixture is susceptible to shoving under traffic loading, the CRS-2 emulsion is not able to provide the tacking strength necessary for the surface layer to remain bonded to the lower layer, leading to delamination.

- In Rutherford County where some pavement sections may contain relatively higher amounts of baghouse fines due to intermittent purging, the PG64-22 binder used as tack coat appeared to provide sufficient bonding that may prevent asphalt layer from delaminating even though mixtures may undergo slight moisture damage.

Apart from intermittently purging baghouse fines into mixes, the pavement sections in Rutherford and Buncombe counties used CRS-2 emulsion and PG64-22 binder as tack coat. The improper use of tack coat could be a contributory factor to delamination distresses observed in those counties. It was, therefore, decided to investigate the contribution of prime and tack coat bond strength contribution to the integrity of pavements in relation to overlay AC thickness. A survey was conducted across all the state highway departments and agencies to acquire information about the use of prime and tack coats in the field. Of the 26 responding agencies, ten reported that there was no requirement on use of prime coat for new construction. A majority of the remaining sixteen used a combination of cutbacks and emulsions for prime coats. In cases where cutbacks were preferred to emulsions, the reasons were absence of curing problems and waiting time. For prime and tack coats, there was no objective test to ensure proper curing. This could, potentially, lead to problems during the service life.

DSR test results on residual binders from emulsions could be used to determine their PG grade. Generally, when using higher PG rated binder, greater shear strength can be expected. Using rolling wheel compaction, composite AC-AC, and PCC-AC specimens were fabricated in the lab. The target air void content for all AC specimens was 4%. Problems encountered in fabricating CTB slabs, required CTB-AC composite fabrication in gyratory molds. Before paving the overlay, the lower layer was tacked or primed, and the emulsions were allowed to cure for 24 hours. The rate of application was 0.06 and 0.24 gallons per square yard for tack coat and prime coat, respectively. The samples were then cored and cut to 6 inch diameter and 2 inch height before being tested in simple shear at various temperatures.

Shear displacement rates of 1.0 and 2.5 mm per minute were used to determine the bond strength of the specimens. The test results concluded that:

- Non-bonded surfaces have extremely low strengths compared to bonded surfaces. Therefore, use of a bonding agent (tack or prime coat) is always recommended during construction.
- For AC-AC composites, the performance of PG64-22 binder as a tack coat is better than CMS-2 emulsion. This is supported by higher axial and shear strengths of PG64-22 tacked specimens compared to CMS-2 specimens.

- For PCC-AC specimens, the behavior of PG64-22 as tack coat is comparable to CMS-2. One reason for this could be due to the fact that the rate of application of residual asphalt could be higher for PG64-22 than for CMS-2. In particular, it was found that PG64-22 performance at higher temperature and lower strain rate was relatively poor. The bond strengths recorded for PCC-AC combination were substantially lower compared to AC-AC. Secondly; the relative imperviousness of PCC (vis-à-vis AC) could lead to less absorption of asphalt from tack coat and, consequently, a poorer bond at high temperature and low strain rate. The relative differences in PCC and AC moduli could also be a contributory factor as well as the absence of corrugations on the PCC slab. In the field, the underlying concrete pavement has grooves or milled surface that increases the friction between the overlay and the PCC slab.
- The bond development in CTB-AC case was due to a contribution of the prime coat as well as aggregate interlock. CSS-1h emulsion performed better than EA-P and EPR-1 emulsions as prime coat.

Using FSCH and axial frequency sweep tests, the dynamic moduli of asphalt mix was determined at various temperatures and, properties for PCC were determined at 28 days. Based on the pavement temperature at various depths, the dynamic moduli and interfacial bond strengths were interpolated to yield temperature-corrected values. These values (dynamic moduli) coupled with the standard 18 kip loading data were, then, input into the ASP program developed in this investigation. The program computed the stresses, strains and displacements at various points in the pavement structure as function of vertical as well as horizontal shear loading. The maximum shear stresses were computed at the interface for different loading conditions. The variation of maximum mobilized shear stresses was then plotted against the interpolated bond strengths to obtain the required minimum design thicknesses.

For AC-AC, at 7-day maximum average temperatures, the overlay design thickness using CMS-2 and PG64-22 tack coat and shear rate of 1.0 mm/minute was comparable (3.5 inch); however at 2.5 mm/minute strain rate PG64-22 (2.5 inch) gave a lower design thickness than CMS-2 (3.25 inch) indicating a superior performance. Mechanistic analysis indicates that delamination will not be a problem for AC-AC combination at 20 °C as the bond strengths are much higher than the mobilized interfacial shear stresses. For PCC-AC combination, at 20 °C and 2.5 mm/minute strain rate, the design thickness for AC overlay is slightly higher than 2-inch; at the same temperature and 1.0 mm/minute the design thickness for CMS-2 and PG64-22 is 2.5 and 4 inch, respectively. Therefore, it can be concluded that CMS-2 yields lower thickness for PCC-AC combination than PG64-22 binder. As indicated earlier, this could be due to excess PG64-22 (compared to the residual asphalt in CMS-2), smooth PCC surface, and low rate of tack coat absorption by the PCC surface. At 7-day maximum temperature, for PCC-AC combination, the interpolated bond strengths are much lower than the mobilized shear stresses. Therefore, the choice of tack coats is dependent not only on the types of interfaces under consideration but also on the rate of application. Higher rate of tack coat is undesirable when using impervious and smooth surfaces such as PCC. At higher temperature, instead of providing a good bond, it will actually act as a slippage surface. In severe cases it may even lead to bleeding on the thin AC overlay layer.

For CTB-AC interface, CSS-1h emulsion seems to be better than EA-P and EPR-1. Overall, based on the results of this study, the following conclusions can be drawn:

- Addition of baghouse fines could cause stiffening of AC mixes. However, appropriate amounts of anti-strip additive need to be added to counteract the added moisture susceptibility due to the presence of baghouse fines.
- The contribution of tack coat to the bond strength is dependent on the grade of the residual asphalt as well as the interfaces under consideration. PG64-22 performs slightly better for the AC-AC case whereas CMS-2 performs marginally better for PCC-AC case.
- For thin pavement sections, the use of prime coats is recommended to increase the bond between the AC layer and the underlying layers. Similarly, use of a suitable tack coat is recommended for all overlay construction with minimum AC layer thickness of 2.5-3.5 inches when PG64-22 or CMS-2 emulsion is used as tack coat. If a different tack coat is used, the minimum thickness can be obtained for the given site using the design guidelines developed in this study.

- CSS-1h performs better as a prime coat than EA-P and EPR-1 emulsions.
- For emulsions used as prime and tack coats, it is necessary to ensure complete curing before paving new layer. Any inappropriate curing could reduce the bond as well as trap moisture causing problems later in service.
- The choice of proper tack coat (CMS-2 versus PG64-22) should be based on operational considerations. Use of PG64-22 as tack coat enables the tacked section to be open to traffic immediately after application. Further the convenience of night time paving as well as minor effect on exposure moisture outweighs the trouble of dealing with hot asphalt. Curing problems with emulsions prevail over the uniformity and ease of their application.

A Mechanistic Approach to Evaluate Contribution of Prime and Tack Coat In Composite Asphalt Pavements, Part II – 3D-Analysis, Finite Layer Computer Program

by

M. S. Rahman, Ph.D.

Akhtarhusein A. Tayebali, Ph.D., P.E.

Qingxia Xu

Moreshwar B. Kulkarni

11 Analysis of Stresses in Pavements: Literature Review

11.1 Introduction

Distresses and failures in pavements are caused by stress-strain-displacement fields developed under mechanical and environmental loads. While the mechanical loads are caused by wheel loads from the moving vehicles, the environmental loads are due primarily to temperature and moisture variation.

Our main objective is to study the layer delamination due to mechanical loads. The mechanism of this distress in pavements can fully be investigated only through a comprehensive model for the analysis of stress-strain-displacement fields within the pavements. In this section we present a brief description of the required features of a model, the available modeling techniques and the modeling approach to be taken for this study.

11.2 Pavement Modeling

A pavement may be idealized as a system of horizontal layers extending infinitely in all three directions. These layers are of varying thickness and different material types with anisotropic properties.

The forces applied by the tires of moving vehicles not only involve the vertical forces due to the self-weight of the vehicle, but also horizontal force due to breaking, turning and acceleration. These horizontal forces may be large and may contribute significantly to the deformation of the pavement. The stress-strain-displacement fields contributed by the horizontal forces at the pavement surface are expected to play an important role in the layer delamination problem.

11.2.1 Analytic Methods

Many analytical solutions have been developed for layered materials subjected to vertical loads over circular area. Burmister [14] and Fox [19] have presented solutions for two layer systems with the underlying layer being infinitely deep. Solutions have also been obtained for a three-layer system by Jones [27], and Ueshita and Meyerhof [46], where again the underlying layer was infinitely deep. Gerrard [20] has presented solutions for a strip loading on a layered system. He considered a two-layered system with finite thickness including the effect of anisotropy. Many researchers have examined the problem of horizontal loading, and analytic solutions have been obtained by Scott [34], for a uniform horizontal loading applied over a strip on the surface of an infinitely deep elastic layer, and Barber [11] who considered the case where the load was applied to a circular region. For layered soils, solutions have been presented by Westman [49] for uniform shear loading over a circular region where a surface layer of material overlies an infinitely deep layer of another material. When several layers of material are involved analytic solutions become difficult, and presentation of results becomes complex because of the many different combinations of layer thickness and moduli.

11.2.2 Numerical Methods

Various numerical methods of analyses may be used for evaluating the stress-strain-displacement fields in a pavement. The finite difference method (Forsythe and Wasow, [18]), finite element method (Zienkiewicz, [51]), the boundary element method (Banerjee and Butterfield, [10]). Finite difference and finite element methods are quite powerful tools and can handle non-homogeneity of the system. However, since they require models of finite extent, the boundary conditions must be idealized at a distance far enough from the loads which then results in large number of elements and thus making these methods rather inefficient for problems involving infinitely extended horizontal layers. A very powerful finite difference code FLAC [26] can also be used. It uses an explicit Lagrangian calculation scheme and the mixed discretization technique by Marti and Cundall, [29]. This code has many useful features including the availability of many nonlinear material models, and can nicely incorporate the boundaries at infinity. With the types of geometry and loading in pavements, it seems that a combined boundary element-finite element methods by Zienkiewicz et al [52] may offer a realistic modeling and efficient solution. Subei [41] have indeed used this approach for the analysis of pavement distress.

11.2.3 Semi-Analytic Finite Element Method

Orthogonal series and integral transforms have long been used for the analysis of engineering problems. These methods involve using a series representation of the loadings and displacements in one or two directions and consequently reducing a three-dimensional problem into a two or one-dimensional problem resulting in a highly efficient solution. In case of a layered system, only a single spatial dimension (vertical) remains explicitly involved in the solution. In this category of methods, a finite layer method has been developed which make use of Fourier or Hankel transforms (Small and Booker [39, 40]), or Fourier series (Tham and Cheung [44]) to greatly simplify the solution process. The basic formulation in this method is analytical, while the solution is generated numerically. Some preliminary application of this method has been made in pavement analysis (Cheung and Fan, [16]; Booker and Small, [13]).

11.3 Approach to be used

The pavement will be modeled primarily as a layered system of linear elastic materials with the possibility of treating the surface asphalt layer as linear viscoelastic material. Anisotropy will also be incorporated.

The vertical and horizontal forces will be uniformly distributed over circular regions. These applied loads will be defined from the consideration of vehicle-road interaction (Cebon, [15]).

As suggested by a quick review of the available modeling techniques presented above, in this study we will use the framework of finite layer method to develop an efficient model and method of analysis. The basic formulation of Small and Booker [39, 40] and Booker and Small [13] will be used to develop the model with all the features needed for out problem. The developed model will be verified against the analytic solutions available for two and three layer systems.

A detailed parametric study will be conducted to investigate the effect of system parameters including layer thickness and stiffness on the stress-stain-displacement fields induced in the pavement. The effect of vehicle load characteristics on the response will also be examined. An attempt will be made to present the solutions (specially the response variables at the layer interfaces) in simplified graphical forms to be used for preliminary analyses by practicing pavement engineers.

12 3-D Analysis of Layered Linear Elastic Pavement System under Vertical and Horizontal Loading

12.1 General Approach and Formulation

The model for pavement system subjected to normal and shear circular loadings on the surface is depicted in Figure 12-1. The solution of the problem is equivalent to the superposition of the solutions of the pavement system subjected to normal load and shear load respectively. The following assumptions are made:

1. Each layer consists of homogeneous, isotropic or cross-anisotropic, elastic materials, which obey Hooke's law.

2. The layers are of infinite extent in the horizontal direction, but of finite thicknesses in vertical direction.

3. The base of the system is rough and rigid.

4. There is no relative movement at layer interfaces.

Finite Layer theory is used to solve this problem. To illustrate the basic idea of finite layer method, let us start with the solution procedure of axial symmetric circular load on layered system.

12.1.1 Vertical Load over a Circular Area on Layered System

The vertical load applied to the surface is uniformly distributed over a circular area, which leads to an axially symmetric problem. The equations of the theory of elasticity for the three-dimensional problem in cylindrical coordinates as used in this study are summarized in the following.

Equations of equilibrium:

$$\frac{\partial s_r}{\partial r} + \frac{\partial t_{rz}}{\partial z} + \frac{s_r - s_q}{r} = 0 \qquad (12\text{-}1)$$

$$\frac{\partial t_{rz}}{\partial r}+\frac{\partial s_z}{\partial z}+\frac{t_{rz}}{r}=0 \tag{12-1b}$$

Stress- strain relationship:

$$\underset{\sim}{s}=\underset{\approx}{D}\underset{\sim}{e} \tag{12-2}$$

where $\underset{\sim}{s}=(s_r, s_q, s_z, t_{rz})^T$ is the vector of stress components, and

$\underset{\sim}{e}=(e_r, e_q, e_z, g_{rz})^T$ is the vector of strain components and $\underset{\approx}{D}$ is the matrix of elastic constants:

$$\underset{\approx}{D}=\begin{bmatrix} a & b & c & 0 \\ b & a & c & 0 \\ c & c & d & c \\ 0 & 0 & 0 & f \end{bmatrix}$$

in which for isotropic materials $a=d=\dfrac{(1-v)E}{(1+v)(1-2v)}$, $b=c=\dfrac{vE}{(1+v)(1-2v)}$ and

$f=\dfrac{E}{2(1+v)}$, in which E is the modulus of elasticity, and v is Poisson's ratio.

Strain-displacement relationship:

$$\begin{bmatrix} e_r \\ e_q \\ e_z \\ g_{rz} \end{bmatrix}=-\begin{bmatrix} \frac{\partial}{\partial r} & 0 & 0 \\ \frac{1}{r} & 0 & 0 \\ 0 & 0 & \frac{\partial}{\partial z} \\ \frac{\partial}{\partial z} & 0 & \frac{\partial}{\partial r} \end{bmatrix}\begin{bmatrix} u_r \\ u_q \\ u_z \end{bmatrix} \tag{12.3}$$

In order to solve the preceding equations (12.1), (12.2) and (12.3), the following Hankel transformations are used:

$$U_z=\int_0^{\infty} r u_z J_0(ar)\,dr \tag{12.4a}$$

$$(U_r, U_q) = \int_0^\infty r(u_r, u_q) J_1(ar) dr \tag{12.4b}$$

where J_0 and J_1 are zero order and first order Bessel functions of the first type respectively, and a is the radial wave number. The corresponding inverse transformations are

$$u_z = \int_0^\infty a U_z J_0(ar) da \tag{12.5a}$$

$$(u_r, u_q) = \int_0^\infty a U_r J_1(ar) da \tag{12.5b}$$

By applying Hankel transform to strain-displacement relationship equation (12.3), strain components can be expressed as the function of transformed displacement, then stresses in terms of the transformed displacements are available by using the stress-strain relationship. Substituting these values of stress into the equations of equilibrium results in governing equations in terms of only one spatial co-ordinate z and wave number α.

$$-a\left[a a U_r + c\frac{\partial U_z}{\partial z}\right] - \frac{\partial}{\partial z}\left[a U_z - \frac{\partial U_r}{\partial z}\right] f = 0 \tag{12.6a}$$

$$-a\left[a U_z - \frac{\partial U_r}{\partial z}\right] f + \frac{\partial}{\partial z}\left[a c U_r + d\frac{\partial U_z}{\partial z}\right] = 0 \tag{12.6b}$$

To solve the equations (12.6a) and (12.6b) in transformed space, make the substitutions,

$$H = a a U_r + c\frac{\partial U_z}{\partial z} \tag{12.7a}$$

$$T = \left[-a U_z + \frac{\partial U_r}{\partial z}\right] f \tag{12.7b}$$

$$N = a c U_r + d\frac{\partial U_z}{\partial z} \tag{12.7c}$$

Substituting *H*, *T*, *N* into equations (12.6a) and (12.6b) results in

$$\underset{\approx}{M}(a, z)\underset{\sim}{S} = 0 \tag{12.8}$$

where

$$\underset{\sim}{S} = (M, N, T)^T$$

$$\underset{\approx}{M}(a, z) = \begin{bmatrix} a & 0 & -\partial/\partial z \\ 0 & -\partial/\partial z & -a \end{bmatrix}$$

The equations (12.8) can be satisfied by introducing the Airy stress function f such that

$$H = \partial^2 f / \partial z^2 \qquad (12.9a)$$

$$T = a\ \partial f / \partial z \qquad (12.9b)$$

$$N = -a^2 f \qquad (12.9c)$$

Using these definitions of H, T, and N in addition to equations (12.7a)(12.7b)(12.7c) leads to

$$aU_r = A\partial^2 f / \partial z^2 + Ba^2 f \qquad (12.10a)$$

$$\frac{\partial U_z}{\partial z} = -B\partial^2 f / \partial z^2 - Ca^2 f \qquad (12.10b)$$

$$\frac{\partial U_r}{\partial z} - aU_z = Fa\ \partial f / \partial z \qquad (12.10c)$$

where $A = d/(ad - c^2)$, $B = c/(ad - c^2)$, $C = a/(ad - c^2)$, and $F = 1/f$.

Elimination of U_r, U_z from the equations (12.10a), (12.10b), and (12.10c) leads to the following fourth-order ordinary differential equation in f

$$A\frac{\partial^4 f}{\partial z^4} + a^2(2B - F)\frac{\partial^2 f}{\partial z^2} + a^4 Cf = 0 \qquad (12.11)$$

Suppose that this differential equation has four Eigenvalues $l = \pm p$ and $l = \pm q$, where

$$\left(\frac{p}{a}\right)^2 = \left\{-(2B - F) + \sqrt{(2B - F)^2 - 4AC}\right\} / 2A \qquad (12.12a)$$

$$\left(\frac{q}{a}\right)^2 = \left\{-(2B - F) - \sqrt{(2B - F)^2 - 4AC}\right\} / 2A \qquad (12.12b)$$

Then the general solution to equation (12.11) can be written as

$$f = L_a \cosh(pz) + M_a \cosh(qz) + L_b \sinh(pz) + M_b \sinh(qz) \qquad (12.13)$$

Equation sets (12.9) (12.10) and equation (12.13) as well as the boundary conditions can be used to find the flexibility relationship for each layer as presented in the following.

For a given layer, there would be normal stress and shear stress at its top surface N_a, T_a and bottom surface N_b, T_b as in Figure 12-2. The subscript "a" and "b" denotes top surface and bottom surface of a layer respectively, and we use the notation $N_a = N(+h)$, $N_b = N(-h)$ etc. Because N_a, T_a and N_b, T_b are related to the stress function f, the relationship between L_a, M_a, L_b, M_b and N_a, T_a and N_b, T_b can be established. Therefore, f can also be expressed as a function with respect to N_a, T_a and N_b, T_b. Based on the relationship between the displacements U_r, U_z and f as expressed in equation set (12.10), we can finally get the flexibility relationship at the top and bottom surfaces for each layer, which can be written as

$$\underset{\sim}{d}^{\,i} = \underset{\approx}{F}^{\,i}\, \underset{\sim}{P}^{\,i} \qquad (12.14)$$

where

$$\underset{\sim}{d}^{\,i} = (U_{za}, U_{ra}, -U_{zb}, -U_{rb})^T$$

$$\underset{\sim}{P}^{\,i} = (N_a, T_a, N_b, T_b)^T$$

$\underset{\approx}{F}^{\,i}$ is the flexibility matrix for the ith layer, which is a 4×4 symmetric matrix.

The layered system is subjected to a uniformly distributed circular pressure s_0 over an area with radius a on the top of surface layer, which can be treated mathematically in transformed domain as

$$N\big|_{z=0} = \int_0^{\infty} s_0 r J_0(a\ r)dr = s_0 a J_1(a\ a) \qquad (12.15)$$

It is generally assumed that the layered system has a rough and rigid base; therefore, the displacements at the bottom of the last layer are all zeros, namely, $U_z = 0$, $U_r = 0$ there.

Since it is assumed that the two adjacent layers are bonded together and there is no slippage at the layer interface, stresses and displacements should be continuous just above and just below the interface. Continuity condition is shown in Figure 12-3, which can be written as

$$(N_b)_i = (N_a)_{i+1}$$

$$(T_b)_i = (T_a)_{i+1}$$

$$(U_{zb})_i = (U_{za})_{i+1}$$

$$(U_{xb})_i = (U_{xa})_{i+1} \tag{12.16}$$

In the analysis outlined above, it is shown that each layer can be treated as an element (compared to the finite element method), and each layer has a flexibility matrix associated with it. If every layer flexibility matrix is assembled into a global one, and so does the displacement vector, the following relationship can be obtained.

$$\underset{\sim}{d} = \underset{\approx}{F}\,\underset{\sim}{P} \tag{12.17}$$

Because of the displacement continuity at the interface as illustrated in equation (12.16), the global displacement vector $\underset{\sim}{d}$ consists largely of zeros. If no special displacement boundary conditions specified, $\underset{\sim}{d}$ would be all zeros. Solving the above set of equations, the normal stresses and shear stresses at the top and bottom of each layer can be obtained. To get the displacements, we only need to multiply the layer flexibility matrix by the stresses associated with that layer.

At this point, variables N, T, U_r, U_z at the top and bottom of each layer in transformed domain are available. To get stresses, strains and displacements in space domain, inverse transformation is needed. For instance, u_z, u_r can be solved by using equations (12.5a) (12.5b), s_z and t_{rz} can be obtained by

$$s_z = \int_0^{\infty} aNJ_0(ar)\,da \tag{12.18}$$

$$t_{rz} = \int_0^{\infty} aTJ_1(ar)\,da \tag{12.19}$$

To solve s_r, firstly, use stress-strain relationship equation (12.2) to get $s_r = ae_r + be_q + ce_z$. Then plug in e_r, e_q and e_z, which are expressed in terms of the already solved transformed variables. The solution can be written as follows:

$$s_r = \int_0^\infty a \left\{ \left[aaU_r + c\frac{\partial U_z}{\partial z} \right] J_0(ar) - (a-b)U_r . \frac{J_1(ar)}{r} \right\} da \qquad (12.20)$$

Similarly

$$s_q = \int_0^\infty a \left[\left\{ aU_r \left[\frac{1}{A} - (a-b) \right] + \left(\frac{B}{A} \right) N \right\} J_0(ar) + \{(a-b)U_r\} \frac{J_1(ar)}{r} \right] da \qquad (12.21)$$

In equations like (12.18), (12.19), (12.20), (12.21) etc., the integral upper limit is infinite. In numerical analysis, the infinite range of integration is truncated at such a point that the contribution from the omitted portion is negligible. Then the finite part of the range is equally divided into a number of sub-sections, as shown in Figure 12-4. The integrals are evaluated over each sub-section separately. For each sub-section, twenty a values are chosen according to Gauss quadrature rule. The final result is the sum of the solution for each a, for example,

$$s_r = \sum_{i=1}^{K} a_i \left\{ \left[a_i aU_r + c\frac{\partial U_z}{\partial z} \right] J_0(a_i r) - (a-b)U_r \frac{J_1(a_i r)}{r} \right. \qquad (12.22)$$

In summary, the basic procedure is: (1) apply Hankel transform with respect to radial coordinate *r* to reduce the problem to that of only one dimension in terms of coordinate *z;* (2) solve the one dimensional problem for each wave number by the finite layer method; (3) apply inverse Hankel transform to get the solution in space domain. The flowchart is presented in Figure 12-5.

12.1.2 Horizontal Load over a Circular Area on Layered System

Uniformly distributed horizontal shear loading over a circular area on the surface of a layered system is a three dimensional problem. Theory of elasticity for the three-dimensional problem in Cartesian coordinates is employed.

Firstly, vectors $\underset{\sim}{s} = (s_{xx}, s_{yy}, s_{zz}, t_{xy}, t_{yz}, t_{xz})^T, \underset{\sim}{e} = (e_{xx}, e_{yy}, e_{zz}, g_{xy}, g_{yz}, g_{xz})^T$,

$\underset{\sim}{u} = (u_x, u_y, u_z)^T$ are used to denote the vector of stress components, vector of strain components and vector of displacement components respectively.

Equations of equilibrium:

$$
\begin{gathered}
\frac{\partial s_{xx}}{\partial x} + \frac{\partial t_{xy}}{\partial y} + \frac{\partial t_{xz}}{\partial z} = 0 \\
\frac{\partial t_{yx}}{\partial x} + \frac{\partial s_{yy}}{\partial y} + \frac{\partial t_{yz}}{\partial z} = 0 \qquad (12.23) \\
\frac{\partial t_{zx}}{\partial x} + \frac{\partial t_{zy}}{\partial y} + \frac{\partial s_{zz}}{\partial z} = 0
\end{gathered}
$$

Stress-strain law:

$$\underset{\sim}{s} = \underset{\approx}{D}\underset{\sim}{e} \qquad (12.24)$$

where $\underset{\approx}{D}$ is the matrix of elastic constants:

$$\underset{\approx}{D} = \begin{bmatrix} a & b & c & 0 & 0 & 0 \\ b & a & c & 0 & 0 & 0 \\ c & c & d & 0 & 0 & 0 \\ 0 & 0 & 0 & f & 0 & 0 \\ 0 & 0 & 0 & 0 & f & 0 \\ 0 & 0 & 0 & 0 & 0 & f \end{bmatrix}$$

Strain-displacement relationship:

$$\underset{\sim}{e} = -\partial \underset{\sim}{u} \qquad (12.25)$$

Where

$$\partial = \begin{bmatrix} \frac{\partial}{\partial x} & 0 & 0 \\ 0 & \frac{\partial}{\partial y} & 0 \\ 0 & 0 & \frac{\partial}{\partial z} \\ \frac{\partial}{\partial y} & \frac{\partial}{\partial x} & 0 \\ 0 & \frac{\partial}{\partial z} & \frac{\partial}{\partial y} \\ \frac{\partial}{\partial z} & 0 & \frac{\partial}{\partial x} \end{bmatrix}$$

To solve the problem, a procedure similar to that of vertical load is used. The difference is that to reduce the problem to a one dimensional problem in transformed domain, a double Fourier transforms with respect to both x and y coordinates are employed.

Apply double Fourier transformations to displacements and stresses as follows:

$$(U_x, U_y, U_z) = \frac{1}{4p^2} \int_{-\infty}^{+\infty}\int_{-\infty}^{+\infty} (iu_x, iu_y, u_z) e^{i(ax+by)} dxdy \tag{12.26}$$

$$(S_{xx}, S_{yy}, S_{zz}, T_{xy}, T_{yz}, T_{xz}) = \frac{1}{4p^2} \int_{-\infty}^{+\infty}\int_{-\infty}^{+\infty} (s_{xx}, s_{yy}, s_{zz}, it_{xy}, it_{yz}, it_{xz}) e^{i(ax+by)} dxdy \tag{12.27}$$

where a denotes wave number in the x direction and b denotes wave number in the y direction.

The corresponding inverse Fourier transformations for equations (12.26) and (12.27) are

$$(u_x, u_y, u_z) = \int_{-\infty}^{+\infty}\int_{-\infty}^{+\infty} (-iU_x, -iU_y, U_z) e^{-i(ax+by)} dadb \tag{12.28}$$

$$(s_{xx}, s_{yy}, s_{zz}, t_{xy}, t_{yz}, t_{xz}) = \int_{-\infty}^{+\infty}\int_{-\infty}^{+\infty} (S_{xx}, S_{yy}, S_{zz}, -iT_{xy}, -iT_{yz}, -iT_{xz}) e^{-i(ax+by)} dadb \tag{12.29}$$

It is observed that since the variables on the left hand sides of equations (12.28) and (12.29) satisfy the equations of elasticity, so do the variables on the right hand sides as follows.

$$(\tilde{u}_x, \tilde{u}_y, \tilde{u}_z) = (-iU_x(a,b,z), -iU_y(a,b,z), U_z(a,b,z)) e^{-i(ax+by)} \tag{12.30}$$

$$(\tilde{s}_{xx}, \tilde{s}_{yy}, \tilde{s}_{zz}, \tilde{t}_{xy}, \tilde{t}_{yz}, \tilde{t}_{xz}) = (S_{xx}(a, b, z), S_{yy}(a, b, z), S_{zz}(a, b, z), -iT_{xy}(a, b, z),$$
$$-iT_{yz}(a, b, z), -iT_{xz}(a, b, z))e^{-i(ax+by)} \quad (12.31)$$

This means that equations (12.30) and (12.31) satisfy the equations of elasticity for every pair of wave number a in the x direction and b in the y direction. It is further noticed that the following axis transformations

$$x = x\cos e + y\sin e \quad (12.32a)$$

$$h = -x\sin e + y\cos e \quad (12.32b)$$

$$a = r\cos e \quad (12.32c)$$

$$b = r\sin e \quad (12.32d)$$

lead to $e^{-i(ax+by)} = e^{-irx}$, which means that for a certain pair of wave numbers a and b, if an axis transformation is made with an angle of e between the new coordinate system(x, h) and the old coordinate system (x, y) on the horizontal plane as indicated in Figure 12-6, all the displacements and stresses for a certain point (x, y, z) would only be dependent on the coordinates (?, z). Based on the advantage of axis transformation, it is possible to solve the problem in transformed domain with transformed coordinate system$x$, h, z, then apply axis transformation back to (x, y, z) still in transformed domain, and finally apply inverse Fourier transformation back to space domain. The following is about the solution procedure in transformed space with transformed axes.

Stress-strain relationship:

Since the material is isotropic or cross anisotropic (transversely isotropic in the x-y plane), the same stress-strain relationship as equation (12.24) can also be written with respect to transformed axis x, h, z in transformed space as

$$\underset{\sim}{\tilde{s}} = \underset{\approx}{D}\,\underset{\sim}{\tilde{e}} \quad (12.33)$$

where

$$\underset{\sim}{\tilde{e}} = (\tilde{e}_{xx}, \tilde{e}_{hh}, \tilde{e}_{zz}, \tilde{g}_{xh}, \tilde{g}_{hz}, \tilde{g}_{zx})^T$$

$$\underset{\sim}{\tilde{s}} = (\tilde{s}_{xx}, \tilde{s}_{hh}, \tilde{s}_{zz}, \tilde{t}_{xh}, \tilde{t}_{hz}, \tilde{t}_{zx})^T$$

Equations of equilibrium:

Because all the stresses are independent of coordinate h , the equations of equilibrium now become

$$\frac{\partial \tilde{s}_{xx}}{\partial x} + \frac{\partial \tilde{t}_{xz}}{\partial z} = 0 \qquad (12.34a)$$

$$\frac{\partial \tilde{t}_{xz}}{\partial x} + \frac{\partial \tilde{s}_{zz}}{\partial z} = 0 \qquad (12.34b)$$

$$\frac{\partial \tilde{t}_{hx}}{\partial x} + \frac{\partial \tilde{t}_{hz}}{\partial z} = 0 \qquad (21.34c)$$

It should be noted that equations (12.34a), (12.34b) are uncoupled from equation (12.34c).

Since all the strains are independent of h , then

$$\tilde{e}_{hh} = \frac{\partial \tilde{u}_h}{\partial h} = 0 \qquad (12.35)$$

Under the condition of equation (12.35), the stress-strain relationship equation (12.33) and the strain-displacement relationship, the following equations can be arrived at:

$$\tilde{e}_{xx} = A\tilde{s}_{xx} - B\tilde{s}_{zz} \qquad (12.36a)$$

$$\tilde{e}_{zz} = -B\tilde{s}_{xx} + C\tilde{s}_{zz} \qquad (12.36b)$$

$$\tilde{g}_{xz} = F\tilde{t}_{xz} \qquad (12.36c)$$

$$\frac{\partial \tilde{u}_h}{\partial x} = F\tilde{t}_{xh} \tag{12.36d}$$

$$\frac{\partial \tilde{u}_h}{\partial z} = F\tilde{t}_{hz} \tag{12.36e}$$

where $A = d/(ad - c^2)$, $B = c/(ad - c^2)$, $C = a/(ad - c^2)$, $F = 1/f$

In the same way as equations (12.30), (12.31), let the solutions be

$$(\tilde{u}_x, \tilde{u}_h, \tilde{u}_z) = (-iU_x, -iU_h, U_z)e^{irx} \tag{12.37}$$

$$(\tilde{e}_{xx}, \tilde{e}_{zz}, \tilde{g}_{xz}) = (E_{xx}, E_{zz}, -iG_{xz})e^{irx} \tag{12.38}$$

$$(\tilde{s}_{xx}, \tilde{s}_{zz}, \tilde{t}_{xz}, \tilde{t}_{xh}, \tilde{t}_{hz}) = (S_{xx}, S_{zz}, -iT_{xz}, S_{xh}, -iS_{hz})e^{irx} \tag{12.39}$$

It is observed that equations (12.36a), (12.36b) and (12.36c) combined with equations (12.34a) and (12.34b) can be solved together. Substituting the corresponding components in equations (12.38) (12.39) into stress-strain equations (12.36a) (12.36b) (12.36c) leads to

$$\underset{\sim}{E} = \begin{bmatrix} A & -B & 0 \\ -B & C & 0 \\ 0 & 0 & F \end{bmatrix} \underset{\sim}{S} \tag{12.40}$$

where $\underset{\sim}{E} = (E_{xx}, E_{zz}, G_{xz})^T$ and $\underset{\sim}{S} = (S_{xx}, S_{zz}, T_{xz})^T$.

Similarly, the equations of equilibrium (12.34a) and (12.34b) become

$$\underset{\approx}{M}(r, z)\underset{\sim}{S} = 0 \tag{12.41}$$

where

$$\underset{\approx}{M}(r, z) = \begin{bmatrix} r & 0 & -\frac{\partial}{\partial z} \\ 0 & -\frac{\partial}{\partial z} & -r \end{bmatrix}$$

The strain-displacement relationship becomes

$$\underset{\sim}{E} = -\underset{\approx}{N}(r, z)\underset{\sim}{U} \tag{12.42}$$

where

$$\underset{\approx}{N}(r, z) = \begin{bmatrix} r & 0 \\ 0 & \dfrac{\partial}{\partial z} \\ \dfrac{\partial}{\partial z} & -r \end{bmatrix}$$

$$\underset{\sim}{U} = (U_x, U_z)^T$$

Introducing the Airy stress function f and let

$$S_{xx} = \partial^2 f / \partial z^2$$

$$S_{xz} = r\, \partial f / \partial z \tag{12.43}$$

$$S_{zz} = -r^2 f$$

The stress-strain and strain-displacement relationships then lead to

$$rU_x = A\partial^2 f / \partial z^2 + Br^2 f$$

$$\frac{\partial U_z}{\partial z} = -B\partial^2 f / \partial z^2 - Cr^2 f \tag{12.44}$$

$$\frac{\partial U_x}{\partial z} - rU_z = Fr\, \partial f / \partial z$$

Equations (12.43) (12.44) are exactly in the same form as those of equations (12.9a-c), (12.10a-c). Following exactly the same procedure as that for vertical loading case, the element flexibility matrix for each layer and the global flexibility matrix for the whole system can be obtained.

For the uncoupled equilibrium equation (12.34c), plugging the corresponding components from equation (12.39) results in

$$-rS_{xh} + \frac{\partial S_{hz}}{\partial z} = 0 \tag{12.45}$$

Plugging the corresponding components from equations (12.37)(12.39) into equations (12.36d) (12.36e) leads to

$$rU_h = \frac{1}{f} S_{xh} \tag{12.46}$$

$$\frac{\partial U_h}{\partial z} = \frac{1}{f} S_{hz} \tag{12.47}$$

The above three equations (12.45), (12.46), (12.47) result in

$$\frac{\partial^2 S_{hz}}{\partial z^2} = r^2 S_{hz} \tag{12.48}$$

The general solution for the above ordinary differential equation is

$$S_{hz} = C_1 \cosh(rz) + C_2 \sinh(rz) \tag{12.49}$$

where C_1 and C_2 are constants.

The equations (12.49), (12.45) and (12.46) lead to

$$U_h = \frac{1}{f}\left[C_2 \cosh(rz) + C_1 \sinh(rz)\right] \tag{12.50}$$

which finally yields the flexibility relationship as

$$\begin{bmatrix} U_{ha} \\ -U_{hb} \end{bmatrix} = \frac{1}{fr} \begin{bmatrix} \cot anh(2rh) & -\cos ech(2rh) \\ -\cos ech(2rh) & \cot anh(2rh) \end{bmatrix} \begin{bmatrix} S_{hza} \\ S_{hzb} \end{bmatrix} \tag{12.51}$$

Since the flexibility relationship for a single layer is obtained, it is easy to get the global flexibility relationship for multiple layers by the use of continuous conditions at the layer interface.

Boundary condition and final solution:

When uniformly distributed shear loading t is applied over a circular area, the boundary conditions in transformed domain in terms of coordinates x, y, z can be expressed as

$$T_{xz} = \frac{1}{4p^{2}}\int_{-\infty}^{+\infty}\int_{-\infty}^{+\infty} it \; e^{i(a\;x+by)}dxdy \tag{12.52}$$

Change the Cartesian coordinate to cylindrical coordinate as

$$\begin{aligned} x &= r\cos q \\ y &= r\sin q \\ a &= r\cos e \\ b &= r\sin e \end{aligned} \tag{12.53}$$

Then equation (12.52) becomes

$$T_{xz} = \frac{i}{4p^{2}}\int_{0}^{+\infty}\int_{0}^{2p} t \quad e^{irr\cos(q-e)}rdrd \quad q \tag{12.54}$$

Making substitution of $j = q - e$ yields

$$T_{xz} = \frac{i}{4p^{2}}\int_{0}^{+\infty}\int_{0}^{2p} t\,e^{irr\cos j}\,rdrd \quad j \tag{12.55}$$

Since it is known that Bessel functions of the first kind can be expressed in integral form [22] as

$$J_n(z) = \frac{1}{i^n p}\int_{0}^{p} e^{iz\cos q}\cos(nq)dq \tag{12.56}$$

Then

$$T_{xz} = \frac{it}{2p}\frac{aJ_1(ra)}{r} \tag{12.57}$$

where a is the radius of the circular loading area.

In x, h, z coordinate system, the boundary condition can be written as

$$T_{xz} = T_{xz}\cos e = \frac{it}{2p}\frac{aJ_1(ra)}{r}\cos e \tag{12.58}$$

$$T_{hz} = T_{xz}\sin e = \frac{it}{2p}\frac{aJ_1(ra)}{r}\sin e \tag{12.59}$$

If the boundary conditions like equations (12.58) and (12.59) are used in equations (12.17) and (12.51), U_z, U_x, S_{zz}, S_{xz} would be multiples of $\cos e$ and U_h, S_{hz} would be multiples of $\sin e$. If we let

$$T_{xz} = T_{xz}^{'}\cos e$$

$$T_{hz} = T_{hz}^{'}\sin e \tag{12.60}$$

Then T_{xz} can be written as

$$T_{xz} = -T_{hz}\sin e + T_{xz}\cos e = -T_{hz}^{'}\sin^2 e + T_{xz}^{'}\cos^2 e \tag{12.61}$$

By inverse transformation

$$t_{xz} = -i\int_{-\infty}^{+\infty}\int_{-\infty}^{+\infty} T_{xz}e^{-i(a\ x+by)}dadb \tag{12.62}$$

Using cylindrical coordinate system as indicated in equation (12.53) and substituting equation (12.61) into equation (12.62) leads to

$$t_{xz} = -i\int_{0}^{+\infty}\int_{0}^{2p}\left\{\left(\frac{T_{xz}^{'}+T_{hz}^{'}}{2}\right)\cos 2e + \left(\frac{T_{xz}^{'}-T_{hz}^{'}}{2}\right)\right\}e^{-irr\cos(q-e)}\, rdrde \tag{12.63}$$

Put $-q+e=j$, then we get

$$1st\ \ term = -i\int_{0}^{+\infty}\int_{0}^{2p}\left(\frac{T_{xz}^{'}+T_{hz}^{'}}{2}\right)(\cos 2q\cos 2j - \sin 2q\sin 2j)e^{-irr\cos j}\, dj\, rdr$$

Since the ‘sine’ part of the above integral is zero and with the use of integral expression of Bessel function of the first order, the 1st term becomes

$$1st\ \ term = 2pi\int_{0}^{+\infty}\left(\frac{T_{xz}^{'}+T_{hz}^{'}}{2}\right)\cos 2qJ_2(rr)rdr$$

Similarly, for 2nd term,

$$2nd\ \ term = -i \int_{-\infty}^{+\infty} \int_{0}^{2p} \left(\frac{T_{xz}^{'} - T_{hz}^{'}}{2} \right) e^{-irr\cos j}\ rdrdj$$

$$= -2pi \int_{0}^{+\infty} \left(\frac{T_{xz}^{'} - T_{hz}^{'}}{2} \right) J_0(rr)rdr$$

Finally, t_{xz} in x, y, z coordinate system can be expressed in term of the solution in x , h , z coordinate system in transformed domain as

$$t_{xz} = 2pi \int_{0}^{+\infty} \left\{ \left(\frac{T_{xz}^{'} + T_{hz}^{'}}{2} \right) \cos 2qJ_2(rr) - \left(\frac{T_{xz}^{'} - T_{hz}^{'}}{2} \right) J_0(rr) \right\} rdr \qquad (12.64)$$

In the same way, s_{zz} can be obtained as

$$s_{zz} = \int_{-\infty}^{+\infty} \int_{-\infty}^{+\infty} S_{zz} e^{-i(ax+by)} da\,db$$

$$= \int_{0}^{+\infty} \int_{0}^{2p} S_{zz}^{'} \cos e e^{-irr\cos(q-e)}\ rdrde \qquad (12.65)$$

$$= 2p \cos q \int_{0}^{+\infty} S_{zz}^{'} J_1(rr)rdr$$

Following the same procedure, the other variables can be obtained as

$$s_{xx} = 2p \int_{0}^{+\infty} \left\{ \left(\frac{3S_{xx}^{'} + S_{hh}^{'} + 2S_{xh}^{'}}{4} \right) \cos qJ_1(rr) + \left(\frac{S_{xx}^{'} - S_{hh}^{'} - 2S_{xh}^{'}}{4} \right) \cos(3q) J_3(rr) \right\} rdr \qquad (12.66)$$

$$s_{yy} = 2p \int_{0}^{+\infty} \left\{ \left(\frac{S_{xx}^{'} + 3S_{hh}^{'} - 2S_{xh}^{'}}{4} \right) \cos qJ_1(rr) + \left(\frac{-S_{xx}^{'} + S_{hh}^{'} + 2S_{xh}^{'}}{4} \right) \cos(3q) J_3(rr) \right\} rdr \qquad (12.67)$$

$$t_{xz} = 2p \int_{0}^{+\infty} \left\{ \left(\frac{T_{xz}^{'} + T_{hz}^{'}}{2} \right) \cos 2qJ_2(rr) - \left(\frac{T_{xz}^{'} - T_{hz}^{'}}{2} \right) J_0(rr) \right\} rdr \qquad (12.68)$$

$$t_{yz} = 2p \int_{0}^{+\infty} \left(\frac{T_{xz}^{'} + T_{hz}^{'}}{2} \right) \sin 2qJ_2(rr)rdr \qquad (12.69)$$

$$\tau_{xy} = 2\pi \int_0^{+\infty} \left\{ \frac{1}{2}\left(\frac{\Sigma'_{xx} - \Sigma'_{\eta\eta}}{2} - \Sigma'_{x\eta} \right) \cos\theta J_1(\rho r) + \frac{1}{2}\left(\frac{\Sigma'_{xx} - \Sigma'_{\eta\eta}}{2} + \Sigma'_{x\eta} \right) \cos(3\theta) J_3(\rho r) \right\} \rho d\rho \quad (12.70)$$

$$u_x = 2\pi \int_0^{+\infty} \left\{ \left(\frac{U'_x + U'_\eta}{2} \right) \cos 2\theta J_2(\rho r) + \left(\frac{U'_x - U'_\eta}{2} \right) J_0(\rho r) \right\} \rho d\rho \quad (12.71)$$

$$u_y = 2\pi \int_0^{+\infty} \left\{ \left(\frac{U'_x + U'_\eta}{2} \right) \sin 2\theta J_2(\rho r) \rho d\rho \right. \quad (12.72)$$

$$u_z = 2\pi \int_0^{+\infty} \{ U'_z \cos\theta J_1(\rho r) \rho d\rho \quad (12.73)$$

12.2 Test Problems

In order to validate the semi-analytical method illustrated in the preceding section, some test problems are analyzed. Stresses generated by the theory in this study were compared to those generated by conventional analytical methods for the same problem.

12.2.1 Stresses under a Uniform Vertical Load: Half Space

Vertical stresses beneath the center of a uniformly and vertically loaded circular area on the surface of a half space were found to be [24]

$$\sigma_z = q\left[1 - \frac{z^3}{(a^2 + z^2)^{1.5}} \right] \quad (12.74)$$

where q is the uniform pressure and z denotes the depth and a is the radius of the area.

For the test problem, the uniform pressure and radius were selected as q = 100psi and a = 0.5 inches respectively; the elastic Young's modulus and Poisson's ratio for the half space were chosen to be E = 100,000psi and v = 0.5 respectively. The vertical stress distribution beneath the loading center can be obtained by analytical solution equation (12.74), while for the semi-analytical finite layer method, the half space is treated as a single layer with a very high value for layer thickness. The results by these two solutions are shown in Figure 12-7. As we can see, the results by the two methods are in good agreement.

12.2.2 Stresses under Uniform Vertical Load: 3-Layered System

The next validation test performed is for a uniform vertical circular surface load on a three-layered system. The vertical load applied at the surface was 100 psi and the radius of loaded area was 1 inch. The first layer was 2.5 inches thick with an elastic modulus value of 200,000 psi and a Poisson's ratio of 0.5. The second layer was also 2.5 inches thick with a Poisson's ratio of 0.5 and elastic modulus of 100,000 psi. The third and final layer was infinitely deep with an elastic modulus value of 5,000 psi and Poisson's ratio 0.5. The normal stress values found by semi-analytical method are on the axis of symmetry below the circular loaded area and at the interfaces between the layers, which are compared with those based on Jones' tables [27]. Once again, the results by semi-analytical finite layer method match almost perfectly with the conventional analytical method as presented in Figure 12-5.

12.2.3 Stresses under Uniform Horizontal Load: Half Space

This test problem is about a uniformly distributed horizontal pressure over a circular area on the surface of an elastic half space. The radius of the loading area is denoted by a, normal stresses and shear stresses along certain coordinate lines (as shown in Figure 12-9) at the horizontal surface $z = a$ are calculated by the semi-analytical finite layer method and compared with those presented by Barber [11]. During the analysis by the semi-analytical method, a single layer with very high value of thickness is used to represent the half space. It can be seen in Figure 12-9 that excellent agreement could be achieved for the two results.

12.2.4 Stresses under Uniform Horizontal Load: 2-Layered System

The last validation test was done on a two-layered system with a uniform horizontal circular surface load. The results used for validation in this case are from R. A. Westman [49]. The two-layered system he analyzed is shown in the Figure 12-10, the thickness of the first layer is represented by h and the second layer is a half space. Elastic Young's modulus and Poisson's ratio for both the upper layer and the half space are denoted by E_1, v_1 and E_2, v_2 respectively. A concentrated surface shear force Q is applied over a circular area with radius a. During the analysis of this problem by the semi-analytical finite layer method, some measures are taken: firstly, the half space of infinite thickness is substituted with a layer of a very high value of thickness; secondly, the concentrated surface shear force Q is divided by the loading area to convert concentrated shear force to uniformly distributed shear force.

The results are parameterized by a load concentration factor *h/a* (ratio of first layer thickness to radius of loaded area) and Young's modulus ratio E_1/E_2 (ratio of Young's modulus of the first layer to that of the half space). Here, only the results for interface shearing stress coefficient $I_{t_{zr}}$ are compared for both methods under certain load concentration factor *h/a* and Young's modulus ratio E_1/E_2. To do that, results for interface shearing stress t_{zr} are first obtained by the semi-analytical method and then corresponding shear stress coefficients are solved according to the following equation

$$t_{zr}(r/a, q, h) = \frac{Q}{a^2}\cos(q) I_{t_{zr}} \tag{12.75}$$

The results presented in Figure 12-10 are for the coordinate line $q = 0$ at the interface. As we can see, the results match well.

12.3 Pavement Delamination Analysis

In the design of pavement, the most commonly used method for rehabilitation of deteriorated pavements is to apply an AC overlay onto them. Before paving a rehabilitation asphalt layer, the top surface of the existing layer is cleaned and a tack coat is applied to bond the new surface being paved and the underlying layer. A strong bonding between layers is critical to dissipate shear stresses into the entire pavement structure. Lack of interface bonding may lead to slippage cracking, delamination and activate distress mechanisms that will rapidly lead to total failure of the pavement. Such failure has usually occurred in the wheel path and in the areas where the vehicles make sharp turns or apply sudden brakes. Typically a slippage crack is crescent shaped [17] as shown in Figure 12-11.

There might be some other reasons for the crescent shaped crack to occur such as [17]: tensile stress in the overlay behind the tire exceeded the tensile strength of the material, causing a crack behind the braking tire; compressive strength of the overlay was exceeded, causing shoving in front of the braking tire, etc. In this study, it is assumed that the delamination is caused only by inadequate bonding strength so that shear stress produced by traffic load exceeds the shear strength of the layer interface.

Two measures can be taken to prevent delamination: (1) reducing the shear stress at the interface by increasing the overlay thickness; (2) increasing the interface shear strength. The first solution is less economical than the second one. For both of these considerations, it is necessary to determine the magnitude of shear stress at the interface for a certain pavement structure subjected to certain loading condition. The semi-analytical finite layer analysis can be a useful tool. The semi-analytical finite layer method as illustrated in preceding sections are used to examine the shear stress distribution at the interface in a multi-layered pavement system subjected to vertical and/or horizontal loadings at the surface.

The pavement system we consider consists of 5 layers and elastic properties for each layer are presented in Figure 12-12. The load applied to the surface is a dual tire load 4500 lb each with center to center distance 12". If the tire pressure is 100 psi each, the contact radius of each tire is 3.785". Suppose that the two tires were put on the y-axis with the center of the first load stationed at point (0, 0) and that of second load stationed at the point (0, 12). The two tires moving in +x direction results in +x direction surface shear load on the pavement.

In the 1986 AASHTO Guide for Pavement Design [1], there is some information about the braking effect of a vehicle on the pavement including the coefficient of friction. It is shown in Table 12-1 that the coefficient of friction varies with the speed of the vehicle. The maximum coefficient of friction is 0.68 at the speed of 30 mph. If the coefficient of friction at certain speed is available, the horizontal pressure applied to the pavement surface can be obtained by multiplying the coefficient of friction with the uniform pressure on one tire.

In this study, some factors affecting the interface shear stress, such as overlay thickness, loading combination and material properties are discussed and some results are presented as follows.

12.3.1 Effect of Various Magnitude of Horizontal Load and Constant Vertical Load on Interlayer Shear Stress

On the surface of the pavement structure shown in Figure 12-12, let the 100 psi vertical load held constant for each tire while six kinds of horizontal shear loads assigned to each tire: 0, 20, 30, 40, 50, and 68 psi. Each case corresponds to a certain vehicle speed. Distribution of shear stress t_{xz} at the interface (z = 1.5") along y-axis is presented in Figure 12-13, where distance ratio denotes the ratio of distance from the origin to the radius of contact area.

If only 100 psi vertical pressure with no horizontal pressure is assigned to each tire, then no shear stress t_{xz} will occur at the points on y-axis. The greater the applied horizontal load, the greater the shear stress. The shear stress increases linearly with the applied horizontal load. It is shown that along y-axis the maximum shear stress occurs at the center of each tire.

The distribution of shear stress t_{xz} along x-axis at the interface (z = 1.5") is shown in Figure 12-14. If only vertical load 100 psi is assigned to each tire, maximum t_{xz} occurs at the two edges of each tire. The two peak shear stresses are equal in value but in opposite direction. If +x direction horizontal shear load is applied, the shear stress in the +x part will increase while shear stress in the -x part will decrease due to neutralization. In the case of 68 psi horizontal pressure plus 100 psi vertical pressure, the maximum shear stress t_{xz} is 58 psi.

The shear stress resultants due to t_{xz}, t_{yz} at the interface under loading combination of 68 psi horizontal pressure plus 100 psi vertical pressure are also calculated and their absolute values (without considering the direction) are presented in three-dimensional graph in Figure 12-15.

Comparing Figure 12-13 and Figure 12-14, we can see that maximum interlayer shear stress t_{xz} along x-axis is much higher than that along y-axis. The maximum shear stress resultants occur within the region close to the tire edges with coordinates (3.785, 0) and (3.785, 12.0). Therefore, the maximum shear stress resultant along x-axis should be very close to that of the whole interface. In later analysis, emphasis is focused on the shear stress distribution along x-axis at certain interface.

12.3.2 Effect of Overlay Thickness on Interlayer Shear Stress: Only Horizontal load Applied

Similar pavement structure in Figure 12-12 is used except with some changes about the thickness of the first layer and load combination. Only apply 68 psi horizontal pressure to each tire and observe the variation of shear stress at the first interface under various overlay thickness 1.0", 1.5", 2.0", 2.5", 3.0", 3.5". The shear stress resultant t versus distance ratio *d/a* is shown in Figure 12-16, where *d* is the distance from the origin to a point on x axis, *a* is the radius of the load area. It is shown that when the layer is thinner, say, *d=1.0"* and *d=1.5"*, the maximum shear stress occurs at the point right below the center of the circular load. As the thickness increases the locus of the maximum t will move along x-axis with distance to the center increasing. It is obvious that the peak shear stress resultant decreases as the thickness increases. For 1" thickness, $t_{\max}$ is about 42% of the applied stress, for 3.5" thickness, $t_{\max}$ is less than 10% of the applied stress. A conclusion can be drawn here that surface shear stress can affect only the upper shallow part of the pavement system.

12.3.3 Effect of Overlay Thickness on Interlayer Shear Stress: Both Vertical and Horizontal Loadings Applied

Set the thickness of the first layer of the pavement structure in Figure 12-12 with various values: 1.0", 1.5", 2.0", 2.5", 3.0" and 3.5". Each tire is applying normal stress 100 psi and shear stress 68psi over the pavement surface. Variation of shear stress resultant t along x-axis at the first interface is presented in Figure 12-17. $t_{\max}$ is located exactly at the edge of the tire for thinner layer, say *d=1.0", 1.5"*. $t_{\max}$ decreases while the thickness of the first layer increases and the locus of $t_{\max}$ moves a little outside, but not far from the tire edge, as indicated in Figure 12-17. Beyond certain depth, 3.5" for this case, shear stress is generated mainly by vertical load. Vertical load has a deeper affecting zone than horizontal load.

12.3.4 Effect of Anisotropic Properties of Layer Material on Shear Stress at the Interface

Due to the layered structure of pavement, we can describe each layer with the cross-isotropic elastic model, which is characterized by 5 independent elastic constants.

E_h = modulus of elasticity in horizontal direction

E_v = modulus of elasticity in vertical direction

n_h = Poisson's ratio, effect of horizontal strain on complementary horizontal strain

n_{hv} = Poisson's ratio, effect of horizontal strain on vertical strain

n_{vh} = Poisson's ratio, effect of vertical strain on horizontal strain

G_v = shear modulus

$$\frac{E_h}{E_v} = \frac{n_{hv}}{n_{vh}}$$

We still use the pavement profile similar to that in Figure 12-12 but will change the material properties of the first and second layer to see any difference of shear stress at the first interface.

Anisotropy in the first layer only

We keep the material properties of 2nd, 3rd, 4th, and 5th layer unchanged and assign a set of anisotropic properties to the first layer, which is as follows.

E_h/E_v	G_v/E_v	E_h (psi)	E_v (psi)	G_v (psi)	n_h	n_{hv}	n_{vh}
0.5	0.4	484500	969000	387600	0.4	0.2	0.4

Comparisons between anisotropic case as list above and isotropic case as in Figure 12-12 under various load combinations are shown in Figure 12-18 through Figure 12-20. In Figure 12-18, under vertical pressure 100 psi for both tires, the anisotropic material will generate a shear stress less than that by isotropic material. Figure 12-19 shows the comparison under 50 psi horizontal pressure for both tires, anisotropic material gives higher shear stress, especially in the range $-1.0 \le r/a \le 1.0$. Under load combination of 100 psi vertical pressure and 50 psi horizontal pressure, however, the peak t_{xz} values for two cases do not vary much, as shown in Figure 12-20.

Anisotropy in the second layer only

Assign anisotropic properties to the second layer as follows and keep isotropic properties of other layers unchanged.

E_h/E_v	G_v/E_v	E_h (psi)	E_v (psi)	G_v (psi)	n_h	n_{hv}	n_{vh}
0.5	0.4	312000	624000	249600	0.4	0.2	0.4

Comparisons are shown in the Figure 12-21 through Figure 12-23. There are almost no differences for t_{xz} at the first interface for both cases under 100 psi vertical pressure for both tires. Under 50 psi horizontal pressure, difference exists in the range $-1.0 \le r/a \le 1.0$. However, anisotropic material will generate less shear stress, which is contrary to the result of anisotropic case of first layer. Under the load combination 100 psi vertical pressure and 50 psi horizontal pressure, there is not much difference in the peak t_{xz} values for the two cases as shown in Figure 12-23.

Anisotropy in both the first layer and the second layer

When we change the material properties of both the first and second layer, there is not much variation on the maximum shear stress distribution at the first interface as shown in Figure 12-24.

12.3.5 Effect of Layer Modulus on Maximum Interlayer Shear Stress

Because asphalt concrete modulus is temperature and frequency dependent, we assume the modulus of both the first and second layer in Figure 12-12 varying between 100,000 psi and 1000,000 psi. The corresponding maximum interlayer shear stresses are listed in Table 12-2.

It is observed that if the first layer and the second layer are composed of same material and have same modulus at any condition, then maximum t_{xz} increases as modulus increases, as presented in Figure 12-25. This may apply to the case: when temperature decreases or frequency increases, maximum t_{xz} increases and vise versa.

If the second layer is of comparatively higher stiffness with modulus varying between 500,000 psi and 1,000,000 psi, then there is not much great difference on maximum t_{xz} whether the first layer is comparatively weaker (100,000 psi) or stronger (1,000,000 psi). The maximum t_{xz} is mainly controlled by the thickness of the first layer.

If the second layer is of low stiffness (100,000 ~ 300,000psi) and the stiffness of the first layer is greater or higher than the second one, then the higher the stiffness of the first layer, the lower the maximum t_{xz}, as shown in Figure 12-26. It indicates that a weaker underlay can help dissipate shear stress to some extent.

In the case of both upper layers are of high stiffness, it is most possible to generate maximum t_{xz}. In the case of a layer with very high stiffness overlay a layer with low stiffness, comparatively smaller maximum t_{xz} will occur.

12.4 Summary

A semi-analytical method has been presented which may be used to obtain solutions to the problem of a circular vertical and/or horizontal loading applied to the surface of a multi-layered system. Corresponding software package has been developed and user's manual is attached in Appendix G.

The software is used to analyze the delamination problem in layered pavements. Parameter study has been performed to check the maximum shear stress occurred at the layer. Through the analyses in this study, we can see that higher loading leads to higher maximum interface shear stress and increasing overlay thickness is an effective way to reduce maximum interface shear stress. The maximum interface shear stress can be approximately found at the tire edges for a vehicle applying both normal and shear stresses to the pavement surface. If the asphalt concrete is treated as an anisotropic material, the resulting maximum shear stress at the interface doesn't differ much with the results obtained by treating asphalt concrete as an isotropic material. Temperature and loading frequency have some effect on the maximum shear stress by affecting the layer modulus.

After the maximum interface shear stress is available, it can be used to compare with the bond strength obtained through simple direct shearing testing, so that appropriate interface binder can be chosen.

Table 12-1 Braking Effect and Force Transferred to the Pavement due to Skid Resistance [1]

Vehicle Speed (mph)	Coefficient of Friction (f)[8]		Braking Distance $D = V^2/(30f)$ (ft)		Braking Time $t = 1.3636*D/V$ (Sec)		Deceleration $a = -1.075*V^2/D$ (ft/sec/sec)	
	Dry Pavement	Wet Pavement	Dry Pavement	Wet Pavement	Dry Pavement	Wet Pavement	Dry Pavement	Wet Pavement
20	0.66	0.4	20	33	1.364	2.25	21.5	13.04
25	0.675	0.38	31	55	1.691	3	21.7	12.2
30	0.68	0.35	44	86	2	3.91	22	11.25
35	0.675	0.34	60	127	2.34	4.95	21.9	10.37
40	0.66	0.32	81	167	2.76	5.69	21.2	10.3
45	0.64	0.31	105	218	3.182	6.61	20.7	9.99
50	0.62	0.30	134	278	3.65	7.58	20.1	9.67
55	0.60	0.30	168	336	4.16	8.33	19.37	9.68
60	0.58	0.29	207	414	4.7	9.41	18.7	9.35
65	0.56	0.29	251	486	5.26	10.2	18.1	9.35
70	0.54	0.28	302	583	5.88	11.4	17.5	9.04

[8] Note: Horizontal Force Transferred from Wheel to the Pavement on Applying Brakes.
H = f * Weight On One Wheel

Table 12-2 Maximum shear stress produced by various moduli of the first and second layers

E1(psi) / E2 (psi)	1e5	2e5	3e5	4e5	5e5	6e5	7e5	8e5	9e5	1e6
1e5	52.548	48.255	44.728	41.887	39.545	37.570	35.871	34.387	33.074	31.900
2e5	56.711	55.411	53.490	51.577	49.804	48.188	46.720	45.382	44.157	43.031
3e5	57.762	58.012	57.196	56.050	54.822	53.606	52.437	51.327	50.297	49.291
4e5	58.002	59.101	59.017	58.444	57.661	56.791	55.897	55.008	54.140	53.300
5e5	57.968	59.550	59.962	59.814	59.381	58.799	58.143	57.452	56.749	56.050
6e5	57.831	59.694	60.446	60.616	60.460	60.115	59.661	59.142	58.588	58.016
7e5	57.659	59.683	60.673	61.082	61.145	60.995	60.711	60.342	59.919	59.462
8e5	57.479	59.591	60.747	61.338	61.576	61.587	61.447	61.207	60.898	60.544
9e5	57.302	59.456	60.729	61.459	61.837	61.981	61.963	61.834	61.627	61.363
1e6	57.134	59.299	60.654	61.491	61.982	62.236	62.323	62.29	62.171	61.998

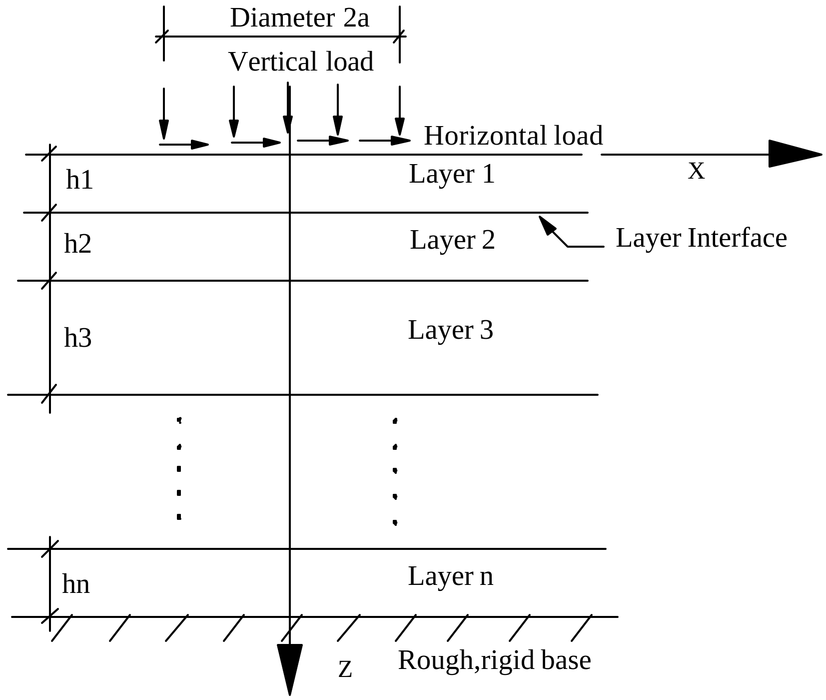

Figure 12-1 Model of layered pavement system

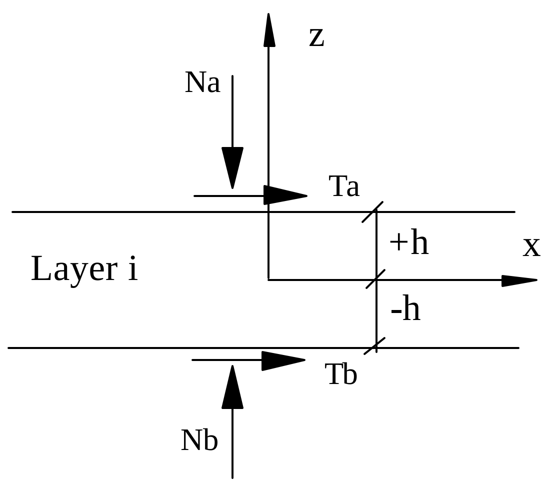

Figure 12-2 Illustration of normal stress and shear stress at the interface

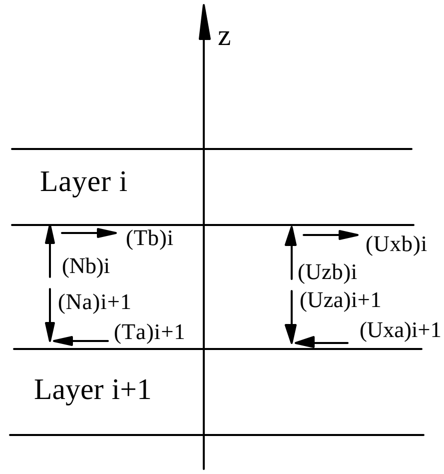

Figure 12-3 Continuity condition at the interface

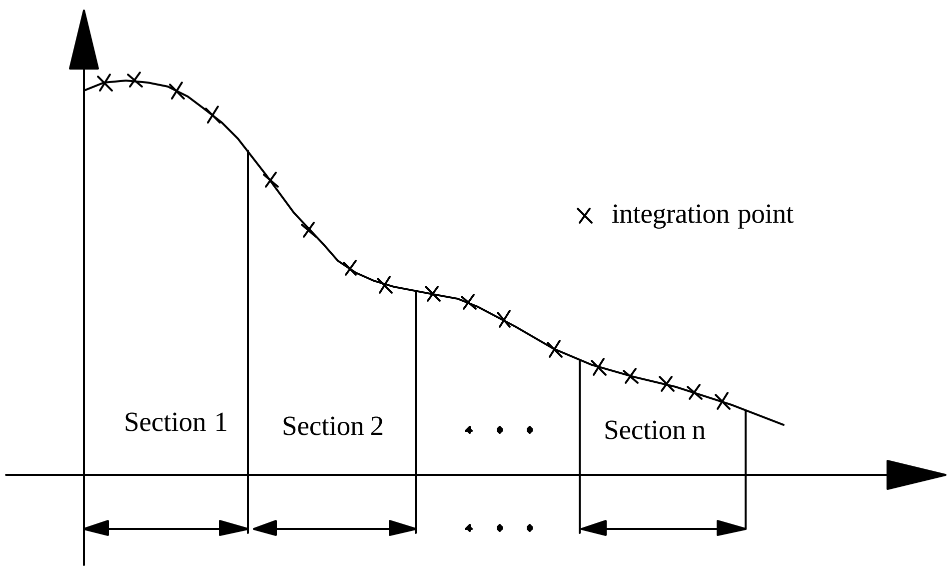

Figure 12-4 Integration Scheme

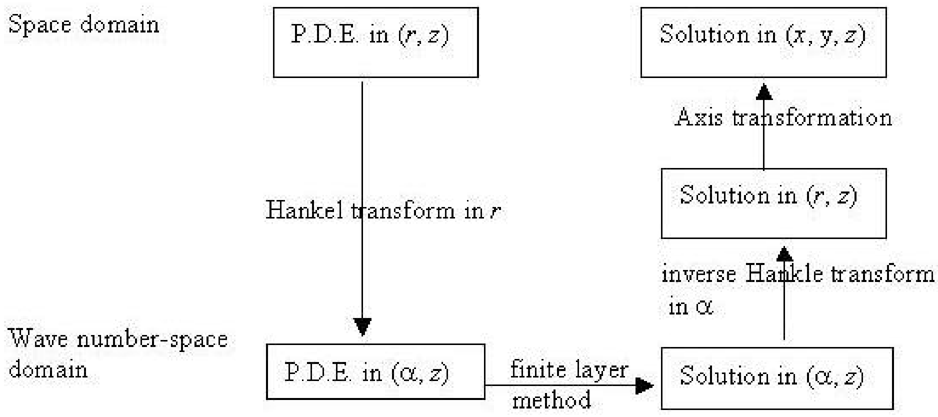

Figure 12-5 Flow chart for solution procedure

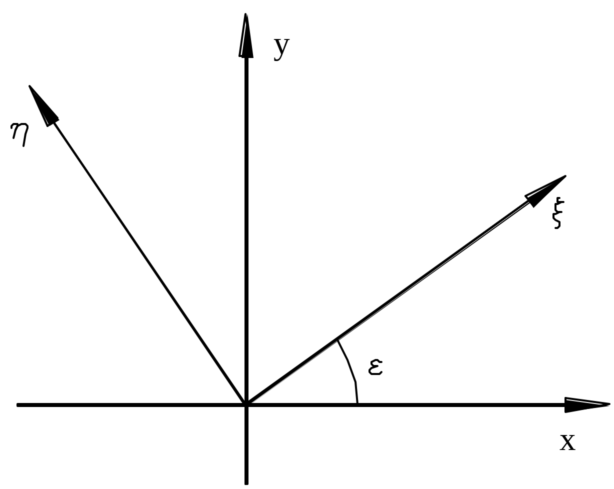

Figure 12-6 Axis transformation

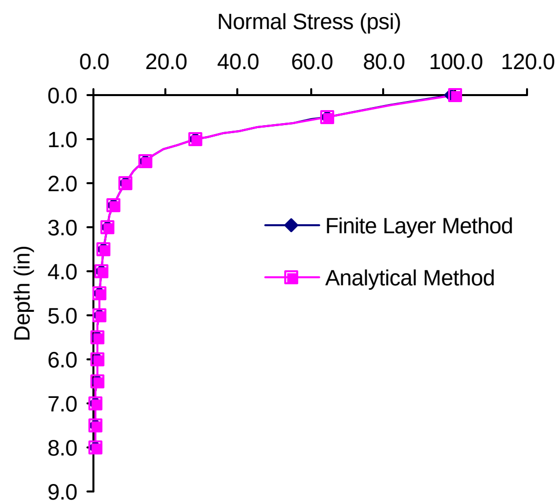

Figure 12-7 Normal stress distributions along the centerline for single layer

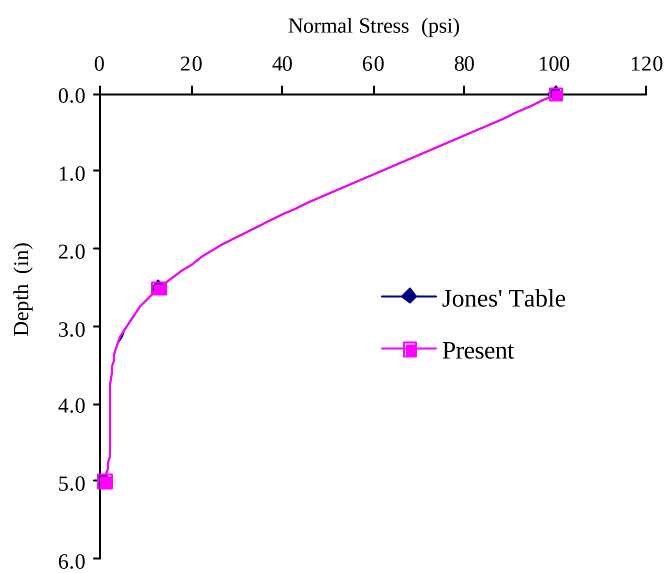

Figure 12-8 Normal stress distributions along the centerline for a three-layered system

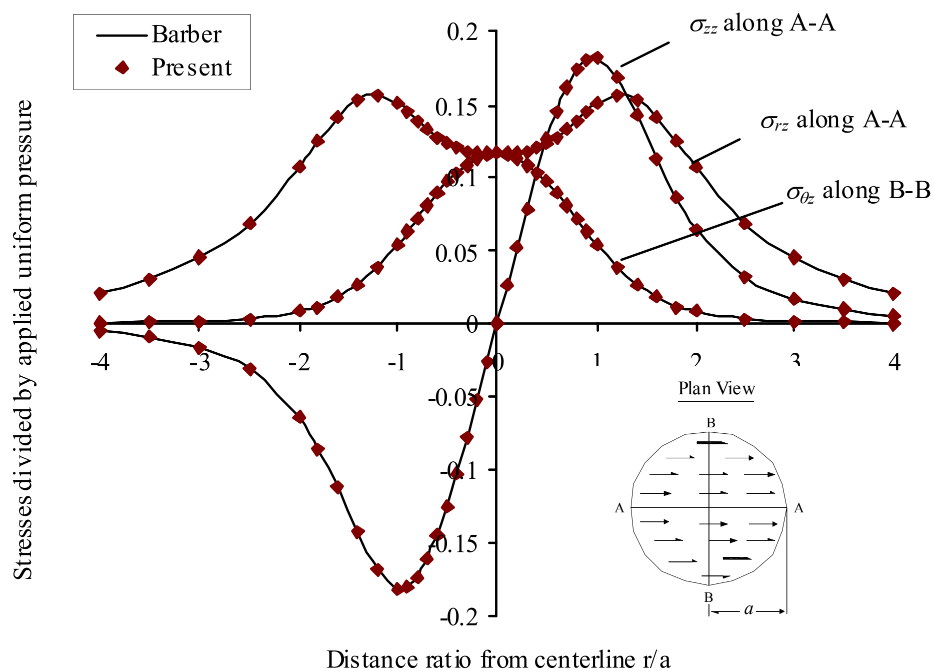

Figure 12-9 Distribution of stresses at surface *z/a* = 1 for a half space

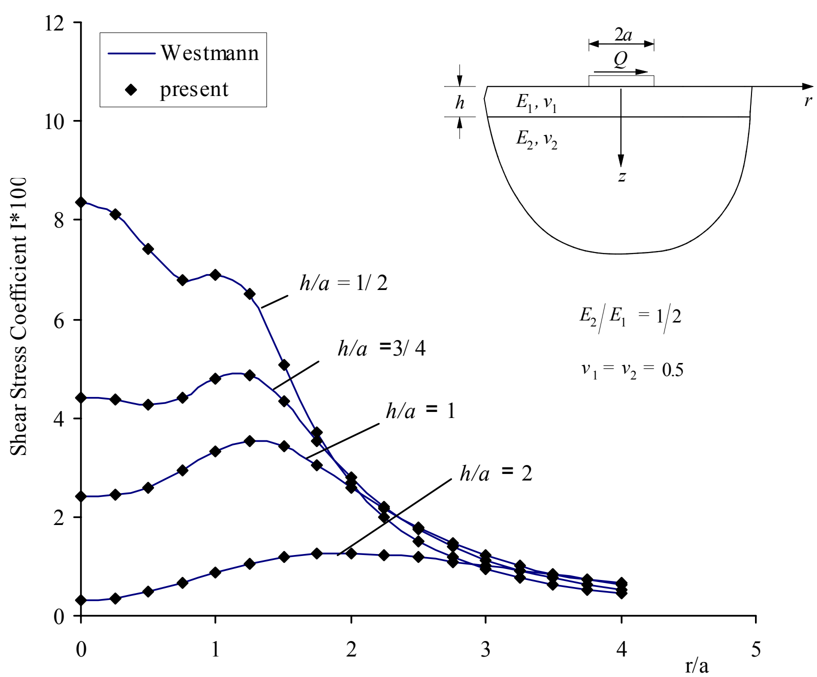

Figure 12-10 Interface shear stress for a two-layered system subjected to circular shear load at surface

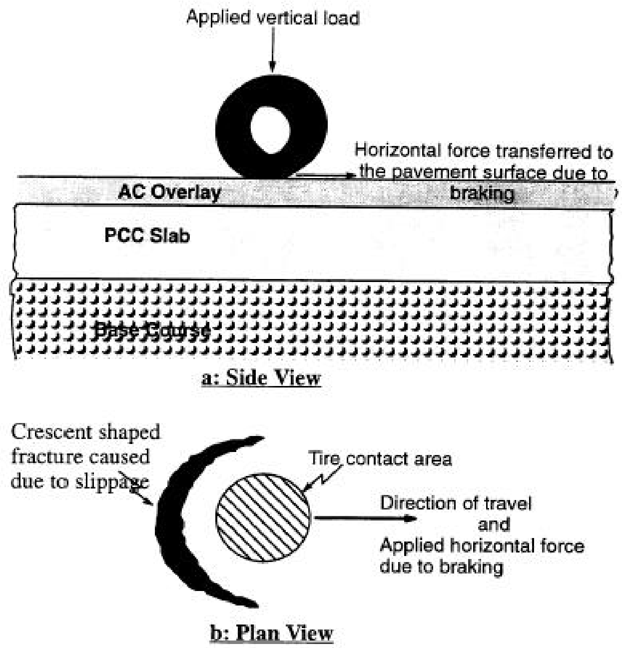

Figure 12-11 Typical slippage failure [17, 32]

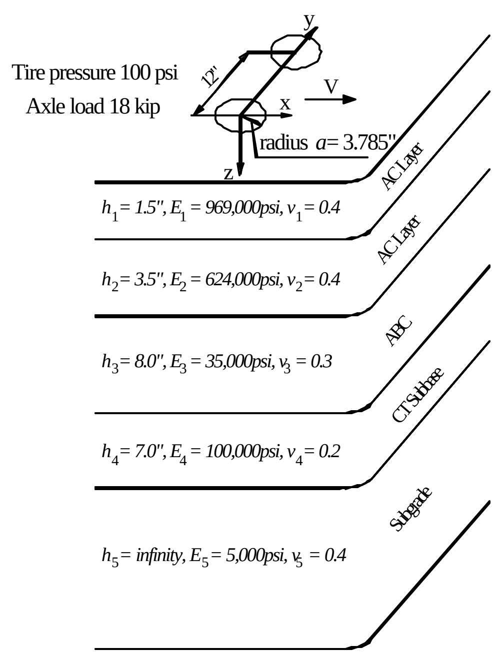

Figure 12-12 Pavement model used in the analysis

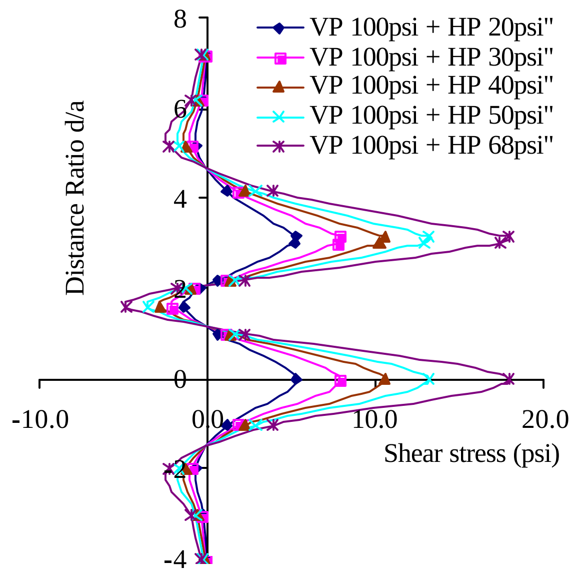

Figure 12-13 Distribution of shear stress t_{xz} at the interface (z=1.5") along y-axis (VP: vertical pressure, HP: horizontal pressure)

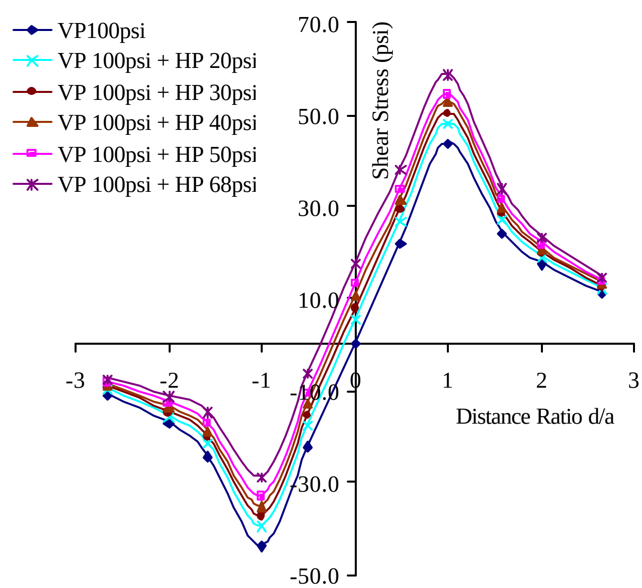

Figure 12-14 Distribution of shear stress t_{xz} at the interface (z=1.5") along x-axis (VP: vertical pressure, HP: horizontal pressure)

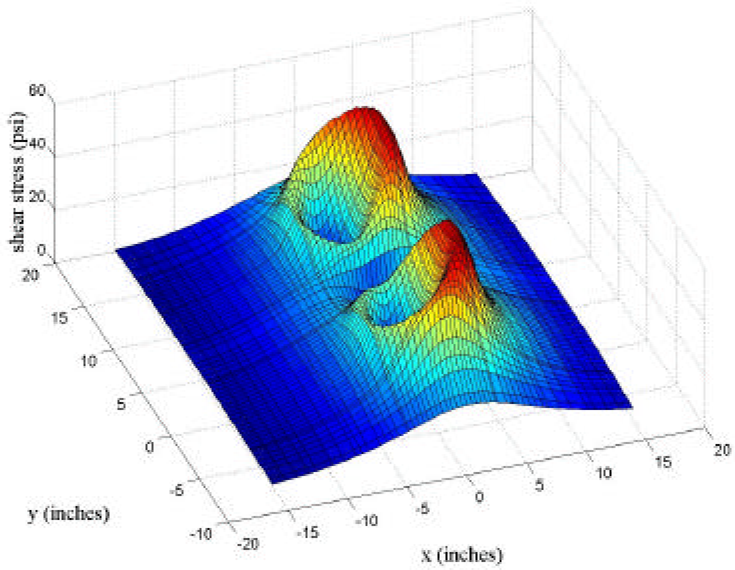

Figure 12-15 3-D presentation of shear stress resultant at the interface (z=1.5²)

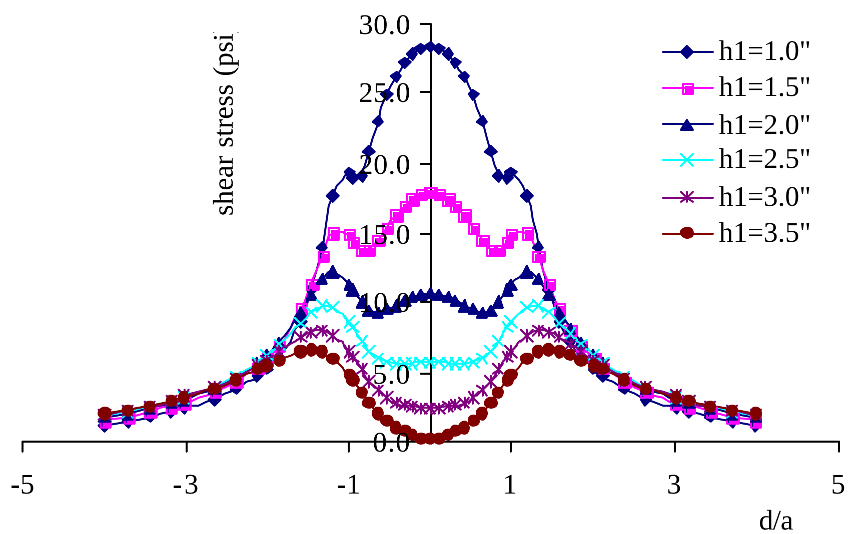

Figure 12-16 Distribution of shear stress resultant at the interface (z = 1.5²) for various thickness of the overlay and only 68psi horizontal load being applied

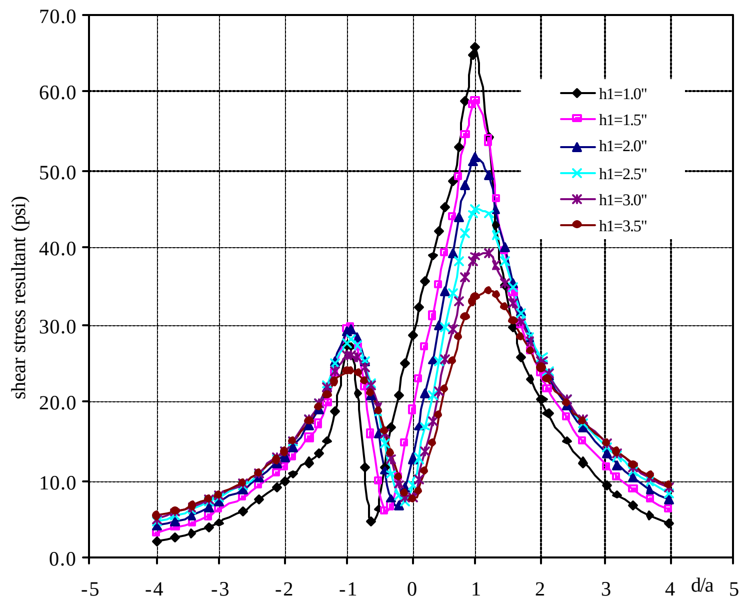

Figure 12-17 Distribution of shear stress at the interface (z = 1.5²) for various thickness of the first layer with 100psi vertical pressure and 68psi horizontal pressure being applied

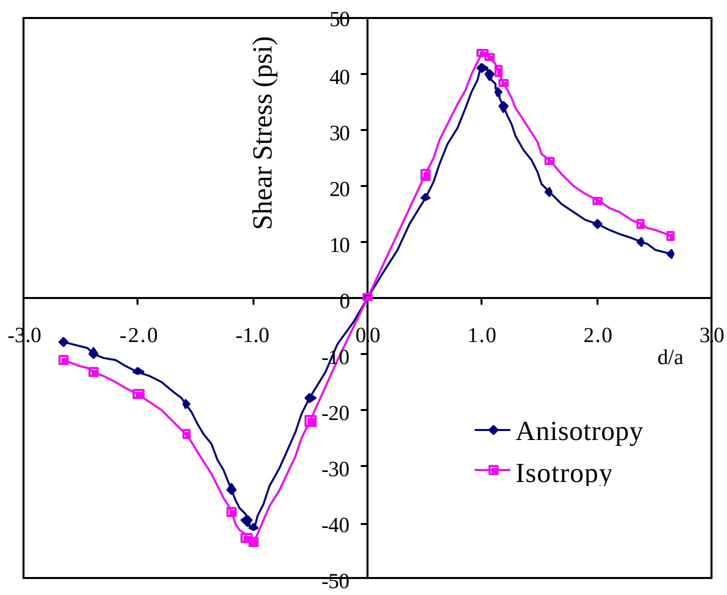

Figure 12-18 Comparison of shear stress at the first interface between isotropic and anisotropic cases of first layer under 100psi vertical pressure of both tires

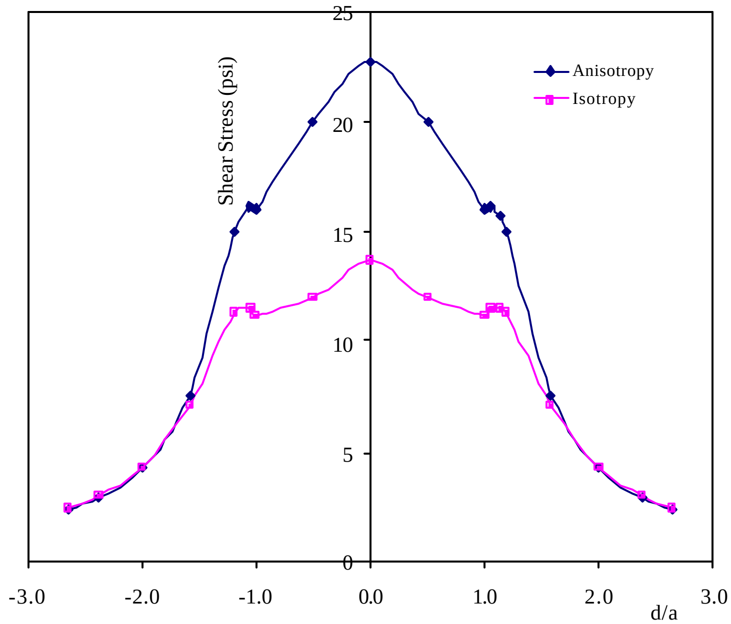

Figure 12-19 Comparison of shear stress at the first interface between isotropic and anisotropic cases of first layer under 50psi horizontal pressure of both tires

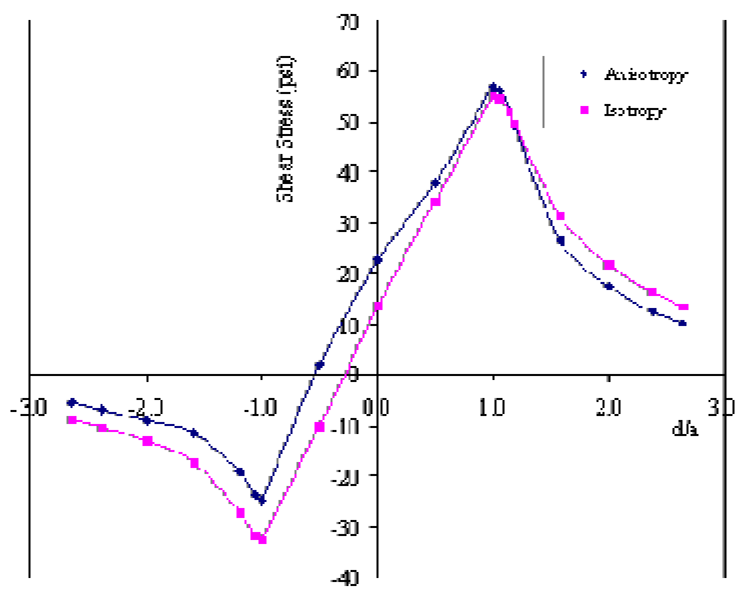

Figure 12-20 Comparison of shear stress at the first interface between isotropic and anisotropic cases of first layer under 100psi vertical pressure and 50psi horizontal pressure of both tires

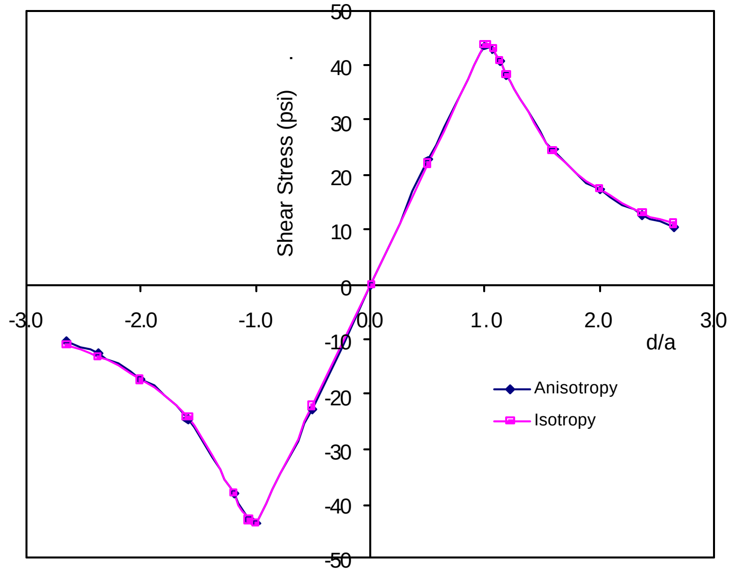

Figure 12-21 Comparison of shear stress at the first interface between isotropic and anisotropic cases of second layer under 100psi vertical pressure of both tires

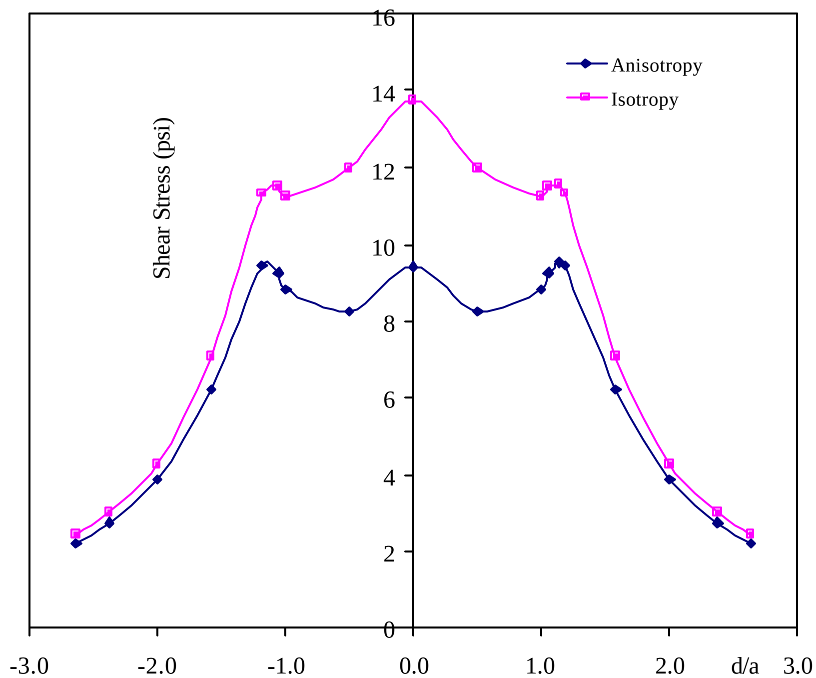

Figure 12-22 Comparison of shear stress at the first interface between isotropic and anisotropic cases of second layer under 50psi horizontal pressure of both tires

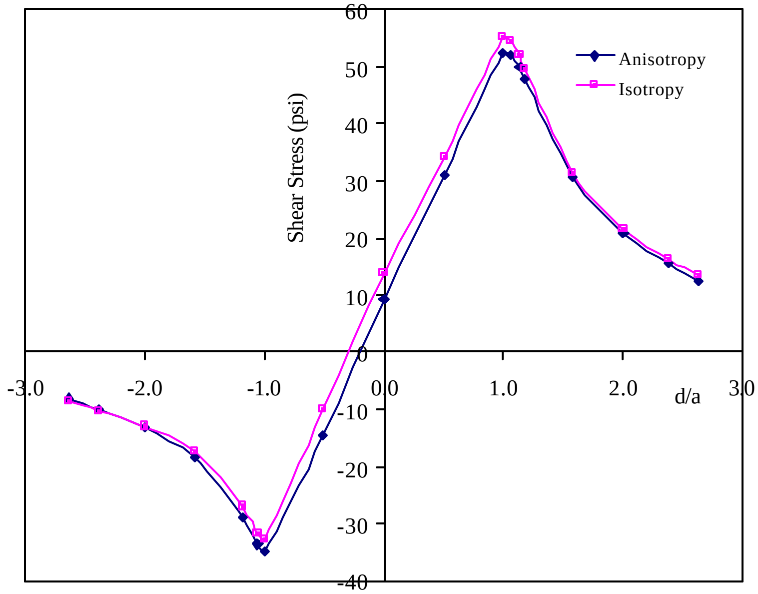

Figure 12-23 Comparison of shear stress at the first interface between isotropic and anisotropic cases of second layer under 100psi vertical pressure and 50psi horizontal pressure of both tires

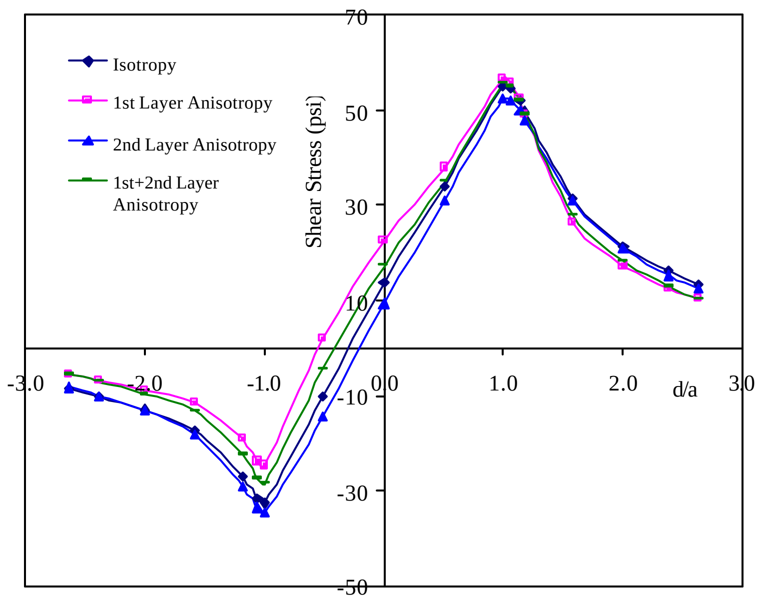

Figure 12-24 Comparison of shear stress at the first interface among 4 cases under 100psi vertical pressure and 50psi horizontal pressure of both tires

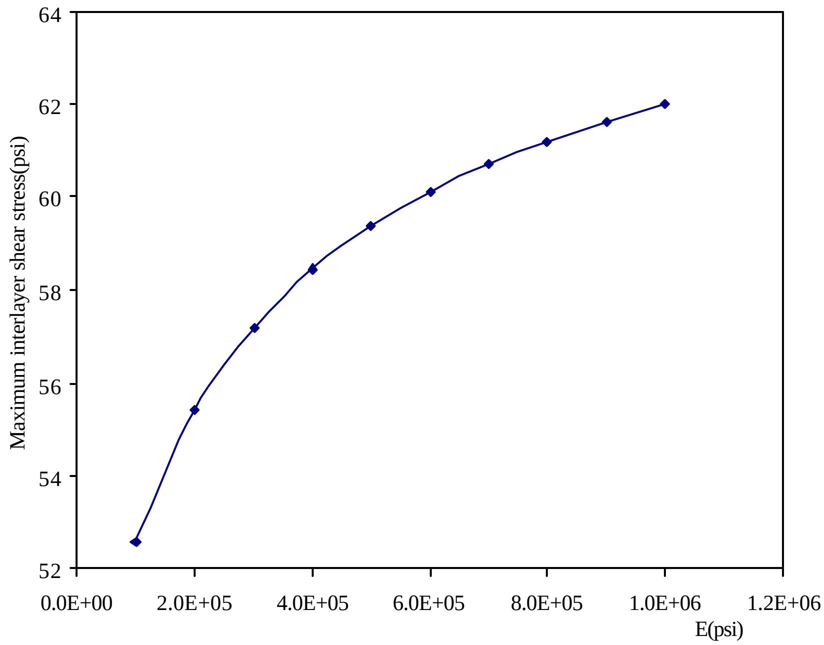

Figure 12-25 Relationship between maximum shear stress and modulus when upper two layers are of same modulus

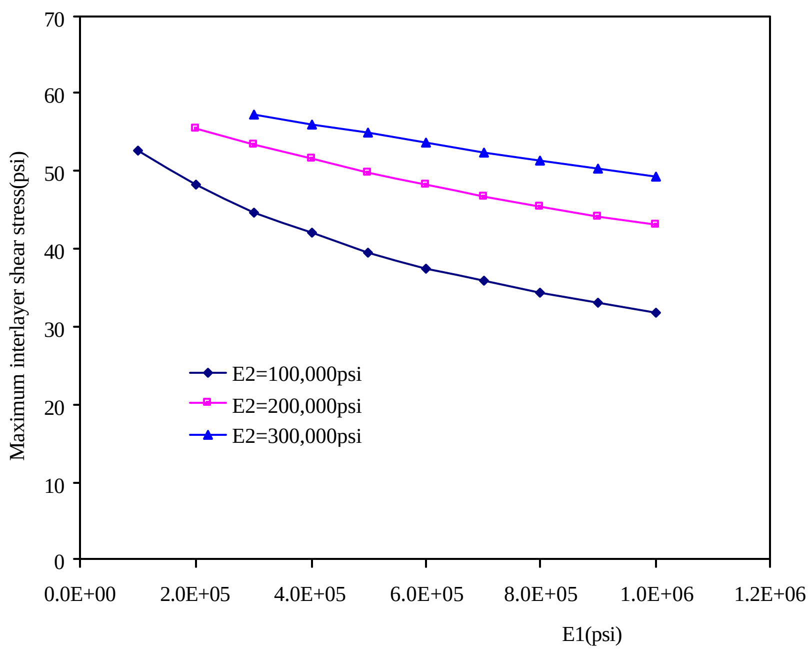

Figure 12-26 Variation of maximum shear stress with modulus of first layer higher than second layer

13 References

1. American Association of State Highway and Transportation Officials, “AASHTO Guide for Design of Pavement Structures,” 1986.

2. American Association of State Highway and Transportation Officials, “AASHTO Guide for Design of Pavement Structures,” pp. II-23, 1993.

3. American Association of State Highway and Transportation Officials, “Standard Specification for Performance Graded Asphalt Binder,” *AASHTO Designation MP1*, 1996.

4. American Association of State Highway and Transportation Officials, “Standard Method for Preparing and Determining the Density of Hot Mix Asphalt (HMA) Specimens by Means of the SHRP Gyratory Compactor,” *AASHTO Designation TP4*, 1996.

5. American Association of State Highway and Transportation Officials, “Standard Test Method for Determining the Rheological Properties of Asphalt Binder Using a Dynamic Shear Rheometer (DSR),” *AASHTO Designation TP5*, 1996.

6. American Association of State Highway and Transportation Officials, “Standard Test Method for Determining the Permanent Deformation and Fatigue Cracking Characteristics of Hot Mix Asphalt using a Simple Shear Test Device,” *AASHTO Designation TP7*, 1996.

7. Ameri-Gaznon, M., and Little, D., “Octahedral Shear Stress Analyses on an ACP Overlay on a Rigid Base,” *Proceedings of the Association of Asphalt Paving Technologists*, vol. 59, pp. 443-479, 1990.

8. Arellano, D., and Thompson, M. R., “Stabilized Base Properties (Strength, Modulus, Fatigue) for Mechanistic-based Airport Pavement Design,” *Technical Research Report,* University of Illinois at Urbana-Champaign, February 1998.

9. Asphalt Institute, “Asphalt in Pavement Maintenance,” *Manual Series No. 16 (MS-16),* Third Edition, 1996.

10. Banerjee, P. K., and Butterfield, R., "Boundary Elements Methods in Engineering," *McGraw Hill*, London, 1981.

11. Barber, E. S., "Shear Loads on Pavements," *Public Roads*, vol. 32, no. 6, pp. 141-144, 1963.

12. Bonnaure, F., Gavois, A., and Udron, J., "A New Method for Predicting the Fatigue Life of Bituminous Mixes," *Proceedings of the Association of Asphalt Paving Technologists,* vol. 49, pp. 499-529, 1980.

13. Booker, J. R., and Small, J. S., "Finite Layer Analysis of Layered Pavement subjected to Horizontal Loading," *Proceedings of 6th International Conf. Num. Meth., Geomechanics,* Innsbruck, Austria, 1988.

14. Burmister, D. M., "The General Theory of Stresses and Displacements in Layered Systems," *Journal of Applied Physics*, vol. 16, pp. 89-94, pp. 126-127, pp. 296-302, February 1945.

15. Cebon, D., "Handbook of Vehicle-Road Interaction," Smets and Zeitlinger.

16. Cheung, Y. K., and Fan, S. C., "Analysis of Pavements and Layered Foundations by the Finite Layer Method," *Third International Conference on Numerical Methods in Geomechanics,* Aachen, 3, pp. 1129-1135, 1979.

17. Epps, J. A., and Button, J. W., "The Slippage Question on Airport Pavements," Texas Transportation Institute, *Interim Report,* RF3424-2.

18. Forsythe, G. E., and Wasow, W. R., "Finite Difference Methods for Partial Differential Equations," John Wiley and Sons, Inc, New York, 1960.

19. Fox, L., "Computations of Traffic Stresses in a Simple Road Structure," *Proc. 2nd Int. Conf. Soil Mech. Found. Eng.,* 2, pp. 236-246, 1948.

20. Gerrard, C. M., "Stresses and Displacement in Layered Cross-Anisotropic Elastic Systems," *Proc. 5th Aust-NZ Conf. Soil. Mech. Found. Eng.*, pp. 205, 1967.

21. Hachiya, Y., and Sato, K., “Effect of Tack Coat on Bonding Characteristics at Interface between Asphalt Concrete Layers,” *Proceedings of 8th International Conference on Asphalt Pavements,* vol. 1, pp. 349-362, 1997.

22. “Handbook of Mathematical Functions,” Dover Publications, Inc., New York.

23. Harris, B. M., and Stuart, K. D., “Analysis of Mineral Fillers and Mastics used in Stone Matrix,” *Proceedings of the Association of Asphalt Paving Technologists,* vol. 64, pp. 54-95, 1995.

24. Huang, Y. H., “Pavement Analysis and Design,” Pearson Prentice Hall, second edition, 2004.

25. Ishai, I., and Livneh, M., “Functional and Structural Role of Prime Coat in Asphalt Pavement Structures,” *Proceedings of the Association of Asphalt Paving Technologists*, vol. 53, pp. 98-118, 1984.

26. Itasca Consulting Group, Inc. “FLAC, Fast Lagrangian Analysis of Continua, User’s Guide,” 1999.

27. Jones, A., “Tables of Stress in Three Layer Elastic Systems,” *Highway Research Board*, bulletin 342, pp. 176-214, 1962.

28. Kummer, H. W., and Meyer, W. E., “Tentative Skid-Resistance Requirements for Main Rural Highways,” *NCHRP Report 37,* Highway Research Board, 1967.

29. Marti, J., and Cundall, P. A., “Mixed Discretization Procedure for Accurate Solution of Plasticity Problems,” *Int. J. Num. Methods and Anal. Methods in Geomech.*, vol. 6, pp. 129-139, 1982.

30. Metcalf, J. B., “Accelerated Pavement Testing, a Brief Review Directed Towards Asphalt Interests,” *Proceedings of the Association of Asphalt Paving Technologists*, vol. 67, pp. 553-572, 1998.

31. Mohammad, L. N., Raqib, M. A., and Huang, B., “Influence of Asphalt Tack Coat Materials on Interface Shear Strength,” *Transportation Research Record,* no 1789, pp. 56-65, 2002.

32. Mukhtar, M. T., and Dempsey, B. J., "Interlayer Stress Absorbing Composite (ISAC) for Mitigating Reflection Cracking in Asphalt Concrete Overlays," *Final Report Project IHR-533,* Illinois Cooperative Highway Research Program, June, 1996.

33. Paul, H. R., and Scherocman, J. A., "Friction Testing of Tack Coat Surfaces," *Transportation Research Record,* no. 1616, pp. 6-12, 1998.

34. Scott, R. F., "Principles of Soil Mechanics," Addison-Wesley, 1963.

35. Shahin, M. Y., Kirchner, K., Blackmon, E.W., and Tomita, H., "Effect of Layer Slippage on Performance of Asphalt-Concrete Pavements," *Transportation Research Record,* no. 1095, pp. 79-85, 1986.

36. "SHRP Superpave Binder Selection Program – SHRPBIND," version 2.1, *Federal Highway Administration,* Pavement Performance Division, McLean, Virginia, 1985.

37. "SHRP-A-415 Permanent Deformation of Asphalt Aggregate Mixes," *Strategic Highway Research Program,* National Research Council, Washington DC, 1994.

38. Sholar, G. A., Page, G. C., Musselman, J. A., Upshaw, P. B., Moseley, H. L., "Preliminary Investigation of a Test Method to Evaluate Bond Strength of Bituminous Tack Coats," *Proceedings of the Association of Asphalt Paving Technologists,* Preprints, pp. 107-137, 2004.

39. Small, J. C., and Booker, J. R., "Finite Layer Analysis of Layered Elastic Materials Using a Flexibility Approach. Part 1 – Strip Loadings," *International Journal for Numerical Methods in Engineering,* vol. 20, pp. 1025-1037, 1984.

40. Small, J. C., and Booker, J. R., "Finite Layer Analysis of Layered Elastic Materials Using a Flexibility Approach. Part 2 – Circular and Rectangular Loadings," *International Journal for Numerical Methods in Engineering,* vol. 23, pp. 959-978, 1986.

41. Subei, N. Saxena, S. K, Mohammadi, J., "A BEM-FEM Approach for Analysis of Distresses in Pavement," *Int. J. Num. And Anal. Methods in Geomech.,* vol. 15, pp. 103-119, 1991.

42. Tayebali, A. A., Fischer, W. K., Huang, Y. X., and Kulkarni, M. B., "Effect of Percentage Baghouse Fines on the Amount and Type of Anti-Stripping Agent Required to Control Moisture Sensitivity," *Final Report*, North Carolina Department of Transportation, June 2003.

43. Tayebali, A. A., Kulkarni, M. B., and Waller, H. F., "Delamination and Shoving of Asphalt Concrete Layers Containing Baghouse Fines," *North Carolina Department of Transportation Project 1999-03,* FHWA/NC/2002-011, May 2000.

44. Tham, L. G., and Cheung, Y. K., "Infinite Rigid Pavement on Layered Foundation," *Proc. Eighth Canadian Cong. App. Mech.,* Moncton, pp. 875-876, 1981.

45. Tschegg, E., Kroer, G., Tan, D., Stanzl-Tschegg, S., and Litzka, J., "Investigation of Bonding between Asphalt Layers on Road Construction," *Journal of Transportation Engineering*, vol. 121, no. 4, pp. 309-316, 1995.

46. Ueshita, K., and Meyerhof, G. G., "Deflection of Multilayer Soil Systems," *Journal of Soil Mechanics Foundation Division*, ASCE, SM5 pp. 257-282, 1967,

47. Uzan, J., "Influence of the Interface Condition on Stress Distribution in a Layered System," *Transportation Research Record,* no. 616, pp. 71-73, 1976.

48. Uzan, J., Livneh, M., and Eshed, Y., "Investigation of Adhesion Properties between Asphaltic-Concrete Layers," *Proceedings of the Association of Asphalt Paving Technologists,* vol. 47, pp. 495-521, 1978.

49. Westman, R. A., "Layered Systems Subjected to Surface Shears," *Journal of Engineering Mechanics Division,* ASCE, vol. 89, EM6, pp. 177-191, 1963.

50. Xu, Q., Rahman, M. S., and Tayebali, A. A., "ASP: A Computer Program for Analysis of Stresses in Pavements," Department of Civil Engineering, North Carolina State University, June 2002.

51. Zienkiewicz, O. C., "The Finite Element Method," McGraw-Hill, third edition, 1976.

52. Zienkiewicz, O. C., Kelly, D. W., and Bettes, P., "The Coupling of Finite Element and Boundary Solution Procedures," *Int. J. Num. Meth. Eng.*, vol. 11, pp. 355-376, 1981.

Appendix A

Questionnaire – ON PRIME AND TACK COATS

A Mechanistic Approach to Evaluate Contribution of Prime and Tack Coat
In Composite Asphalt Pavements
North Carolina Department of Transportation, Project HWY-2001-04

<u>Scope of the Survey:</u> **An evaluation of the effectiveness of emulsified asphalt prime coats as compared to cutback asphalt prime coats, and to make a survey of the state practices with respect to types and rates of application of both prime coats and tack coats.**

Responding Agency:____

Name and Title of Individual Completing Questionnaire:______________________

____

Does your agency require the use of a prime coat on new construction?

Yes ___ NO ____

If the answer to question 1 is yes, what are the required type of material and the normal rate of application?

____

Is the use of prime coat related to asphalt pavement thickness? If so, explain

____

____

Is a specific cure time specified? Yes ___ No ____

If yes, how much cure time? ____

What types of laboratory tests are required for prime coat material(s) ?

____

____

Are any types of field performance test(s) required? Yes ___ NO ___. If yes, please explain ____

____

Have you been able to detect any difference in pavement performance by using or not using a prime coat? Yes ___ No ___. If yes, please explain _____________________

____

Do you have opinion as to the merits of an emulsified asphalt prime as compared to a cutback asphalt prime? Yes ____ NO ___. If yes, please explain ________________

____

What types of asphalt materials are used for tack coats – types and application rates?

____

____

If you use emulsified asphalt tack coats for nighttime paving, what provisions are made for the emulsion breaking prior to placement of the hot-mix asphalt?

____

____

Please return completed questionnaire to:

Prof. Akhtar A. Tayebali, P.E.

North Carolina State University

Department of Civil Engineering

Campus Box 7908

Raleigh, NC 27695-7908

Ph: (919) 515-7611

Completed questionnaires can be faxed at (919) 515-7908. If you prefer to fill this questionnaire in electronic format, please send an e-mail to tayebali@eos.ncsu.edu**.**

Appendix B

State	Prime Coat	Prime Coat Materials	PC Rate (gal/yd^2)	PC relation to AC thickness	Cure Time	How much?	Lab Tests for Prime Coats	Field PT?	Field Performance Test Description	Diff. in perf.?	Explanation	Explanation: why emulsion is better than cutback or vice versa.	Tack Coat Types	Tack Coat Rates (gal/yd^2)	Night time provisions
AK	Y/N	MC-30 or CSS-1	250-750 ml/sq m	N, The application of tack coat is dependent on individual designers and on the paving location.	N		MC-30 must meet M82. CSS-1 must meet M140.	N		N	-	Y, Cutbacks penetrate better than the emulsified asphalts.	Special Tack Emulsion -1	200-400 ml/sq.m	Tack coat may not be placed on a wet surface or when the roadway surface temp is below 5 deg. C.
AL	Y	AE-P, MC-30, MC-70 for tight bases. MC-250, MC 70, RC-250 for open bases, EPR	0.22 - 0.25 20% redn. for CTB	No	N		M81, M82, spot test is not required.	N		Y	Protects base from wind/water erosion and promotes the maintenance of optimum m/c by creating an impermeable membrane.	Better penetration and better coverage from cutback asphalt.	CRS-2, CRS-2h, CSS-1, CSS-1h, CSQ-1hp, PG 67-22	As directed by engr but < 0.07	Eliminating the use of emulsified asphalt tack coats because it is not possible to determine whether emulsion has broken or not.
AR	N	MC cutbacks	0.4	N, Except for a minimum thickness of hot mix on minor roadways.	Y	3 days	Distillation, softening point, penetration, viscosity, spot test.	N		N	-	-	RC cutbacks, emulsions	0.03 - 0.10	Observation of the inspector.
AZ	N	-	-	-	-	-	Kinematic Viscosity	N		N	-	N, MC-250 is the only thing used in AZ.	AC, SS-1	AC @ 0.06, SS-1 & ERA-25 - 1:1 dilute w/ water @ 0.08	Nothing specified. Emulsion must break before paving of AC.
CT	Y	Emulsions.	0.14-0.45 liter/sq. m	No, but prime coats are required only on airports.	Y	Tacky to touch.	Percent residue, viscosity..	N		N	-	-	SS-1, SS-1H	0.14-0.45 liter/sq. m	None.

State	Prime Coat	Prime Coat Materials	PC Rate (gal/yd^2)	PC relation to AC thickness	Cure Time	How much?	Lab Tests for Prime Coats	Field PT?	Field Performance Test Description	Diff. in perf.?	Explanation	Explanation: why emulsion is better than cutback or vice versa.	Tack Coat Types	Tack Coat Rates (gal/yd^2)	Night time provisions
FL	Y	RC-70, RC-250. SS-1, CSS-1, SS-1H diluted with equal parts of water. AE-60, AE-90, AE-150, AE-200, Sp. MS-Emulsion diluted at a ratio of six parts of emulsion to four parts of water. AEP, EP (RS type), EPR-1 Prime.	> 0.1	N	N		Sec. 916-3 and 916-4 of FDOT.	N	-	Y	Prime is thought to act as a barrier to moisture to frequent rains in Florida. Better bond between AC and base course. Also acts as barrier for moisture when penetration happens through cracks. Mr. William Gartner, Jr. was a firm believer of Prime Coat.	-	-	-	-
GA	Y	RC-30, RC-70, MC-30, MC-70, EAP-1	0.7 - 1.4 liters/sq. m	PC required on all soil-cement and lime stabilized bases and on all other bases unless AC > 125 mm	N		T55, T79, T48, T201, T78, T51, T44, T49, T50, T72, T111	N	-	-	-	-	PG 58-22, PG64-22, PG67-22	0.18 - 0.27 liters / sq. m	N/A
ID	N	MC-70, MC-250, CSS-1	0.3	No, related more to the amount of traffic on the base. Helps when thin lifts of asphalt are present	N		M82 - cutbacks T59 - emulsions	N	PC matl. Accepted by certification. Verification samples taken; may or may not be tested.	Y	Thinner pavements (0,2') shove and tear on grades and in curves where prime is not used.	Cutbacks penetrate better but environmental problems.	Diluted CSS-1	0.05	None at this time.
IL	Y	RC-70	0.02	Only on full depth pavements is prime coat required. N	Y	Min. 1 hour.	Sp. Gr, Kin. Visc., Distillation, Test on residue, penetration, ductility, % soluble in TCE	N	-	N	Considered paving without in late 1997. Cost savings considered minimal and not worth the risk.	We allow emulsions for resurfacing projects - with success.	resurfacing: SS-1, SS-1H, CSS-1, CSS-1H, HFE60, HFE90, RC-70	0.05-0.1	Just emulsion breaking.
KS	N	-	-	Not used.	-	-	-	-	-	-	-	Emulsions do not penetrate.	CSS-1H, SS-1H diluted 50%	0.03-0.05	Must break down before overlay.

State	Prime Coat	Prime Coat Materials	PC Rate (gal/yd^2)	PC relation to AC thickness	Cure Time	How much?	Lab Tests for Prime Coats	Field PT?	Field Performance Test Description	Diff. in perf.?	Explanation	Explanation: why emulsion is better than cutback or vice versa.	Tack Coat Types	Tack Coat Rates (gal/yd^2)	Night time provisions
KY	Y	Primer-L: cutback asphalt emulsion.	1.6-2.0 lb/sq. yd	No	Y	"must cure!"	Saybolt Furol, Water Content, Asphalt Content, Coating, Residue Test Float, Solubility in Tri-chloro-ethylene	Y	Sampling of Primer_L @ 1 per 15000 tons of AC and the same tests.	N	-	Cutbacks perform better as sealants but concern about health and environment.	SS-1, SS-1H, CSS-1, CSS-1h, AE-60, RS-1, CRS-1	0.4 lb/sq. yd	It is necessary to have all water to be evaporated before any paving process.
ME	N	-	0.02 for overlays, 0.04 for milled and 0.01 for new mixes tacked at Contractors option	N, Tack coat is not needed for new construction only on overlaid pavement's or lower layers that have been exposed to winter or have got dirty.	N	-	M140 Ductility, Penetration, Sieve test for lumps, Oil content, Float test, Viscosity at 25 deg. C.	N	-	Y	Contractors find easy to densify SUPERPAVE mixes. QA bonus makes up for the cost of the tack. Less delamination and when applied properly it is impossible to separate tacked layers in cores without a saw.	N	Emulsions and are required only when overlaying an old pavement that is dirty or has wintered over.	-	Little night time paving but breaking can be decided in artificial lights.
MN	N	Although the specifications exist in the "handbook" Prime Coat is not used in practice. MC-30, MC-70.	0.45-1.35 liter/sq. m	-		-	-	-	-	-	-	N	MC-250, MC-800, C-70, C-250, C-800, SS-1, SS-1H, MS-2, RS-1, RS-2, CSS-1, CSS-1H, CRS-1, CRS-2	0.23 lit/sq.m for cutbacks and undiluted emulsions. 0.91 lit/sq.m for diluted emulsions. Water may be added upto 0% for SS-1, SS-1H, CSS-1 and CSS-1H.	Currently requiring the emulsion to break completely.

State	Prime Coat	Prime Coat Materials	PC Rate (gal/yd^2)	PC relation to AC thickness	Cure Time	How much?	Lab Tests for Prime Coats	Field PT?	Field Performance Test Description	Diff. in perf.?	Explanation	Explanation: why emulsion is better than cutback or vice versa.	Tack Coat Types	Tack Coat Rates (gal/yd^2)	Night time provisions
MO	Y	RC-70, MC-30 or SS-1	0.2-0.5	Primer not used for plant mix bituminous base with a thickness of 4" or more.	N	-	M81, M82 or M140	N	-	N	We have always required the use of prime coat.	Y, Emulsions have more pickup versus cutback.	SS-1, SS-1H, CSS-1, CSS-1H	0.02-0.1	No provisions for emulsion tack coats during night time paving.
MS	Y	CTB - MC-70, EA-1. Lime treated: EA-1, SS-1, CSS-1, CMS-2h, MS-2h	CTB-0.1-0.25. Lime: 0.25	N	N	-	T59, M82, M140, M208	N	-	Y	Indirectly, we know that unprimed chemically stabilized courses do suffer moisture damage, but it could be related as much to the stabilization effort as it is to the prime coat.	Y, emulsions are easier for contractors to use and work well when applied properly.	SS-1, CSS-1 and some AC-30	-	-
NE	N	-	-	-	-	-	-	-	-	N	-	Y, Environmental Issue.	CSS-1H when diluted with water to reduce AC content to 30% of total vol.	0.1-0.2 on existing or milled surfaces. OR 0.05-0.1 on freshly laid AC.	Required to be broken before placement. But it is not always the case. We have not discovered any problems when unbroken tack was covered with hot mix.
NH	N			PC not required since 1974.				N				N	RS-1, CRS-1	0.025	Emulsion breaking should be very quick.
NJ	Y	MC-30, MC-70	0.68-1.58 liter/sq. m	The engineer may waive the application of prime coat if a minimum of 125 mm of plant AC mix is placed on unbound aggregate course prior to opening to traffic.	N	-	M82	Y	No volatile organic substances under normal use conditions.	N	Currently attempting to eliminate the prime coat requirement. More often eliminated than not on projects.	-	RC-70, RC-T, RS-1, SS-1, SS-1h, CSS-1, CSS-1h. Emulsion used determined by Calendar.	See sec. 404.13	Tacky to touch.

State	Prime Coat	Prime Coat Materials	PC Rate (gal/yd^2)	PC relation to AC thickness	Cure Time	How much?	Lab Tests for Prime Coats	Field PT?	Field Performance Test Description	Diff. in perf.?	Explanation	Explanation: why emulsion is better than cutback or vice versa.	Tack Coat Types	Tack Coat Rates (gal/yd^2)	Night time provisions
NY	N	-	-	-	-	-	-	-	-	-	-	-	HFMS-2h, SS-1h, CSS-1h	diluted application rate: 0.14-0.32 lit./sq. m	Currently under discussion.
OK	Y/N	MC-30, MC-70 or emulsions in Oklahoma, Tulsa and Commanche Counties	0.1-0.4	N	N	Sufficient to allow proper penetration and hardening of prime coat.	Kinematic Viscosity @140 C, Flash Point, % Water, Distillation, Abs Viscosity, Ductility, Solubility in Trichloroethylene, Spot Test.	Y/N	No performance tests but lab tests, viscosity (140), Distillation.	Y	We had one project this year that had significant plane slippage problems due to use of tack coats in lieu of prime coat.	Y, Emulsions to be used where environment is a concern and also if conditions warrant and wherever there is sufficient time for curing.	RS-1, RS-2, MS-1, MS-2, MS-2h, HFMS-1, HFMS-2, HFMS-2h, HFMS-2s, SS-1, SS-1h, CRS-1, CRS-2, CMS-1, CMS-2, CSS-1, CSS-1h	0.1	Emulsions disallowed after sunset.
RI	N	-	-	-	-	-	-	-	-	-	-	-	SS-1	0.05	Emulsions used for night time paving but no provisions exist for breaking prior to placement.
SC	Y	-	0.25-0.3	N	N	-	Saybolt Furol, Residue by Distillation.	N	-	N	-	N	CRS-2, HFMS-1	0.05-0.15 based on residual asphalt.	None, contractors electing to use RS emulsion if needed.
TN	Y	AE-P, CAE-P	0.2-0.5	N	N	-	M140, Saybolt Furol, Settlement, Residue, Distillate, Float, Penetration, Solubility.	N	-	N	-	N	SS-1, CSS-1, PG64-22	0.05 for smooth (max.) and 0.2 (max) for milled.	None

State	Prime Coat	Prime Coat Materials	PC Rate (gal/yd^2)	PC relation to AC thickness	Cure Time	How much?	Lab Tests for Prime Coats	Field PT?	Field Performance Test Description	Diff. in perf.?	Explanation	Explanation: why emulsion is better than cutback or vice versa.	Tack Coat Types	Tack Coat Rates (gal/yd^2)	Night time provisions
TX	Y	MC-30, AEP, PCE, EAP&T. CSS-1 and SS-1	0.1	Emulsions can be used but have to be worked into the top inch and recompacted.	N	-	Item 300 of "Asphalts, Oils and Emulsions."	N	For new materials, testing is required.	N	Compulsory, therefore nothing to compare with.	Y, MC-30 penetrates best. For open bases, emulsion may be good.	diluted SS-1, CSS-1	0.05	Not aware of any special considerations.
WV	Y	SS-1, SS-1h, CSS-1, CSS-1h diluted with water. Inverted emulsions permitted but rarely used.	0.3 - 0.6	N	N	-	M140, M208	N	-	N	-	Cutbacks penetrate better but environmental problems and costly.	Mostly SS emulsions (cationic, anionic, inverted)	0.2 - 0.3; SS-1h diluted with 50% water is commonly used.	No special requirements.
WY	Y	MC-70	3.2 lb/sq yd	No	N	-	M82, Kinematic viscosity, distillation. Have an acceptance schedule based on properties.	N	-	Y	We feel the prime facilitates placing the first lift of pavement and also provides some water proofing.	N	SS-1 or CSS-1	0.25 lb/sq yd	Do very little night time paving.

Appendix C

Job Mix Formula

99410 NORTH CAROLINA DEPARTMENT OF TRANSPORTATION

RALEIGH, NORTH CAROLINA 27611

HOT MIX ASPHALT JOB MIX FORMULA

APAC-CAROLINA, INC

ENKA, NC

PLANT CERTIFICATION NO: DM-310

TYPE MIX: BCSC, TYPE HDS

JOB MIX FORM NO: 93-447-052

EFFECTIVE DATE: 07-27-93

PROJECT NO:

COUNTY: BUNCOMBE

AGGREGATE SOURCES AND BLEND PERCENTAGES

SUPPLIER	LOCATION/SOURCE	MATERIAL	BLEND(%)
VULCAN MATERIALS	ENKA QUARRY	#78M	42
VULCAN MATERIALS	ENKA QUARRY	W.SCRGS.	30
VULCAN MATERIALS	ENKA QUARRY	D.SCRGS.	28

TOTAL: 100.0%

JMF COMBINED GRADATION

SIEVE SIZE	% PASSING
2''	
1 ½ ''	
1''	
¾''	100
½''	98
3/8''	95
NO. 4	72
8	50
16	39
40	24
80	12
200	5.0

ASPHALT CEMENT %(TOT) 5.7

GRADE		PG64-22
EST ASH	11-3-93	0.3
MAX. SP. GV.		2.486
LABORATORY SP. GV.		2.364
VOIDS IN TOTAL MIX %		4.9
MIN. % COMPACTION		95.0
MIX TEMPERATURE F.		285
FLOW (0.01 IN.)		11
STABILITY (LBS.)		3000
NON STRIP ADDITIVE %		0.50
MODIFIER %		0.00

ASPHALT CEMENT SUPPLIER : SPECS.
TACK COAT SUPPLIER : SPECS.
NON-STRIP ADD. SUPPLIER : PAVE BOND LP – CINCINNATI, OHIO
MODIFIER SUPPLIER :

COMMENTS:

% AC DECREASED TO INCREASE VOIDS. BLEND CHANGES TO CONTROL GRADATION & VOIDS IN MIX. #8 SIEVE CHANGE BASED ON FIELD TEST RESULTS.

DATE JMF VOID:

APPROVED BY:
J.E. GRADY, JR.
PAVEMENT CONSTRUCTION ENGR.

99410 NORTH CAROLINA DEPARTMENT OF TRANSPORTATION

RALEIGH, NORTH CAROLINA 27611

HOT MIX ASPHALT JOB MIX FORMULA

THOMPSON CONTRACTORS, INC — TYPE MIX: BCSC, TYPE HDS

RUTHERFORDTON, NC — JOB MIX FORM NO: 93-903-051

EFFECTIVE DATE: 02-07-94

PLANT CERTIFICATION NO: DM-286 — PROJECT NO:

COUNTY: RUTHERFORD

AGGREGATE SOURCES AND BLEND PERCENTAGES

SUPPLIER	LOCATION/SOURCE	MATERIAL	BLEND(%)
THOMPSON CONTRACTORS	MILLER CREEK QUARRY	#78M	47
THOMPSON CONTRACTORS	MILLER CREEK QUARRY	SCRGS.	33
THOMPSON CONTRACTORS	BROAD RIVER	SAND	20
		TOTAL:	**100.0%**

JMF COMBINED GRADATION

SIEVE SIZE	% PASSING
2’’	
1 ½ ’’	
1’’	
¾’’	100
½’’	98
3/8’’	95
NO. 4	69
8	53
16	43
40	24
80	11
200	5.9

ASPHALT CEMENT %(TOT) 6.2

GRADE		PG64-22
EST ASH	11-3-93	0.4
MAX. SP. GV.		2.502
LABORATORY SP. GV.		2.378
VOIDS IN TOTAL MIX %		5.0
MIN. % COMPACTION		95.0
MIX TEMPERATURE F.		285
FLOW (0.01 IN.)		9
STABILITY (LBS.)		1900
NON STRIP ADDITIVE %		0.50
MODIFIER %		0.00

ASPHALT CEMENT SUPPLIER : SPECS.
TACK COAT SUPPLIER : SPECS.
NON-STRIP ADD. SUPPLIER : PERMA-TAC — SCAN ROAD
MODIFIER SUPPLIER :

COMMENTS:

DATE JMF VOID:

APPROVED BY:
J.E. GRADY, JR.
PAVEMENT CONSTRUCTION ENGR.

NORTH CAROLINA DEPARTMENT OF TRANSPORTATION
RALEIGH, NORTH CAROLINA 27611

HOT MIX ASPHALT JOB MIX FORMULA

APAC-CAROLINA, INC.

ENKA, NC

TYPE MIX: BCSC, TYPE I-2

JOB MIX FORM NO: 01-229-161

EFFECTIVE DATE: 05-11-01

PLANT CERTIFICATION NO: DM-310

PROJECT NO:

COUNTY:

AGGREGATE SOURCES AND BLEND PERCENTAGES

SUPPLIER	LOCATION/SOURCE	MATERIAL	BLEND (%)
VULCAN MATERIALS	ENKA QUARRY	78M	26.0
VULCAN MATERIALS	ENKA QUARRY	W.SCRGS.	63.0
VULCAN MATERIALS	ENKA QUARRY	D.SCRGS.	11.0
		TOTAL	100.0%

JMF COMBINED GRADATION

SIEVE SIZE	% PASSING
2 "	100
1 1/2"	100
1 "	100
3/4"	100
1/2"	100
3/8"	97
NO. 4	77
8	62
16	44
40	50
80	13
NO. 200	5.9

ASPHALT CEMENT %(TOT)	7.0
GRADE	PG64-22
EST ASH	
MAX. SP. GV.	2.469
LABORATORY SP. GV.	2.333
VOIDS IN TOTAL MIX %	5.5
MIN. % COMPACTION	95.0
MIX TEMPERATURE F.	300
FLOW (0.01 IN.)	11
STABILITY (LBS.)	2020
NON STRIP ADDITIVE %	0.60
MODIFIER %	0.00

ASPHALT CEMENT SUPPLIER: SOUTH STATES KNOXVILLE
TACK COAT SUPPLIER : SPECS.
NON-STRIP ADD. SUPPLIER: ARR-MAZ LOF 6500
MODIFIER SUPPLIER :

COMMENTS:

DATE JMF VOID:

APPROVED BY:
J.E. GRADY, JR.
PAVEMENT CONSTRUCTION ENGR.

Appendix D

APA Test Results

Rutting Test Data Sheet

Project No. : ~~NC State~~ Test No. : R1210-1 Temperature : ~~50~~ (deg. C)
Mix ID No. : ~~Buncombe Co.~~ Test Date : 12/10/99 Wheel Load : ~~100~~ (lbs)
Mix Type : Data File : R1210_1.ptd Hose Pressure : ~~100~~ (psi)
Operator : Run Status: Complete Run Time 2:14:43 (hh:mm:ss)

Left Sample ID	BNC w			Bulk S Gravity				% Air Void			
Stroke	Temperature		Depth Gauge Reading(mm)					Manual	Net Man	APA-DAS	Percent
Count	F	C	1	2	3	4	5	Average	Deflection	Average	Change
0									0	0	
500										2.467	
1000										3.554	44.1
1500										4.181	17.6
2000										4.592	9.8
3000										5.081	10.7
4000										5.403	6.3
5000										5.653	4.6
6000										5.831	3.2
7000										5.981	2.6
8000										6.152	2.9
8001										6.152	0

Middle Sample ID				Bulk S Gravity				% Air Void			
Stroke	Temperature		Depth Gauge Reading(mm)					Manual	Net Man	APA-DAS	Percent
Count	F	C	1	2	3	4	5	Average	Deflection	Average	Change
0									0	0	
500										0	
1000										0	
1500										0	
2000										0	
3000										0	
4000										0	
5000										0	
6000										0	
7000										0	
8000										0	
8001										0	

Right Sample ID BNC w/o				Bulk S Gravity				% Air Void			
Stroke	Temperature		Depth Gauge Reading(mm)					Manual	Net Man	APA-DAS	Percent
Count	F	C	1	2	3	4	5	Average	Deflection	Average	Change
0									0	0	
500										2.065	
1000										3.294	59.5
1500										3.98	20.8
2000										4.418	11
3000										4.993	13
4000										5.317	6.5
5000										5.595	5.2
6000										5.715	2.1
7000										5.967	4.4
8000										6.128	2.7
8001										6.124	-0.1

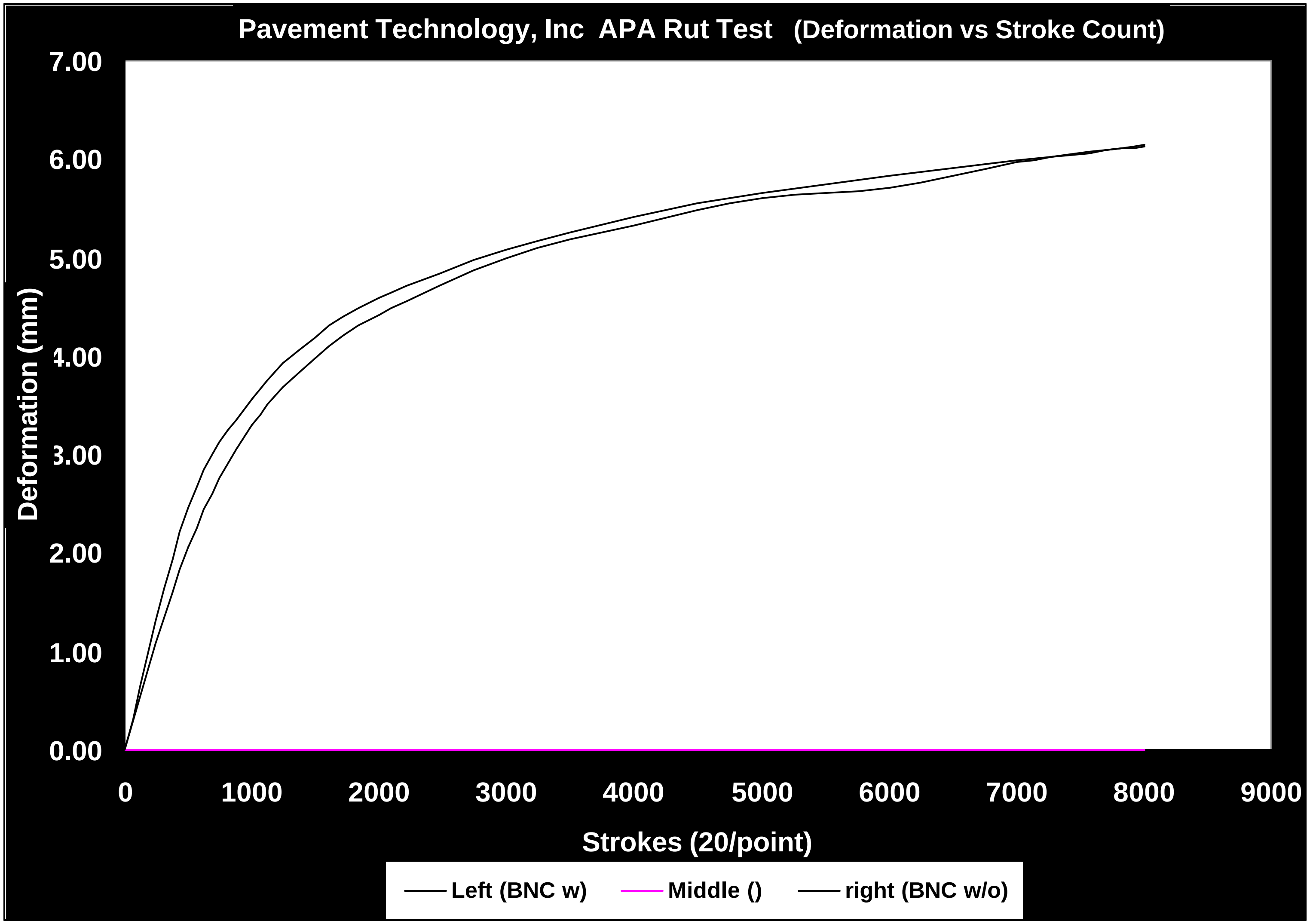

Pavement Technology, Inc APA Rut Test (Deformation vs Stroke Count)
7.00
6.00
5.00
4.00
3.00
2.00
1.00
0.00
Deformation (mm)
0
1000
2000
3000
4000
5000
6000
7000
8000
9000
Strokes (20/point)
Left (BNC w)
Middle ()
right (BNC w/o)

Rutting Test Data Sheet

Project No. :	NC State	Test No. :	R1209-1	Temperature : 50	(deg. C)
Mix ID No. :	Rutherford Co.	Test Date :	12/09/99	Wheel Load : 100	(lbs)
Mix Type :		Data File :	R1209_1.ptd	Hose Pressure : ~~100~~	(psi)
Operator :		Run Status:	Complete	Run Time 2:14:38	(hh:mm:ss)

Left Sample ID	RF w		Bulk S Gravity				% Air Void			
Stroke	Temperature		Depth Gauge Reading(mm)				Manual	Net Man	APA-DAS	Percent
Count	F	C	1	2	3	4	5 Average	Deflection	Average	Change
0								0	0	
500									5.858	
1000									7.328	25.1
1500									8.237	12.4
2000									8.929	8.4
3000									9.953	11.5
4000									10.657	7.1
5000									11.246	5.5
6000									11.691	4
7000									12.01	2.7
8000									12.335	2.7
8001									12.335	0

Middle Sample ID			Bulk S Gravity				% Air Void			
Stroke	Temperature		Depth Gauge Reading(mm)				Manual	Net Man	APA-DAS	Percent
Count	F	C	1	2	3	4	5 Average	Deflection	Average	Change
0								0	0	
500									0	
1000									0	
1500									0	
2000									0	
3000									0	
4000									0	
5000									0	
6000									0	
7000									0	
8000									0	
8001									0	

Right Sample ID BNC w/o			Bulk S Gravity				% Air Void			
Stroke	Temperature		Depth Gauge Reading(mm)				Manual	Net Man	APA-DAS	Percent
Count	F	C	1	2	3	4	5 Average	Deflection	Average	Change
0								0	0	
500									5.616	
1000									6.982	24.3
1500									7.901	13.2
2000									8.602	8.9
3000									9.655	12.2
4000									10.513	8.9
5000									11.197	6.5
6000									11.891	6.2
7000									12.331	3.7
8000									12.782	3.7
8001									12.782	0

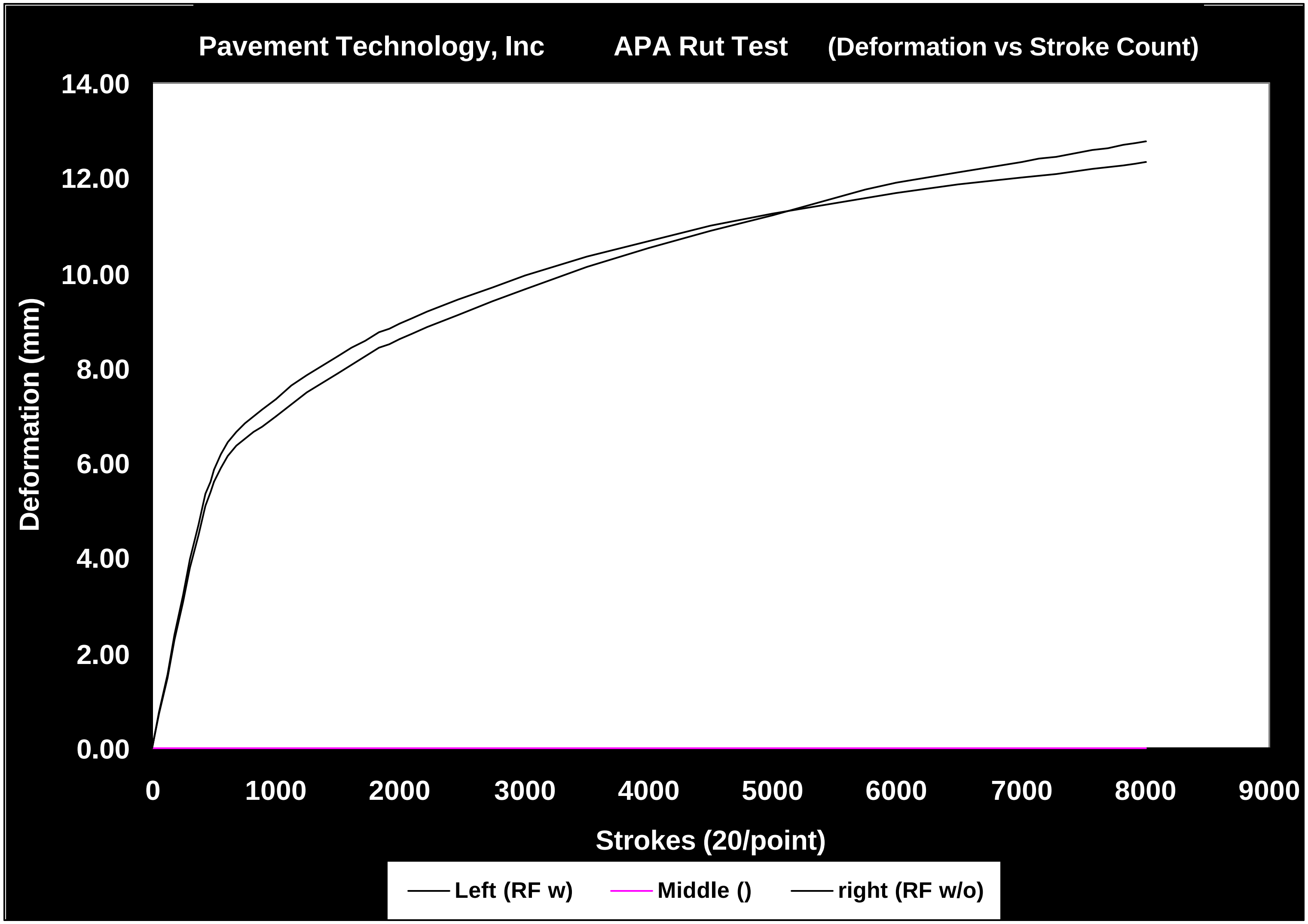

Pavement Technology, Inc APA Rut Test (Deformation vs Stroke Count)
Deformation (mm)
14.00
12.00
10.00
8.00
6.00
4.00
2.00
0.00
0
1000
2000
3000
4000
5000
6000
7000
8000
9000
Strokes (20/point)
Left (RF w)
Middle ()
right (RF w/o)

Appendix E

DSR Test Results

Table E- 1|G*| and d values for binders at 58 °C

Frequency (Hz)	Buncombe County				Rutherford County			
	Virgin		Aged		Virgin		Aged	
	|G*| (Pa)	δ (deg)	|G*| (Pa)	δ (deg)	|G*| (Pa)	δ (deg)	|G*| (Pa)	δ (deg)
1.00E-02	2.13E+01	8.94E+01	5.55E+01	8.93E+01	1.58E+01	8.91E+01	4.79E+01	8.93E+01
5.00E-02	1.06E+02	8.93E+01	2.74E+02	8.82E+01	7.84E+01	8.95E+01	2.35E+02	8.81E+01
1.00E-01	2.12E+02	8.90E+01	5.41E+02	8.72E+01	1.57E+02	8.91E+01	4.63E+02	8.71E+01
1.50E-01	3.16E+02	8.89E+01	8.03E+02	8.65E+01	2.34E+02	8.89E+01	6.86E+02	8.65E+01
5.00E-01	1.03E+03	8.76E+01	2.52E+03	8.42E+01	7.68E+02	8.77E+01	2.15E+03	8.41E+01
1.00E+00	2.00E+03	8.65E+01	4.80E+03	8.28E+01	1.50E+03	8.68E+01	4.10E+03	8.26E+01
1.59E+00	3.11E+03	8.58E+01	7.46E+03	8.16E+01	2.36E+03	8.61E+01	6.35E+03	8.16E+01
5.00E+00	9.22E+03	8.38E+01	2.04E+04	7.87E+01	6.96E+03	8.41E+01	1.73E+04	7.88E+01
1.00E+01	1.75E+04	8.23E+01	3.72E+04	7.69E+01	1.33E+04	8.26E+01	3.17E+04	7.71E+01
2.00E+01	3.30E+04	8.03E+01	6.70E+04	7.49E+01	2.49E+04	8.06E+01	5.64E+04	7.51E+01

Table E- 2 |G*| and d values for binders at 64 °C

Frequency (Hz)	Buncombe County				Rutherford County			
	Virgin		Aged		Virgin		Aged	
	|G*| (Pa)	δ (deg)	|G*| (Pa)	δ (deg)	|G*| (Pa)	δ (deg)	|G*| (Pa)	δ (deg)
1.00E-02	9.10E+00	8.78E+01	2.28E+01	8.97E+01	6.96E+00	8.92E+01	1.94E+01	8.94E+01
5.00E-02	4.49E+01	8.93E+01	1.14E+02	8.92E+01	3.39E+01	8.94E+01	9.63E+01	8.91E+01
1.00E-01	9.00E+01	8.94E+01	2.26E+02	8.86E+01	6.78E+01	8.95E+01	1.93E+02	8.85E+01
1.50E-01	1.35E+02	8.92E+01	3.38E+02	8.82E+01	1.02E+02	8.93E+01	2.88E+02	8.80E+01
5.00E-01	4.46E+02	8.85E+01	1.09E+03	8.62E+01	3.35E+02	8.86E+01	9.27E+02	8.61E+01
1.00E+00	8.81E+02	8.78E+01	2.10E+03	8.50E+01	6.64E+02	8.80E+01	1.79E+03	8.49E+01
1.59E+00	1.35E+03	8.71E+01	3.29E+03	8.40E+01	1.05E+03	8.73E+01	2.77E+03	8.38E+01
5.00E+00	4.18E+03	8.53E+01	9.31E+03	8.14E+01	3.15E+03	8.53E+01	7.92E+03	8.13E+01
1.00E+01	8.02E+03	8.37E+01	1.74E+04	7.96E+01	6.08E+03	8.36E+01	1.48E+04	7.96E+01
2.00E+01	1.53E+04	8.15E+01	3.15E+04	7.74E+01	1.16E+04	8.08E+01	2.70E+04	7.77E+01

Table E- 3 |G*| and d values for binders at 70 °C

Frequency (Hz)	Buncombe County				Rutherford County			
	Virgin		Aged		Virgin		Aged	
	|G*| (Pa)	δ (deg)	|G*| (Pa)	δ (deg)	|G*| (Pa)	δ (deg)	|G*| (Pa)	δ (deg)
1.00E-02	4.24E+00	8.85E+01	9.56E+00	8.93E+01	3.29E+00	8.89E+01	8.25E+00	8.94E+01
5.00E-02	2.05E+01	8.90E+01	4.72E+01	8.95E+01	1.65E+01	8.93E+01	4.02E+01	8.96E+01
1.00E-01	4.10E+01	8.92E+01	9.46E+01	8.93E+01	3.29E+01	8.95E+01	8.12E+01	8.93E+01
1.50E-01	6.17E+01	8.93E+01	1.41E+02	8.90E+01	4.95E+01	8.94E+01	1.21E+02	8.90E+01
5.00E-01	2.05E+02	8.90E+01	4.65E+02	8.77E+01	1.64E+02	8.91E+01	3.99E+02	8.77E+01
1.00E+00	4.09E+02	8.86E+01	9.13E+02	8.67E+01	3.28E+02	8.87E+01	7.82E+02	8.66E+01
1.59E+00	6.33E+02	8.80E+01	1.44E+03	8.57E+01	5.15E+02	8.82E+01	1.22E+03	8.57E+01
5.00E+00	1.98E+03	8.61E+01	4.20E+03	8.33E+01	1.58E+03	8.62E+01	3.59E+03	8.31E+01
1.00E+01	3.86E+03	8.43E+01	7.94E+03	8.14E+01	3.09E+03	8.45E+01	6.80E+03	8.11E+01
2.00E+01	7.49E+03	8.14E+01	1.48E+04	7.87E+01	5.94E+03	8.11E+01	1.27E+04	7.83E+01

Table E- 4 |G*| and d values for baghouse mastics at 58 °C

Frequency (Hz)	Buncombe County				Rutherford County			
	Virgin		Aged		Virgin		Aged	
	|G*| (Pa)	δ (deg)	|G*| (Pa)	δ (deg)	|G*| (Pa)	δ (deg)	|G*| (Pa)	δ (deg)
1.00E-02	2.59E+02	7.95E+01	3.74E+02	8.26E+01	1.63E+02	8.13E+01	1.62E+02	8.20E+01
5.00E-02	1.05E+03	8.37E+01	1.57E+03	8.57E+01	6.14E+02	8.77E+01	5.95E+02	8.78E+01
1.00E-01	1.99E+03	8.51E+01	2.92E+03	8.64E+01	1.20E+03	8.77E+01	1.17E+03	8.78E+01
1.50E-01	2.87E+03	8.56E+01	4.29E+03	8.64E+01	1.80E+03	8.75E+01	1.75E+03	8.76E+01
5.00E-01	8.88E+03	8.64E+01	1.33E+04	8.58E+01	5.77E+03	8.61E+01	5.51E+03	8.56E+01
1.00E+00	1.70E+04	8.66E+01	2.52E+04	8.53E+01	1.13E+04	8.44E+01	1.07E+04	8.38E+01
1.59E+00	2.75E+04	8.66E+01	4.07E+04	8.47E+01	1.71E+04	8.29E+01	1.68E+04	8.26E+01
5.00E+00	7.47E+04	8.93E+01	1.08E+05	8.65E+01	5.11E+04	7.58E+01	4.89E+04	7.47E+01
1.00E+01	1.38E+05	8.28E+01	1.97E+05	8.84E+01	9.99E+04	6.68E+01	9.61E+04	6.48E+01
2.00E+01	**	**	3.71E+05	7.82E+01	2.09E+05	5.33E+01	2.03E+05	5.24E+01

Table E- 5 |G*| and d values for baghouse mastics at 64 °C

Frequency (Hz)	Buncombe County				Rutherford County			
	Virgin		Aged		Virgin		Aged	
	|G*| (Pa)	δ (deg)	|G*| (Pa)	δ (deg)	|G*| (Pa)	δ (deg)	|G*| (Pa)	δ (deg)
1.00E-02	1.19E+02	7.69E+01	1.35E+02	8.30E+01	8.68E+01	7.80E+01	8.08E+01	7.81E+01
5.00E-02	4.41E+02	8.03E+01	5.95E+02	8.62E+01	2.72E+02	8.65E+01	2.64E+02	8.69E+01
1.00E-01	8.19E+02	8.22E+01	1.18E+03	8.67E+01	5.16E+02	8.78E+01	4.99E+02	8.78E+01
1.50E-01	1.21E+03	8.38E+01	1.75E+03	8.72E+01	7.65E+02	8.77E+01	7.43E+02	8.76E+01
5.00E-01	3.67E+03	8.68E+01	5.53E+03	8.79E+01	2.48E+03	8.61E+01	2.42E+03	8.59E+01
1.00E+00	6.67E+03	8.92E+01	1.05E+04	8.84E+01	4.86E+03	8.35E+01	4.74E+03	8.37E+01
1.59E+00	1.05E+04	8.73E+01	1.68E+04	8.91E+01	7.59E+03	8.16E+01	7.45E+03	8.13E+01
5.00E+00	3.16E+04	7.43E+01	4.78E+04	8.34E+01	2.40E+04	7.10E+01	2.31E+04	7.08E+01
1.00E+01	6.65E+04	5.77E+01	9.27E+04	7.22E+01	5.20E+04	5.43E+01	4.94E+04	5.48E+01
2.00E+01	1.79E+05	3.56E+01	2.00E+05	5.34E+01	1.29E+05	3.89E+01	1.27E+05	3.67E+01

Table E- 6 |G*| and d values for baghouse mastics at 70 °C

Frequency (Hz)	Buncombe County				Rutherford County			
	Virgin		Aged		Virgin		Aged	
	|G*| (Pa)	δ (deg)	|G*| (Pa)	δ (deg)	|G*| (Pa)	δ (deg)	|G*| (Pa)	δ (deg)
1.00E-02	5.58E+01	7.27E+01	1.02E+02	7.22E+01	4.33E+01	7.30E+01	4.42E+01	7.23E+01
5.00E-02	1.75E+02	7.91E+01	3.62E+02	7.75E+01	1.36E+02	8.28E+01	1.30E+02	8.43E+01
1.00E-01	3.15E+02	8.11E+01	6.55E+02	7.93E+01	2.31E+02	8.66E+01	2.25E+02	8.68E+01
1.50E-01	4.67E+02	8.28E+01	1.00E+03	8.13E+01	3.38E+02	8.71E+01	3.28E+02	8.70E+01
5.00E-01	1.47E+03	8.82E+01	2.75E+03	8.52E+01	1.10E+03	8.49E+01	1.07E+03	8.45E+01
1.00E+00	2.78E+03	8.57E+01	4.74E+03	8.83E+01	2.20E+03	8.08E+01	2.12E+03	8.08E+01
1.59E+00	5.23E+03	8.23E+01	8.13E+03	8.72E+01	3.31E+03	7.66E+01	3.22E+03	7.73E+01
5.00E+00	1.57E+04	5.25E+01	2.29E+04	6.84E+01	1.25E+04	5.37E+01	1.17E+04	6.05E+01
1.00E+01	4.72E+04	3.06E+01	5.37E+04	4.91E+01	3.38E+04	3.39E+01	2.98E+04	4.23E+01
2.00E+01	1.39E+05	1.80E+01	1.76E+05	2.54E+01	1.13E+05	1.84E+01	1.06E+05	1.93E+01

** Values discarded

Table E- 7 |G*| and d values for P#200 mastics at 58 °C

Frequency (Hz)	Buncombe County				Rutherford County			
	Virgin		Aged		Virgin		Aged	
	|G*| (Pa)	δ (deg)	|G*| (Pa)	δ (deg)	|G*| (Pa)	δ (deg)	|G*| (Pa)	δ (deg)
1.00E-02	1.79E+02	7.95E+01	2.81E+02	8.04E+01	4.26E+03	8.43E+01	1.14E+02	8.63E+01
5.00E-02	6.28E+02	8.68E+01	9.57E+02	8.69E+01	5.96E+04	8.82E+01	5.03E+02	8.85E+01
1.00E-01	1.23E+03	8.74E+01	1.86E+03	8.68E+01	1.72E+04	8.82E+01	9.88E+02	8.78E+01
1.50E-01	1.83E+03	8.73E+01	2.75E+03	8.66E+01	1.00E+03	8.76E+01	1.46E+03	8.74E+01
5.00E-01	5.88E+03	8.62E+01	8.70E+03	8.52E+01	3.23E+03	8.58E+01	4.67E+03	8.54E+01
1.00E+00	1.15E+04	8.47E+01	1.69E+04	8.38E+01	6.36E+03	8.41E+01	9.03E+03	8.34E+01
1.59E+00	1.76E+04	8.35E+01	2.64E+04	8.25E+01	1.01E+06	7.85E+01	1.43E+04	8.23E+01
5.00E+00	5.32E+04	7.72E+01	7.47E+04	7.66E+01	3.02E+04	7.34E+01	4.15E+04	7.27E+01
1.00E+01	1.03E+05	6.82E+01	1.41E+05	7.00E+01	2.06E+07	5.11E+01	8.23E+04	6.65E+01
2.00E+01	2.13E+05	5.58E+01	2.81E+05	5.88E+01	8.87E+07	3.47E+01	1.87E+05	4.67E+01

Table E- 8 |G*| and d values for P#200 mastics at 64 °C

Frequency (Hz)	Buncombe County				Rutherford County			
	Virgin		Aged		Virgin		Aged	
	|G*| (Pa)	δ (deg)	|G*| (Pa)	δ (deg)	|G*| (Pa)	δ (deg)	|G*| (Pa)	δ (deg)
1.00E-02	9.04E+01	7.59E+01	1.35E+02	7.83E+01	3.73E+01	8.14E+01	5.87E+01	8.35E+01
5.00E-02	2.82E+02	8.60E+01	4.26E+02	8.65E+01	1.46E+02	8.66E+01	2.31E+02	8.81E+01
1.00E-01	5.29E+02	8.74E+01	8.18E+02	8.72E+01	2.81E+02	8.79E+01	4.44E+02	8.82E+01
1.50E-01	7.82E+02	8.73E+01	1.21E+03	8.71E+01	4.20E+02	8.77E+01	6.60E+02	8.80E+01
5.00E-01	2.53E+03	8.61E+01	3.92E+03	8.59E+01	1.37E+03	8.54E+01	2.15E+03	8.56E+01
1.00E+00	5.01E+03	8.42E+01	7.66E+03	8.44E+01	2.76E+03	8.25E+01	4.16E+03	8.25E+01
1.59E+00	7.78E+03	8.19E+01	1.20E+04	8.30E+01	4.17E+03	7.96E+01	6.75E+03	8.19E+01
5.00E+00	2.45E+04	6.96E+01	3.55E+04	7.47E+01	1.44E+04	6.17E+01	2.07E+04	7.13E+01
1.00E+01	5.32E+04	5.47E+01	7.02E+04	6.31E+01	3.59E+04	4.19E+01	4.61E+04	5.15E+01
2.00E+01	1.41E+05	3.64E+01	1.47E+05	5.45E+01	1.15E+05	2.22E+01	1.21E+05	3.37E+01

Table E- 9 |G*| and d values for P#200 mastics at 70 °C

Frequency (Hz)	Buncombe County				Rutherford County			
	Virgin		Aged		Virgin		Aged	
	|G*| (Pa)	δ (deg)	|G*| (Pa)	δ (deg)	|G*| (Pa)	δ (deg)	|G*| (Pa)	δ (deg)
1.00E-02	4.82E+01	7.01E+01	6.44E+01	7.39E+01	2.09E+01	8.23E+01	3.56E+01	8.23E+01
5.00E-02	1.46E+02	8.24E+01	2.08E+02	8.44E+01	7.33E+01	8.54E+01	1.29E+02	8.77E+01
1.00E-01	2.49E+02	8.63E+01	3.76E+02	8.68E+01	1.27E+02	8.72E+01	2.47E+02	8.82E+01
1.50E-01	3.62E+02	8.66E+01	5.57E+02	8.70E+01	1.85E+02	8.70E+01	3.61E+02	8.80E+01
5.00E-01	1.18E+03	8.49E+01	1.79E+03	8.54E+01	6.13E+02	8.27E+01	1.18E+03	8.50E+01
1.00E+00	2.36E+03	8.24E+01	3.57E+03	8.31E+01	1.25E+03	7.64E+01	2.36E+03	8.12E+01
1.59E+00	3.72E+03	8.19E+01	5.60E+03	7.98E+01	1.51E+03	6.78E+01	3.59E+03	7.61E+01
5.00E+00	1.25E+04	6.29E+01	1.79E+04	6.37E+01	8.29E+03	4.53E+01	1.31E+04	5.58E+01
1.00E+01	3.53E+04	3.50E+01	4.16E+04	4.71E+01	2.92E+04	2.18E+01	3.11E+04	4.17E+01
2.00E+01	1.13E+05	2.00E+01	1.29E+05	2.30E+01	1.00E+05	1.14E+01	1.02E+05	2.18E+01

Table E- 10 |G*|sin d values for Buncombe County materials, 58 °C

Frequency (Hz)	Binder		Baghouse Mastic		P#200 Mastic	
	Virgin	Aged	Virgin	Aged	Virgin	Aged
1.00E-02	2.13E+01	5.55E+01	2.54E+02	3.71E+02	1.76E+02	2.77E+02
5.00E-02	1.06E+02	2.74E+02	1.05E+03	1.56E+03	6.27E+02	9.56E+02
1.00E-01	2.12E+02	5.41E+02	1.98E+03	2.92E+03	1.22E+03	1.86E+03
1.50E-01	3.16E+02	8.01E+02	2.86E+03	4.28E+03	1.83E+03	2.74E+03
5.00E-01	1.03E+03	2.51E+03	8.86E+03	1.33E+04	5.86E+03	8.67E+03
1.00E+00	2.00E+03	4.76E+03	1.69E+04	2.51E+04	1.14E+04	1.68E+04
1.59E+00	3.10E+03	7.38E+03	2.75E+04	4.05E+04	1.75E+04	2.62E+04
5.00E+00	9.17E+03	2.00E+04	7.47E+04	1.08E+05	5.19E+04	7.26E+04
1.00E+01	1.74E+04	3.62E+04	1.37E+05	1.97E+05	9.60E+04	1.33E+05
2.00E+01	3.25E+04	6.47E+04	**	3.63E+05	1.76E+05	2.40E+05
Average	**6.58E+03**	**1.37E+04**	**3.01E+04**	**7.56E+04**	**3.63E+04**	**5.03E+04**

Table E- 11 |G*|sin d values for Buncombe County materials, 64 °C

Frequency (Hz)	Binder		Baghouse Mastic		P#200 Mastic	
	Virgin	Aged	Virgin	Aged	Virgin	Aged
1.00E-02	9.10E+00	2.28E+01	1.16E+02	1.34E+02	8.77E+01	1.33E+02
5.00E-02	4.49E+01	1.14E+02	4.34E+02	5.94E+02	2.81E+02	4.25E+02
1.00E-01	9.00E+01	2.26E+02	8.12E+02	1.18E+03	5.29E+02	8.17E+02
1.50E-01	1.35E+02	3.37E+02	1.20E+03	1.75E+03	7.82E+02	1.21E+03
5.00E-01	4.46E+02	1.08E+03	3.66E+03	5.53E+03	2.53E+03	3.91E+03
1.00E+00	8.80E+02	2.09E+03	6.67E+03	1.05E+04	4.98E+03	7.63E+03
1.59E+00	1.35E+03	3.27E+03	1.05E+04	1.68E+04	7.71E+03	1.19E+04
5.00E+00	4.16E+03	9.20E+03	3.04E+04	4.75E+04	2.30E+04	3.42E+04
1.00E+01	7.97E+03	1.71E+04	5.62E+04	8.83E+04	4.34E+04	6.26E+04
2.00E+01	1.51E+04	3.08E+04	1.04E+05	1.61E+05	8.39E+04	1.20E+05
Average	**3.02E+03**	**6.42E+03**	**2.14E+04**	**3.33E+04**	**1.67E+04**	**2.43E+04**

Table E- 12|G*|sin d values for Buncombe County materials, 70 °C

Frequency (Hz)	Binder		Baghouse Mastic		P#200 Mastic	
	Virgin	Aged	Virgin	Aged	Virgin	Aged
1.00E-02	4.24E+00	9.56E+00	5.33E+01	9.68E+01	4.53E+01	6.19E+01
5.00E-02	2.05E+01	4.72E+01	1.72E+02	3.53E+02	1.45E+02	2.07E+02
1.00E-01	4.10E+01	9.46E+01	3.11E+02	6.43E+02	2.49E+02	3.76E+02
1.50E-01	6.17E+01	1.41E+02	4.63E+02	9.92E+02	3.61E+02	5.56E+02
5.00E-01	2.05E+02	4.64E+02	1.47E+03	2.74E+03	1.18E+03	1.78E+03
1.00E+00	4.09E+02	9.11E+02	2.77E+03	4.74E+03	2.34E+03	3.54E+03
1.59E+00	6.33E+02	1.43E+03	5.18E+03	8.12E+03	3.69E+03	5.51E+03
5.00E+00	1.98E+03	4.17E+03	1.25E+04	2.13E+04	1.12E+04	1.61E+04
1.00E+01	3.84E+03	7.85E+03	2.40E+04	4.06E+04	2.03E+04	3.05E+04
2.00E+01	7.40E+03	1.45E+04	4.29E+04	7.55E+04	3.87E+04	5.06E+04
Average	**1.46E+03**	**2.96E+03**	**8.97E+03**	**1.55E+04**	**7.81E+03**	**1.09E+04**

Table E- 13 |G*|/sin d values for Buncombe County materials, 58 °C

Frequency (Hz)	Binder		Baghouse Mastic		P#200 Mastic	
	Virgin	Aged	Virgin	Aged	Virgin	Aged
1.00E-02	2.13E+01	5.55E+01	2.63E+02	3.77E+02	1.82E+02	2.85E+02
5.00E-02	1.06E+02	2.74E+02	1.06E+03	1.57E+03	6.29E+02	9.59E+02
1.00E-01	2.12E+02	5.42E+02	1.99E+03	2.93E+03	1.23E+03	1.86E+03
1.50E-01	3.16E+02	8.04E+02	2.88E+03	4.30E+03	1.83E+03	2.75E+03
5.00E-01	1.03E+03	2.53E+03	8.90E+03	1.33E+04	5.89E+03	8.73E+03
1.00E+00	2.01E+03	4.84E+03	1.70E+04	2.53E+04	1.15E+04	1.70E+04
1.59E+00	3.12E+03	7.54E+03	2.76E+04	4.08E+04	1.78E+04	2.67E+04
5.00E+00	9.28E+03	2.08E+04	7.47E+04	1.08E+05	5.46E+04	7.68E+04
1.00E+01	1.77E+04	3.82E+04	1.39E+05	1.97E+05	1.11E+05	1.50E+05
2.00E+01	3.34E+04	6.94E+04	**	3.79E+05	2.58E+05	3.28E+05
Average	**6.72E+03**	**1.45E+04**	**3.04E+04**	**7.73E+04**	**4.63E+04**	**6.14E+04**

Table E- 14 |G*|/sin d values for Buncombe County materials, 64 °C

Frequency (Hz)	Binder		Baghouse Mastic		P#200 Mastic	
	Virgin	Aged	Virgin	Aged	Virgin	Aged
1.00E-02	9.11E+00	2.28E+01	1.23E+02	1.36E+02	9.32E+01	1.38E+02
5.00E-02	4.49E+01	1.14E+02	4.47E+02	5.97E+02	2.83E+02	4.27E+02
1.00E-01	9.00E+01	2.26E+02	8.27E+02	1.18E+03	5.30E+02	8.19E+02
1.50E-01	1.35E+02	3.37E+02	1.22E+03	1.75E+03	7.83E+02	1.21E+03
5.00E-01	4.46E+02	1.08E+03	3.67E+03	5.54E+03	2.54E+03	3.93E+03
1.00E+00	8.82E+02	2.09E+03	6.67E+03	1.05E+04	5.03E+03	7.70E+03
1.59E+00	1.35E+03	3.27E+03	1.06E+04	1.68E+04	7.86E+03	1.21E+04
5.00E+00	4.19E+03	9.20E+03	3.28E+04	4.81E+04	2.62E+04	3.68E+04
1.00E+01	8.06E+03	1.71E+04	7.87E+04	9.74E+04	6.51E+04	7.87E+04
2.00E+01	1.54E+04	3.08E+04	3.07E+05	2.50E+05	2.38E+05	1.81E+05
Average	**3.06E+03**	**6.42E+03**	**4.42E+04**	**4.32E+04**	**3.46E+04**	**3.23E+04**

Table E- 15 |G*|/sin d values for Buncombe County materials, 70 °C

Frequency (Hz)	Binder		Baghouse Mastic		P#200 Mastic	
	Virgin	Aged	Virgin	Aged	Virgin	Aged
1.00E-02	4.24E+00	9.56E+00	5.84E+01	1.07E+02	5.13E+01	6.71E+01
5.00E-02	2.05E+01	4.72E+01	1.78E+02	3.71E+02	1.48E+02	2.09E+02
1.00E-01	4.10E+01	9.46E+01	3.19E+02	6.67E+02	2.50E+02	3.77E+02
1.50E-01	6.17E+01	1.42E+02	4.70E+02	1.01E+03	3.62E+02	5.57E+02
5.00E-01	2.05E+02	4.65E+02	1.47E+03	2.76E+03	1.19E+03	1.79E+03
1.00E+00	4.09E+02	9.14E+02	2.79E+03	4.74E+03	2.38E+03	3.59E+03
1.59E+00	6.34E+02	1.44E+03	5.28E+03	8.14E+03	3.76E+03	5.69E+03
5.00E+00	1.99E+03	4.23E+03	1.98E+04	2.47E+04	1.41E+04	2.00E+04
1.00E+01	3.88E+03	8.03E+03	9.27E+04	7.10E+04	6.16E+04	5.68E+04
2.00E+01	7.57E+03	1.51E+04	4.50E+05	4.11E+05	3.31E+05	3.31E+05
Average	**1.48E+03**	**3.05E+03**	**5.73E+04**	**5.25E+04**	**4.14E+04**	**4.20E+04**

Table E- 16 |G*|cos d values for Buncombe County materials, 58 °C

Frequency (Hz)	Binder		Baghouse Mastic		P#200 Mastic	
	Virgin	Aged	Virgin	Aged	Virgin	Aged
1.00E-02	2.26E-01	6.48E-01	4.72E+01	4.81E+01	3.24E+01	4.66E+01
5.00E-02	1.31E+00	8.63E+00	1.15E+02	1.17E+02	3.47E+01	5.23E+01
1.00E-01	3.56E+00	2.63E+01	1.69E+02	1.85E+02	5.64E+01	1.02E+02
1.50E-01	6.31E+00	4.84E+01	2.18E+02	2.71E+02	8.54E+01	1.61E+02
5.00E-01	4.36E+01	2.54E+02	5.57E+02	9.76E+02	3.90E+02	7.23E+02
1.00E+00	1.21E+02	6.05E+02	1.01E+03	2.08E+03	1.06E+03	1.81E+03
1.59E+00	2.27E+02	1.09E+03	1.65E+03	3.75E+03	2.00E+03	3.46E+03
5.00E+00	9.92E+02	3.99E+03	8.53E+02	6.62E+03	1.18E+04	1.73E+04
1.00E+01	2.35E+03	8.43E+03	1.74E+04	5.50E+03	3.83E+04	4.83E+04
2.00E+01	5.56E+03	1.75E+04	**	7.60E+04	1.20E+05	1.46E+05
Average	9.31E+02	3.19E+03	2.44E+03	9.55E+03	1.74E+04	2.17E+04

Table E- 17 |G*|cos d values for Buncombe County materials, 64 °C

Frequency (Hz)	Binder		Baghouse Mastic		P#200 Mastic	
	Virgin	Aged	Virgin	Aged	Virgin	Aged
1.00E-02	3.48E-01	1.33E-01	2.71E+01	1.64E+01	2.21E+01	2.74E+01
5.00E-02	5.27E-01	1.57E+00	7.40E+01	3.93E+01	1.97E+01	2.57E+01
1.00E-01	9.81E-01	5.37E+00	1.12E+02	6.83E+01	2.38E+01	3.93E+01
1.50E-01	1.80E+00	1.05E+01	1.31E+02	8.45E+01	3.67E+01	6.15E+01
5.00E-01	1.18E+01	7.16E+01	2.06E+02	2.06E+02	1.71E+02	2.79E+02
1.00E+00	3.31E+01	1.82E+02	9.28E+01	2.89E+02	5.07E+02	7.48E+02
1.59E+00	6.72E+01	3.45E+02	4.90E+02	2.74E+02	1.10E+03	1.46E+03
5.00E+00	3.46E+02	1.40E+03	8.54E+03	5.50E+03	8.56E+03	9.35E+03
1.00E+01	8.76E+02	3.14E+03	3.56E+04	2.84E+04	3.07E+04	3.18E+04
2.00E+01	2.25E+03	6.89E+03	1.45E+05	1.20E+05	1.14E+05	8.56E+04
Average	**3.59E+02**	**1.20E+03**	**1.90E+04**	**1.54E+04**	**1.55E+04**	**1.29E+04**

Table E- 18 |G*|cos d values for Buncombe County materials, 70 °C

Frequency (Hz)	Binder		Baghouse Mastic		P#200 Mastic	
	Virgin	Aged	Virgin	Aged	Virgin	Aged
1.00E-02	1.08E-01	1.18E-01	1.66E+01	3.12E+01	1.64E+01	1.79E+01
5.00E-02	3.40E-01	4.02E-01	3.30E+01	7.81E+01	1.94E+01	2.02E+01
1.00E-01	5.40E-01	1.19E+00	4.88E+01	1.22E+02	1.63E+01	2.08E+01
1.50E-01	7.81E-01	2.45E+00	5.85E+01	1.51E+02	2.12E+01	2.93E+01
5.00E-01	3.46E+00	1.83E+01	4.62E+01	2.32E+02	1.04E+02	1.43E+02
1.00E+00	9.91E+00	5.31E+01	2.06E+02	1.41E+02	3.11E+02	4.31E+02
1.59E+00	2.22E+01	1.06E+02	7.02E+02	3.98E+02	5.23E+02	9.95E+02
5.00E+00	1.35E+02	4.93E+02	9.56E+03	8.45E+03	5.71E+03	7.94E+03
1.00E+01	3.85E+02	1.19E+03	4.06E+04	3.51E+04	2.89E+04	2.83E+04
2.00E+01	1.12E+03	2.90E+03	1.32E+05	1.59E+05	1.06E+05	1.19E+05
Average	**1.68E+02**	**4.77E+02**	**1.83E+04**	**2.04E+04**	**1.42E+04**	**1.57E+04**

Table E- 19 |G*|sin d values for Rutherford County materials, 58 °C

Frequency (Hz)	Binder		Baghouse Mastic		P#200 Mastic	
	Virgin	Aged	Virgin	Aged	Virgin	Aged
1.00E-02	1.58E+01	4.79E+01	1.61E+02	1.61E+02	***	1.14E+02
5.00E-02	7.84E+01	2.35E+02	6.13E+02	5.94E+02	***	5.03E+02
1.00E-01	1.57E+02	4.62E+02	1.20E+03	1.17E+03	***	9.87E+02
1.50E-01	2.34E+02	6.85E+02	1.79E+03	1.75E+03	***	1.46E+03
5.00E-01	7.67E+02	2.14E+03	5.76E+03	5.50E+03	***	4.65E+03
1.00E+00	1.50E+03	4.07E+03	1.12E+04	1.07E+04	***	8.97E+03
1.59E+00	2.36E+03	6.28E+03	1.70E+04	1.66E+04	***	1.41E+04
5.00E+00	6.92E+03	1.70E+04	4.96E+04	4.72E+04	***	3.96E+04
1.00E+01	1.32E+04	3.09E+04	9.18E+04	8.69E+04	***	7.54E+04
2.00E+01	2.45E+04	5.44E+04	1.67E+05	1.61E+05	***	1.36E+05
Average	**4.97E+03**	**1.16E+04**	**3.46E+04**	**3.31E+04**	*******	**2.82E+04**

Table E- 20 |G*|sin d values for Rutherford County materials, 64 °C

Frequency (Hz)	Binder		Baghouse Mastic		P#200 Mastic	
	Virgin	Aged	Virgin	Aged	Virgin	Aged
1.00E-02	6.96E+00	1.94E+01	8.49E+01	7.91E+01	3.69E+01	5.83E+01
5.00E-02	3.38E+01	9.63E+01	2.71E+02	2.63E+02	1.46E+02	2.31E+02
1.00E-01	6.78E+01	1.93E+02	5.15E+02	4.99E+02	2.81E+02	4.44E+02
1.50E-01	1.02E+02	2.88E+02	7.65E+02	7.43E+02	4.20E+02	6.60E+02
5.00E-01	3.35E+02	9.25E+02	2.47E+03	2.41E+03	1.36E+03	2.15E+03
1.00E+00	6.63E+02	1.78E+03	4.83E+03	4.71E+03	2.73E+03	4.12E+03
1.59E+00	1.05E+03	2.76E+03	7.51E+03	7.36E+03	4.10E+03	6.68E+03
5.00E+00	3.14E+03	7.83E+03	2.27E+04	2.18E+04	1.27E+04	1.96E+04
1.00E+01	6.04E+03	1.45E+04	4.22E+04	4.04E+04	2.40E+04	3.61E+04
2.00E+01	1.15E+04	2.64E+04	8.08E+04	7.59E+04	4.34E+04	6.70E+04
Average	**2.29E+03**	**5.48E+03**	**1.62E+04**	**1.54E+04**	**8.91E+03**	**1.37E+04**

Table E- 21|G*|sin d values for Rutherford County materials, 70 °C

Frequency (Hz)	Binder		Baghouse Mastic		P#200 Mastic	
	Virgin	Aged	Virgin	Aged	Virgin	Aged
1.00E-02	3.29E+00	8.24E+00	4.14E+01	4.21E+01	2.07E+01	3.52E+01
5.00E-02	1.65E+01	4.02E+01	1.35E+02	1.29E+02	7.30E+01	1.29E+02
1.00E-01	3.29E+01	8.11E+01	2.30E+02	2.24E+02	1.27E+02	2.47E+02
1.50E-01	4.95E+01	1.21E+02	3.37E+02	3.27E+02	1.85E+02	3.60E+02
5.00E-01	1.64E+02	3.98E+02	1.10E+03	1.07E+03	6.08E+02	1.17E+03
1.00E+00	3.27E+02	7.81E+02	2.17E+03	2.09E+03	1.21E+03	2.33E+03
1.59E+00	5.15E+02	1.22E+03	3.22E+03	3.14E+03	1.39E+03	3.48E+03
5.00E+00	1.58E+03	3.56E+03	1.01E+04	1.01E+04	5.89E+03	1.09E+04
1.00E+01	3.07E+03	6.72E+03	1.89E+04	2.00E+04	1.09E+04	2.07E+04
2.00E+01	5.87E+03	1.24E+04	3.57E+04	3.50E+04	1.98E+04	3.78E+04
Average	**1.16E+03**	**2.54E+03**	**7.19E+03**	**7.23E+03**	**4.02E+03**	**7.71E+03**

Table E- 22 |G*|/sin d values for Rutherford County materials, 58 °C

Frequency (Hz)	Binder		Baghouse Mastic		P#200 Mastic	
	Virgin	Aged	Virgin	Aged	Virgin	Aged
1.00E-02	1.58E+01	4.79E+01	1.65E+02	1.64E+02	***	1.14E+02
5.00E-02	7.84E+01	2.35E+02	6.14E+02	5.95E+02	***	5.03E+02
1.00E-01	1.57E+02	4.64E+02	1.21E+03	1.17E+03	***	9.88E+02
1.50E-01	2.34E+02	6.88E+02	1.80E+03	1.75E+03	***	1.47E+03
5.00E-01	7.68E+02	2.17E+03	5.79E+03	5.53E+03	***	4.68E+03
1.00E+00	1.51E+03	4.13E+03	1.13E+04	1.08E+04	***	9.09E+03
1.59E+00	2.37E+03	6.42E+03	1.73E+04	1.69E+04	***	1.44E+04
5.00E+00	6.99E+03	1.77E+04	5.27E+04	5.07E+04	***	4.35E+04
1.00E+01	1.34E+04	3.25E+04	1.09E+05	1.06E+05	***	8.97E+04
2.00E+01	2.52E+04	5.83E+04	2.60E+05	2.56E+05	***	2.57E+05
Average	**5.07E+03**	**1.23E+04**	**4.60E+04**	**4.50E+04**	*****	**4.21E+04**

Table E- 23 |G*|/sin d values for Rutherford County materials, 64 °C

Frequency (Hz)	Binder		Baghouse Mastic		P#200 Mastic	
	Virgin	Aged	Virgin	Aged	Virgin	Aged
1.00E-02	6.96E+00	1.94E+01	8.87E+01	8.26E+01	3.77E+01	5.91E+01
5.00E-02	3.39E+01	9.63E+01	2.72E+02	2.64E+02	1.47E+02	2.32E+02
1.00E-01	6.78E+01	1.93E+02	5.16E+02	4.99E+02	2.81E+02	4.44E+02
1.50E-01	1.02E+02	2.88E+02	7.66E+02	7.44E+02	4.21E+02	6.60E+02
5.00E-01	3.35E+02	9.29E+02	2.48E+03	2.42E+03	1.37E+03	2.16E+03
1.00E+00	6.64E+02	1.80E+03	4.89E+03	4.77E+03	2.78E+03	4.19E+03
1.59E+00	1.05E+03	2.79E+03	7.67E+03	7.53E+03	4.24E+03	6.81E+03
5.00E+00	3.16E+03	8.02E+03	2.54E+04	2.44E+04	1.63E+04	2.19E+04
1.00E+01	6.11E+03	1.50E+04	6.40E+04	6.04E+04	5.38E+04	5.90E+04
2.00E+01	1.18E+04	2.77E+04	2.05E+05	2.12E+05	3.03E+05	2.18E+05
Average	**2.33E+03**	**5.68E+03**	**3.11E+04**	**3.13E+04**	**3.83E+04**	**3.14E+04**

Table E- 24 |G*|/sin d values for Rutherford County materials, 70 °C

Frequency (Hz)	Binder		Baghouse Mastic		P#200 Mastic	
	Virgin	Aged	Virgin	Aged	Virgin	Aged
1.00E-02	3.29E+00	8.25E+00	4.53E+01	4.64E+01	2.11E+01	3.59E+01
5.00E-02	1.65E+01	4.02E+01	1.37E+02	1.30E+02	7.35E+01	1.29E+02
1.00E-01	3.29E+01	8.12E+01	2.31E+02	2.25E+02	1.27E+02	2.47E+02
1.50E-01	4.95E+01	1.21E+02	3.38E+02	3.28E+02	1.86E+02	3.61E+02
5.00E-01	1.64E+02	3.99E+02	1.11E+03	1.08E+03	6.18E+02	1.18E+03
1.00E+00	3.28E+02	7.84E+02	2.23E+03	2.15E+03	1.28E+03	2.38E+03
1.59E+00	5.15E+02	1.22E+03	3.41E+03	3.30E+03	1.63E+03	3.70E+03
5.00E+00	1.59E+03	3.62E+03	1.56E+04	1.34E+04	1.16E+04	1.59E+04
1.00E+01	3.10E+03	6.88E+03	6.07E+04	4.43E+04	7.85E+04	4.68E+04
2.00E+01	6.02E+03	1.30E+04	3.59E+05	3.22E+05	5.09E+05	2.73E+05
Average	**1.18E+03**	**2.61E+03**	**4.42E+04**	**3.87E+04**	**6.03E+04**	**3.44E+04**

Table E- 25 |G*|cos d values for Rutherford County materials, 58 °C

Frequency (Hz)	Binder		Baghouse Mastic		P#200 Mastic	
	Virgin	Aged	Virgin	Aged	Virgin	Aged
1.00E-02	2.62E-01	6.17E-01	2.47E+01	2.26E+01	***	7.31E+00
5.00E-02	6.74E-01	7.60E+00	2.50E+01	2.30E+01	***	1.33E+01
1.00E-01	2.43E+00	2.33E+01	4.73E+01	4.55E+01	***	3.78E+01
1.50E-01	4.62E+00	4.23E+01	7.72E+01	7.22E+01	***	6.73E+01
5.00E-01	3.04E+01	2.20E+02	3.97E+02	4.21E+02	***	3.75E+02
1.00E+00	8.49E+01	5.27E+02	1.10E+03	1.15E+03	***	1.04E+03
1.59E+00	1.61E+02	9.31E+02	2.10E+03	2.16E+03	***	1.92E+03
5.00E+00	7.18E+02	3.36E+03	1.25E+04	1.29E+04	***	1.23E+04
1.00E+01	1.70E+03	7.07E+03	3.93E+04	4.10E+04	***	3.29E+04
2.00E+01	4.06E+03	1.45E+04	1.25E+05	1.24E+05	***	1.28E+05
Average	**6.76E+02**	**2.67E+03**	**1.80E+04**	**1.82E+04**	*******	**1.77E+04**

Table E- 26 |G*|cos d values for Rutherford County materials, 64 °C

Frequency (Hz)	Binder		Baghouse Mastic		P#200 Mastic	
	Virgin	Aged	Virgin	Aged	Virgin	Aged
1.00E-02	9.46E-02	1.92E-01	1.81E+01	1.67E+01	5.59E+00	6.64E+00
5.00E-02	3.31E-01	1.53E+00	1.66E+01	1.42E+01	8.65E+00	7.70E+00
1.00E-01	5.89E-01	5.08E+00	2.00E+01	1.88E+01	1.02E+01	1.40E+01
1.50E-01	1.29E+00	1.02E+01	3.13E+01	3.08E+01	1.69E+01	2.32E+01
5.00E-01	8.32E+00	6.24E+01	1.69E+02	1.73E+02	1.10E+02	1.65E+02
1.00E+00	2.32E+01	1.60E+02	5.48E+02	5.24E+02	3.59E+02	5.46E+02
1.59E+00	4.96E+01	2.99E+02	1.10E+03	1.12E+03	7.56E+02	9.47E+02
5.00E+00	2.60E+02	1.20E+03	7.84E+03	7.58E+03	6.81E+03	6.65E+03
1.00E+01	6.78E+02	2.66E+03	3.03E+04	2.85E+04	2.67E+04	2.87E+04
2.00E+01	1.85E+03	5.78E+03	1.00E+05	1.02E+05	1.06E+05	1.01E+05
Average	**2.87E+02**	**1.02E+03**	**1.40E+04**	**1.40E+04**	**1.41E+04**	**1.38E+04**

Table E- 27 |G*|cos d values for Rutherford County materials, 70 °C

Frequency (Hz)	Binder		Baghouse Mastic		P#200 Mastic	
	Virgin	Aged	Virgin	Aged	Virgin	Aged
1.00E-02	6.13E-02	8.51E-02	1.26E+01	1.34E+01	2.78E+00	4.73E+00
5.00E-02	2.08E-01	3.10E-01	1.70E+01	1.29E+01	5.89E+00	5.07E+00
1.00E-01	2.73E-01	1.01E+00	1.39E+01	1.24E+01	6.17E+00	7.62E+00
1.50E-01	5.18E-01	2.12E+00	1.73E+01	1.73E+01	9.72E+00	1.23E+01
5.00E-01	2.46E+00	1.60E+01	9.88E+01	1.03E+02	7.80E+01	1.03E+02
1.00E+00	7.19E+00	4.69E+01	3.52E+02	3.40E+02	2.94E+02	3.59E+02
1.59E+00	1.65E+01	9.14E+01	7.69E+02	7.07E+02	5.69E+02	8.63E+02
5.00E+00	1.04E+02	4.32E+02	7.42E+03	5.74E+03	5.82E+03	7.39E+03
1.00E+01	2.93E+02	1.05E+03	2.81E+04	2.20E+04	2.71E+04	2.32E+04
2.00E+01	9.25E+02	2.58E+03	1.07E+05	1.00E+05	9.83E+04	9.43E+04
Average	**1.35E+02**	**4.22E+02**	**1.44E+04**	**1.29E+04**	**1.32E+04**	**1.26E+04**

Appendix F

Mobilized Interfacial Shear Stresses

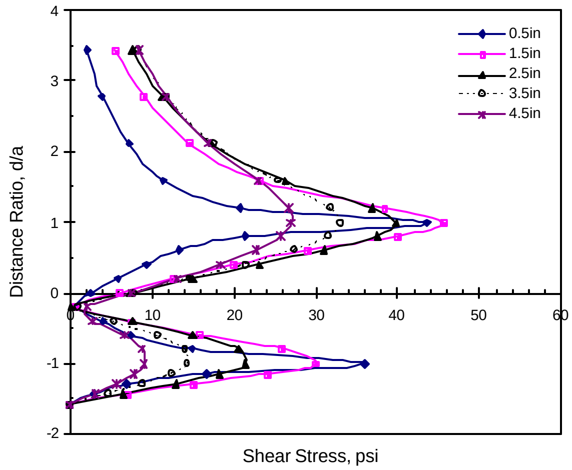

(a) Shear distribution along axle for vertical load with zero horizontal shear

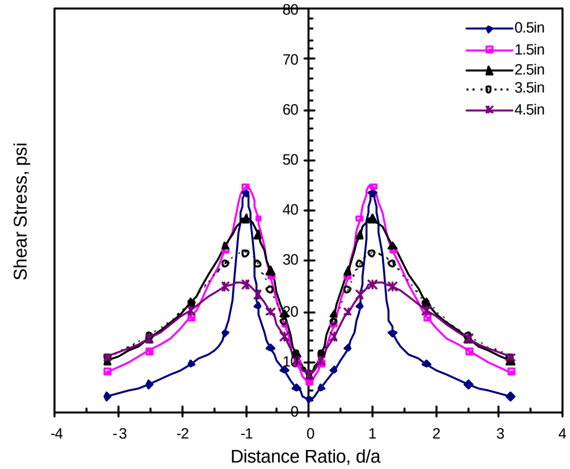

(b) Shear distribution perpendicular to axle for vertical load with zero horizontal shear

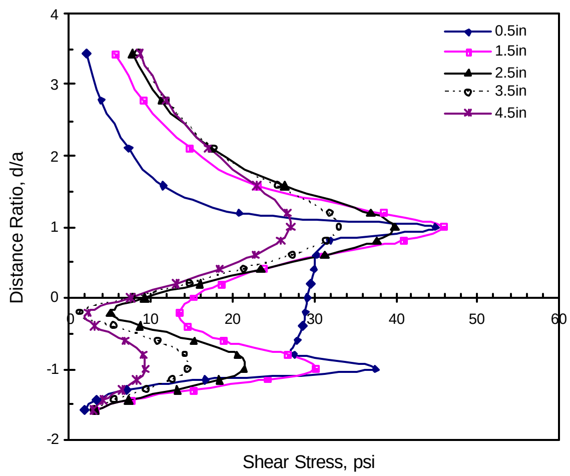

(c) Shear distribution along axle for vertical load with 40% horizontal shear

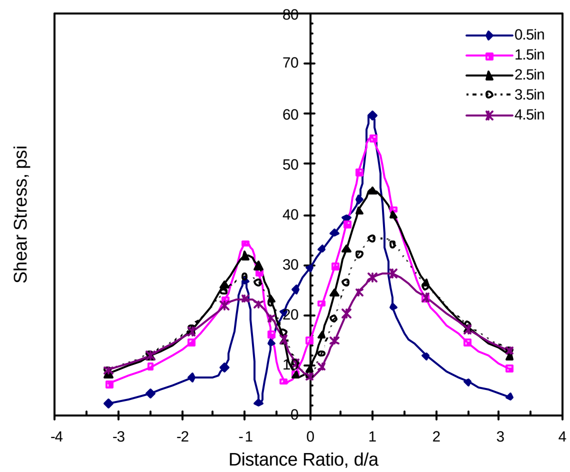

(d) Shear distribution perpendicular to axle for vertical load with 40% horizontal shear

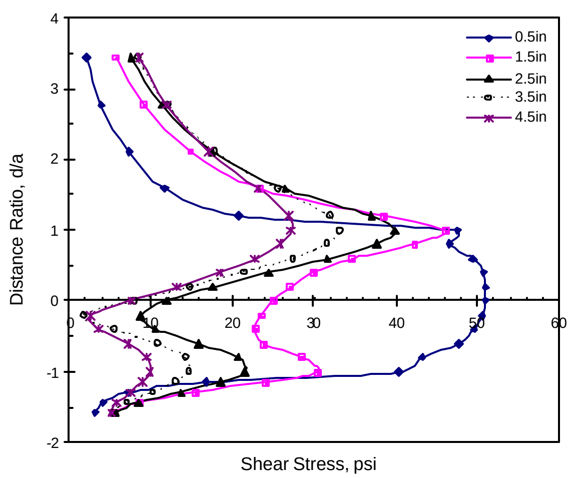

(e) Shear distribution along axle for vertical load with 70% horizontal shear

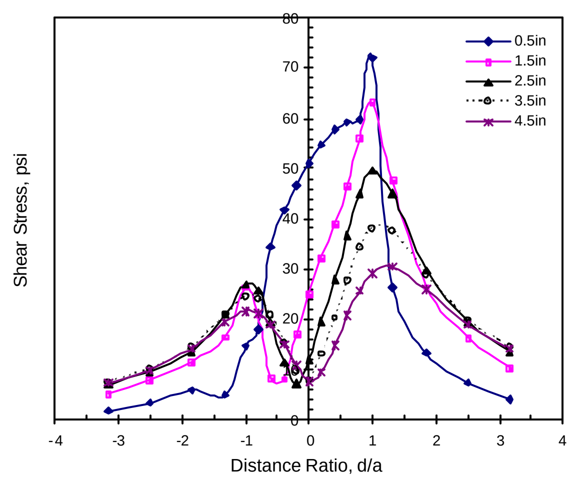

(f) Shear distribution perpendicular to axle for vertical load with 70% horizontal shear

Figure F-1(a-f) Mobilized interfacial shear stresses for AC-AC combination at 20 °C

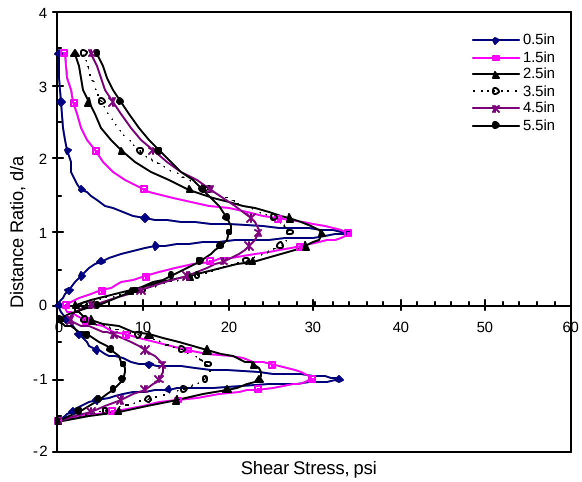

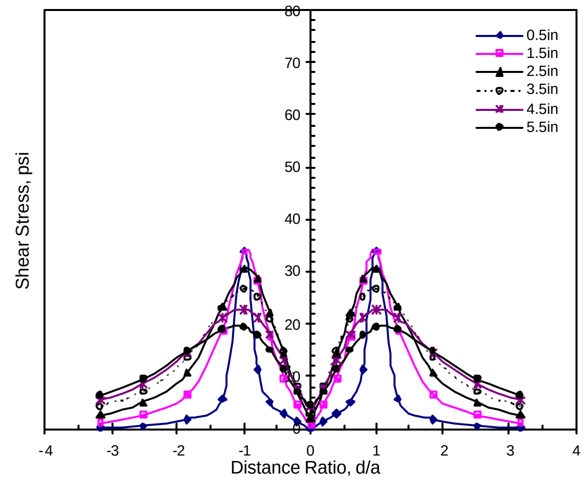

(a) Shear distribution along axle for vertical load with zero horizontal shear

(b) Shear distribution perpendicular to axle for vertical load with zero horizontal shear

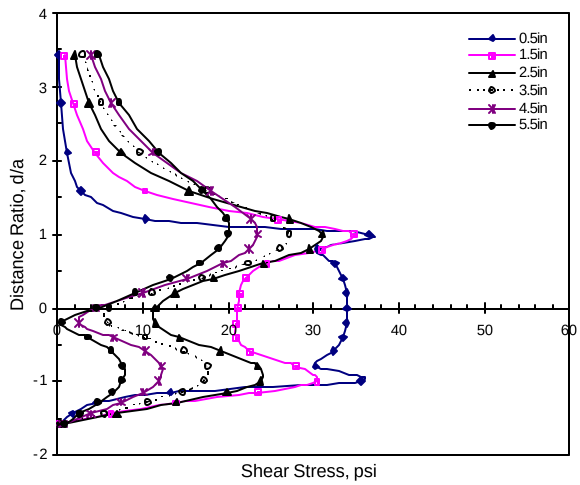

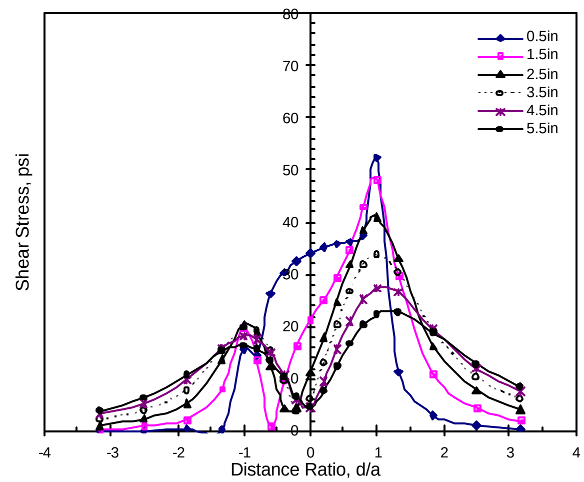

(c) Shear distribution along axle for vertical load with 40% horizontal shear

(d) Shear distribution perpendicular to axle for vertical load with 40% horizontal shear

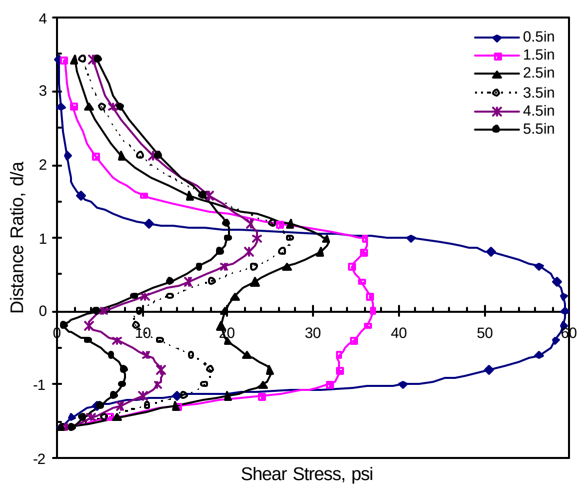

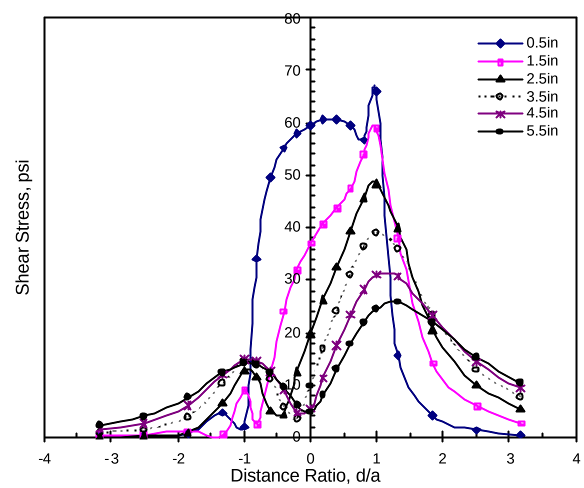

(e) Shear distribution along axle for vertical load with 70% horizontal shear

(f) Shear distribution perpendicular to axle for vertical load with 70% horizontal shear

Figure F-2(a-f) Mobilized interfacial shear stresses for AC-AC, high temp.

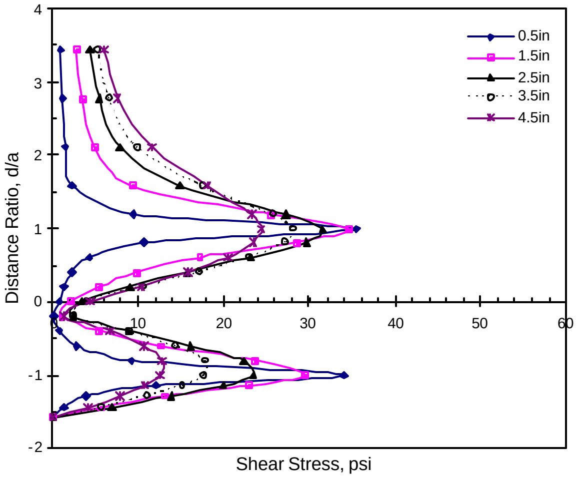

(a) Shear distribution along axle for vertical load with zero horizontal shear

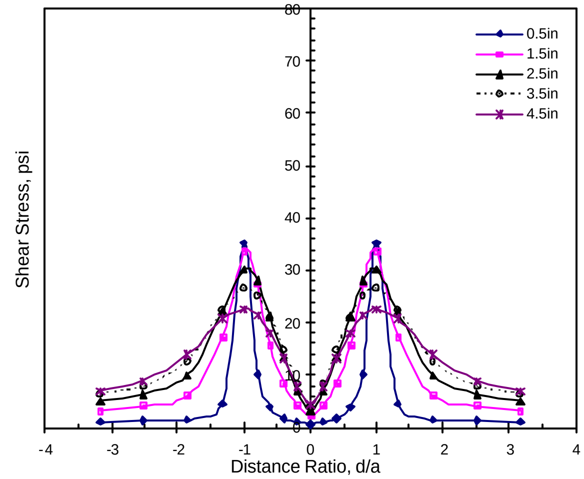

(b) Shear distribution perpendicular to axle for vertical load with zero horizontal shear

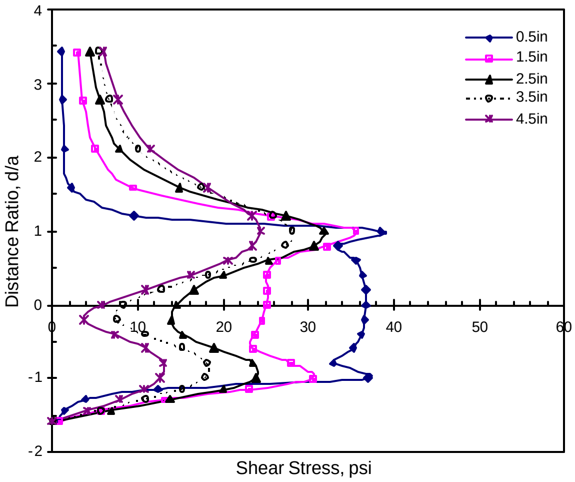

(c) Shear distribution along axle for vertical load with 40% horizontal shear

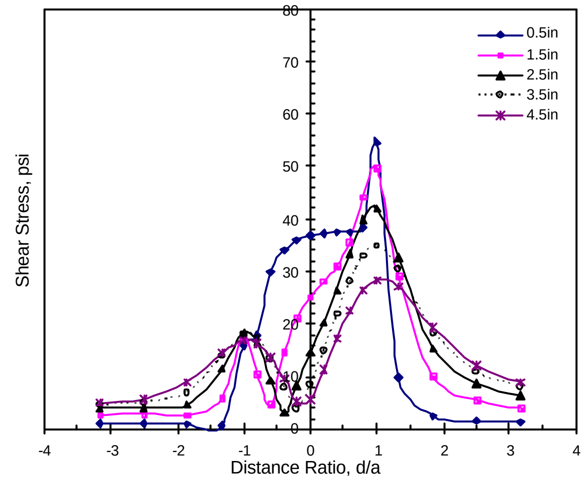

(d) Shear distribution perpendicular to axle for vertical load with 40% horizontal shear

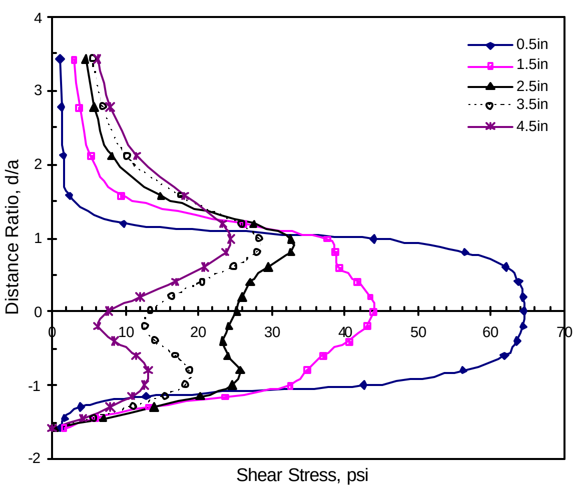

(e) Shear distribution along axle for vertical load with 70% horizontal shear

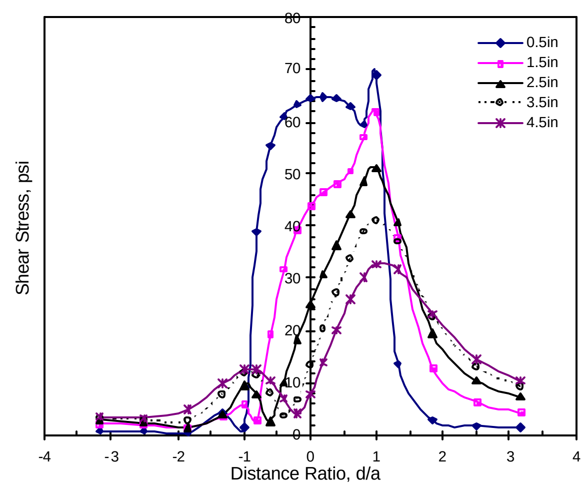

(f) Shear distribution perpendicular to axle for vertical load with 70% horizontal shear

Figure F-3(a-f) Mobilized interfacial shear stresses for PCC-AC, 20 °C

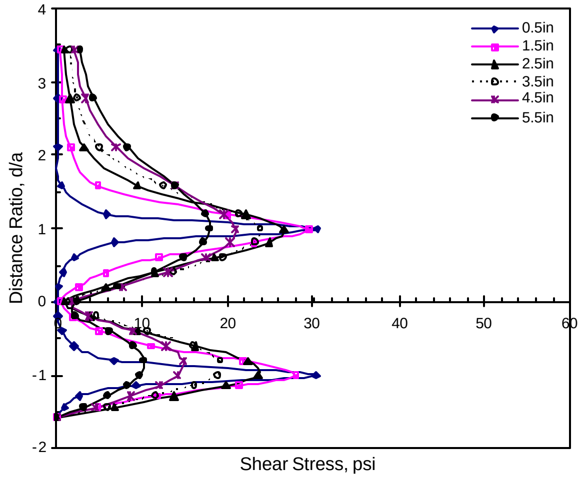

(a) Shear distribution along axle for vertical load with zero horizontal shear

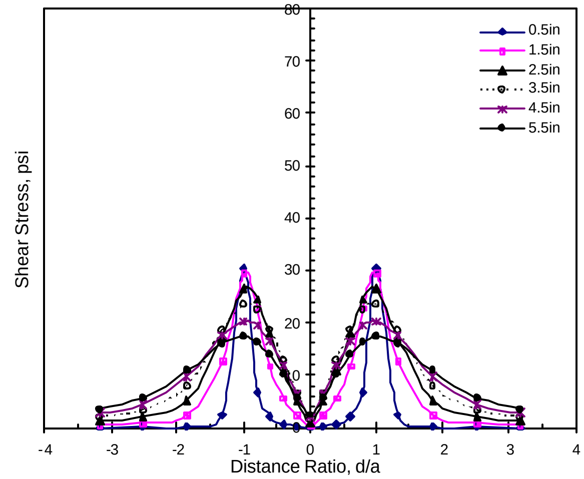

(b) Shear distribution perpendicular to axle for vertical load with zero horizontal shear

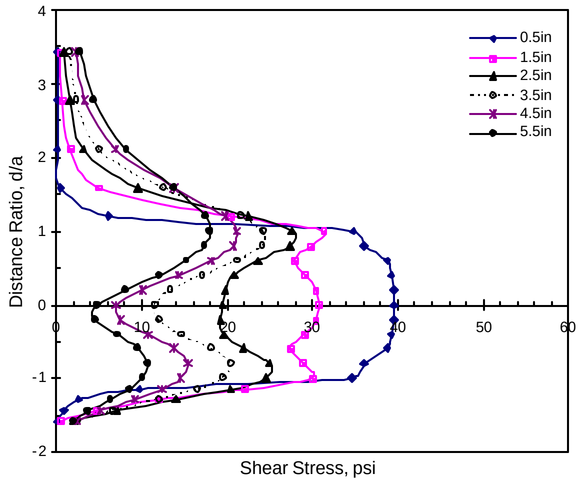

(c) Shear distribution along axle for vertical load with 40% horizontal shear

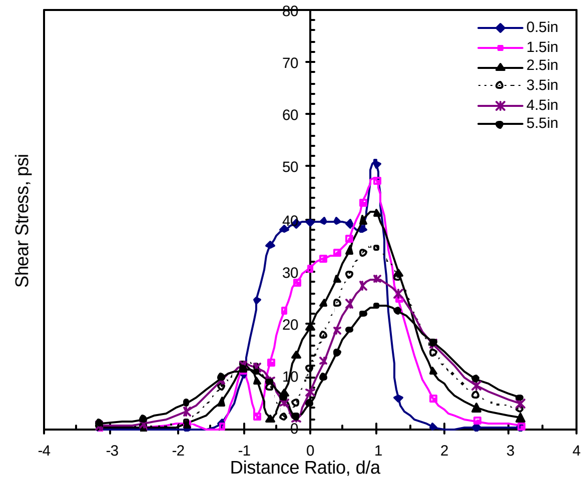

(d) Shear distribution perpendicular to axle for vertical load with 40% horizontal shear

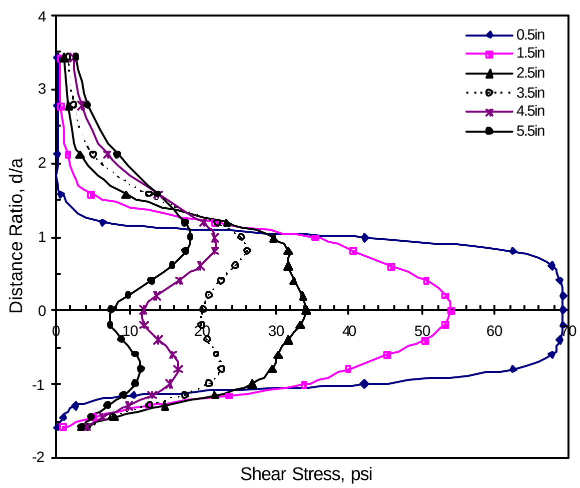

(e) Shear distribution along axle for vertical load with 70% horizontal shear

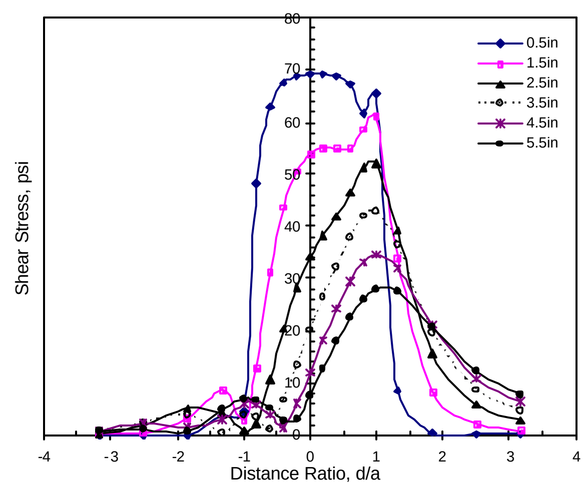

(f) Shear distribution perpendicular to axle for vertical load with 70% horizontal shear

Figure F-4 (a-f) Mobilized interfacial shear stresses for PCC-AC, high temp.

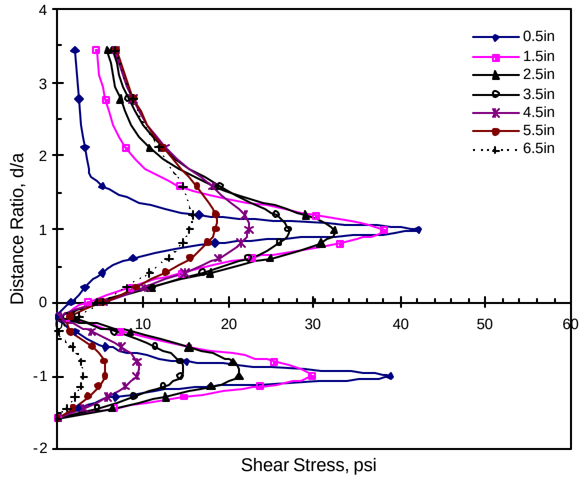

(a) Shear distribution along axle for vertical load with zero horizontal shear

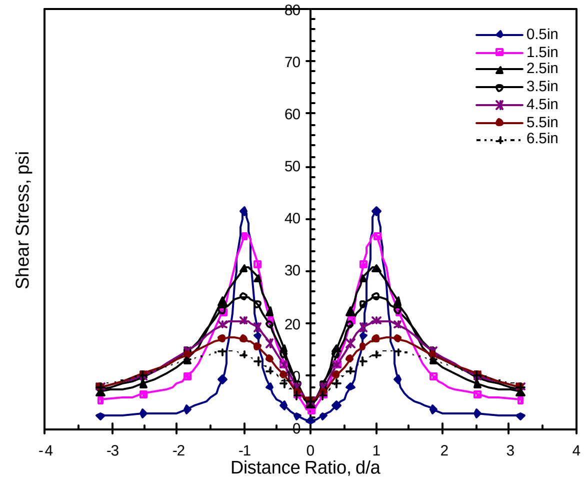

(b) Shear distribution perpendicular to axle for vertical load with zero horizontal shear

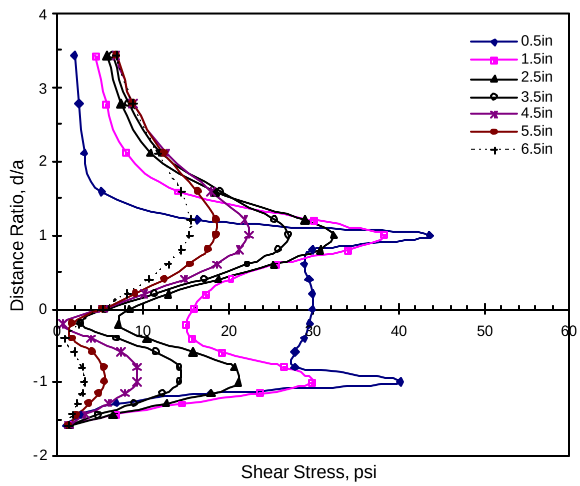

(c) Shear distribution along axle for vertical load with 40% horizontal shear

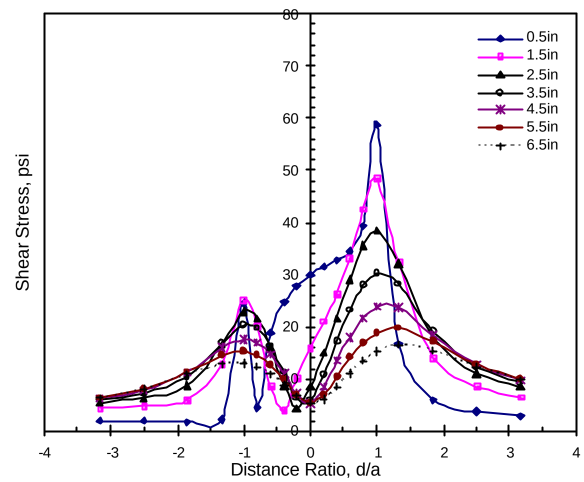

(d) Shear distribution perpendicular to axle for vertical load with 40% horizontal shear

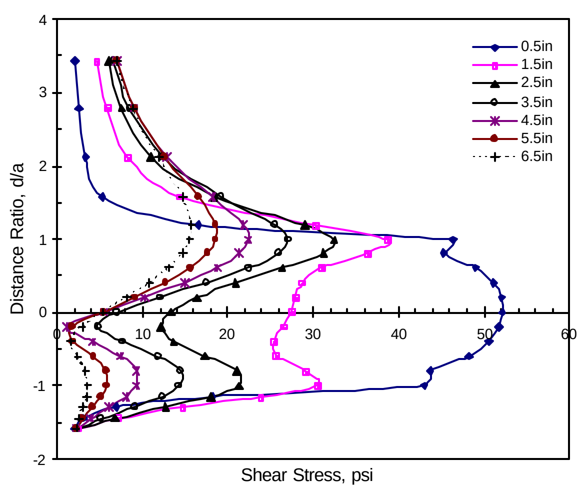

(e) Shear distribution along axle for vertical load with 70% horizontal shear

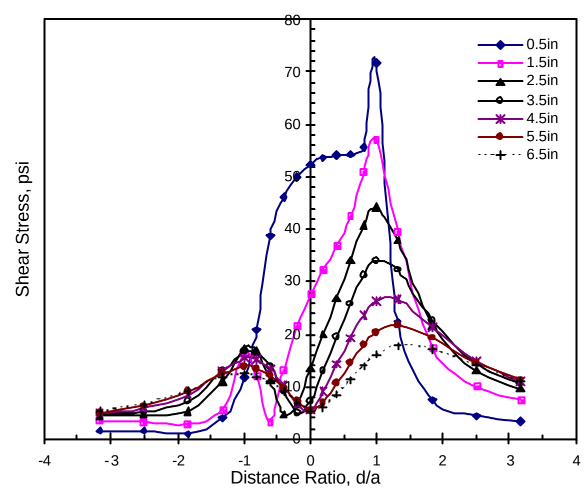

(f) Shear distribution perpendicular to axle for vertical load with 70% horizontal shear

Figure F-5(a-f) Mobilized interfacial shear stresses for CTB-AC, 20 °C

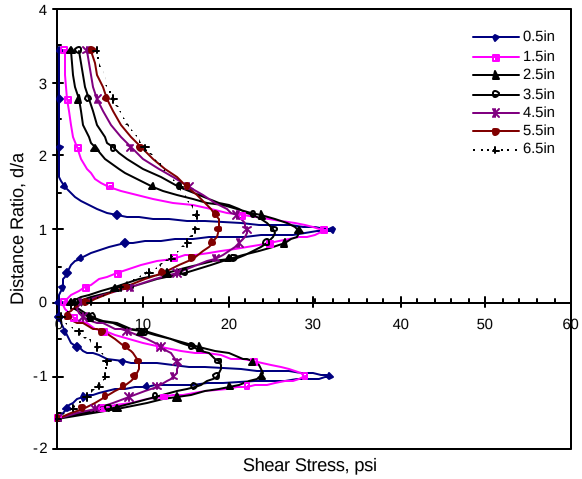

(a) Shear distribution along axle for vertical load with zero horizontal shear

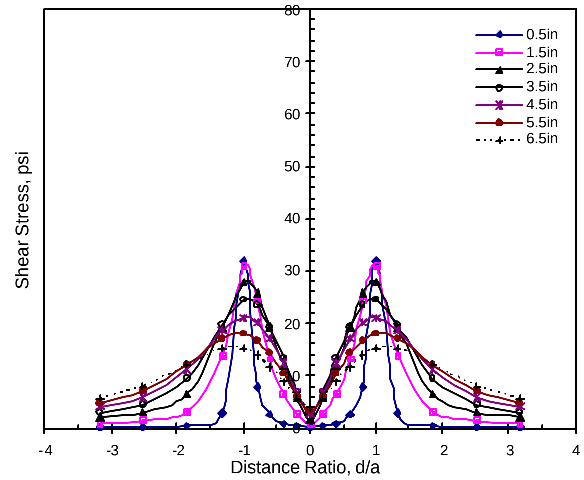

(b) Shear distribution perpendicular to axle for vertical load with zero horizontal shear

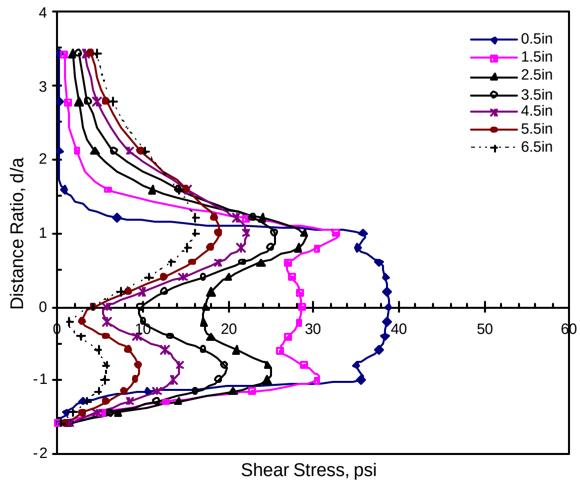

(c) Shear distribution along axle for vertical load with 40% horizontal shear

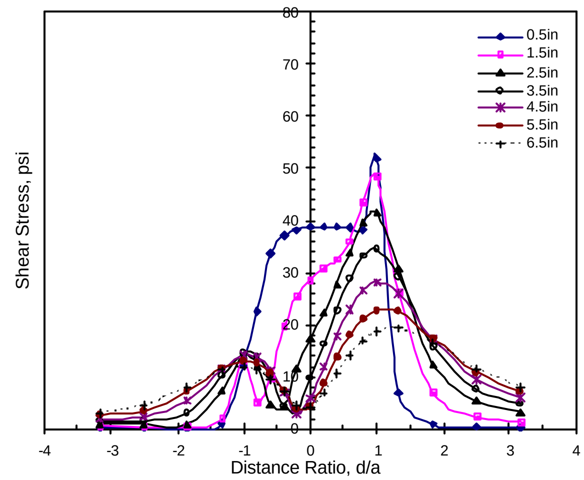

(d) Shear distribution perpendicular to axle for vertical load with 40% horizontal shear

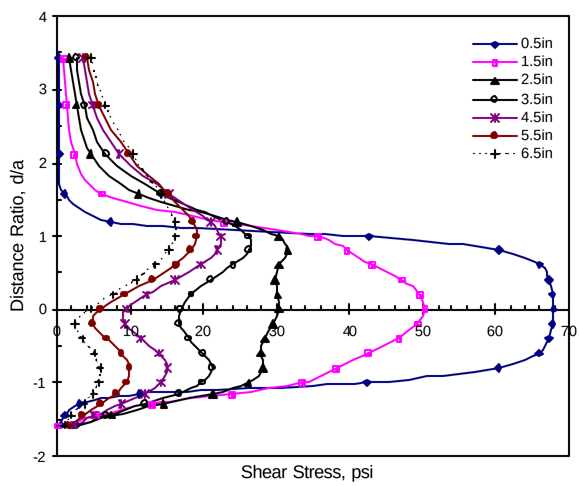

(e) Shear distribution along axle for vertical load with 70% horizontal shear

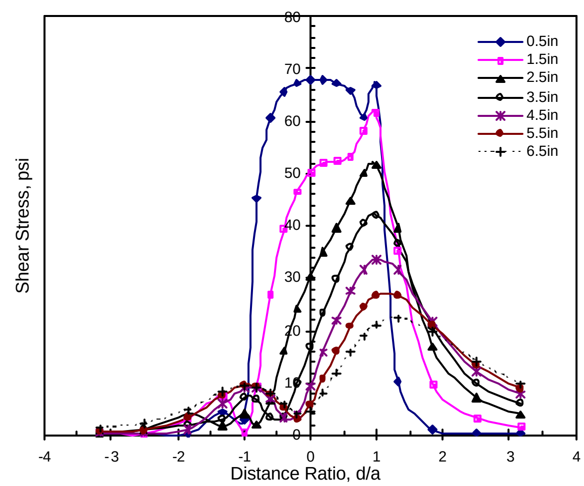

(f) Shear distribution perpendicular to axle for vertical load with 70% horizontal shear

Figure F-6(a-f) Mobilized interfacial shear stresses for CTB-AC, high temp.

Appendix G

Finite Layer Analysis of Stresses in Pavements

FLA: A Computer Program for Analysis of Stresses in Pavements

G1. Introduction

A computer program FLA is developed for the analysis of stresses in pavement subjected to a set of vehicle loads. The materials in the pavement layers are treated as either isotropic or cross-anisotropic elastic. Both the normal and shear loading uniformly distributed over a circular contact area on the pavement surface caused by vehicle tires can be handled.

The formulation underlying FLA is based on finite layer analysis of a layered system by Small and Booker [39, 40]. The program is menu-driven and written in FORTRAN 77 and JAVA v1.2.2, which may be run on a variety of microcomputers.

G2. Installation and Start-Up Procedures

Minimum System Requirements for Windows 98/2000/XP/NT

- IBM compatible computer with 66MHz 486 processor or higher
- Double-speed CD-ROM drive
- VGA color monitor, 256 colors
- 8 MB RAM
- 22 MB hard drive space

Installing the CD-ROM for Windows 98/2000/XP/NT

Insert CD into CD-ROM drive.
The installation will start automatically.
Follow on-screen instructions to complete installation.

The CD-ROM also contains the complete FLA manual in PDF form. The online manual can be accessed directly from the CD-ROM, or it can be copied to another location.

Start Up

The default installation procedure creates an icon for FLA on the desktop. To load FLA, just simply double-click that icon.

G3. Guide User Interface (GUI)

The GUI includes 5 menus: File, Input, Computation, Graphic and Help. The menus may be accessed by

1. Pressing the ALT key and the underlined letter of the menu option or
2. By positioning the mouse track over the menu item and clicking the left mouse button.

You can then select an item on the drop-down menu by either typing the underlined letter for the menu selection (do not press Alt this time), or by clicking on the selection with the mouse.

Once you have opened one of the menus, you can use the right arrow and left arrow keys to move between them. Some of the menu selections may not be available at a given time; these will be shown in gray lettering.

For new users, the following steps are the common steps taken for basic analysis.

Step 1: Select the menu item *General Information* in *Input menu*, input date required.

Step 2: Enter the *Loads*

Step 3: Enter *Layer Properties*

Step 4: Enter *Output Positions* on x-y plane

Step 5: Enter *Depths* which are of interest

Step 6: Enter *Specify Integration* scheme if it is enabled

Step 7: Save the file

Step 8: *Run Analysis*. If any errors are detected by the program, the user should follow the directions shown in the message box to correct the input data.

Step 9: Presentation to the user about computed results. The graphs available under the *Graphics Menu* are provided to aid user in analysis or design.

Detailed information about each menu is stated below.

G3.1 File Menu

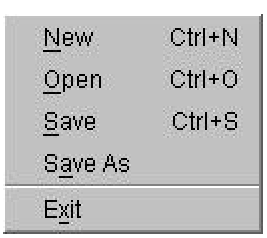

The File Menu pull-down menu controls the commands for file operations. The File Menu options are:

New: To create a new data file. This command closes any open data file and allows you to start entering data for a new file. This file is not actually created until you issue the Save command.

Open: To read a data file from a disk. This command allows the user to enter the name of an existing data to be read for editing. This option will replace any data in the editor with the new data obtained from the input file. If the input file is of inappropriate format, then an error message will pop out.

Save: To save the current data. This command saves any edits to the existing data to the current file if a file with the current file name exists. Otherwise, a Save As dialog box will appear to ask you to type file name. Only file name without extension is needed, an extension *.dat will be automatically added to the file name.

Please note that before performing an analysis, program will ask you to save the current data if it is not saved, or it will automatically save the current file again if it exists.

Save As: To save the current data under a new name. This command writes the data to a new file or overwrites any specified existing file. The user enters the file name to be saved in the Save As dialog box. Only file name without extension is needed, an extension *.dat will be automatically added to the file name.

Exit: To quit the program.

G3.2 INPUT MENU

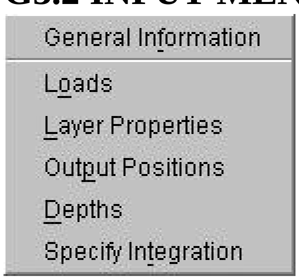

All data to the program is entered by using the program's inbuilt dialog box. For data input, a dialog box is displayed indicating the various items of input data required. If the data is to be read from the screen, valid values must be given. Checking of the data is carried out. For instance, it is not possible to type any characters except numbers, decimal points, plus and minus signs and the exponential symbol E or e. Real numbers may be entered in fixed point format (e.g. 1.20) or in exponential format (e.g. 9.60e5). If you type a character instead of a number, then error message will show up. If no input file is open, only *General Information* menu item will be enabled in the *Input Menu* and only after valid values are typed through General Information dialog box, the other menu items will be activated.

G3.2.1 General Information

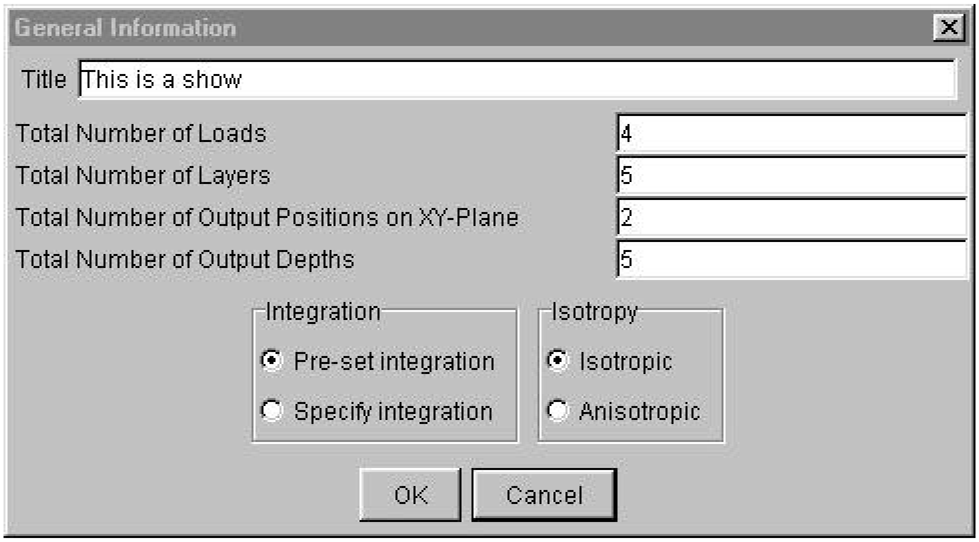

The data entered in the dialog box for General Information are:

Title: Any title or comment can be typed on this line.

Number of Loads : Enter the number of circular loadings. The maximum allowable number of loadings is 10.

Number of Layers : Enter the number of layers. The maximum allowable number of layers is 10.

Number of Output Positions : Enter the number of positions at which response is to be calculated. These are x-y positions. The response is about the stress-strain-displacement at points locating along a line vertically beneath the x-y position. If the output positions with total number greater than two are all on a line parallel to x-axis (y-axis) , then stress-strain-displacement at certain depth along this line can be plotted. Refer to *Horizontal Section*. The maximum allowable number of output positions is 20.

Number of Output Depths : Enter the number of vertical coordinates at which responses are to be computed. The maximum allowable number of output depths is 20.

Integration: Numerical integration is used within the program to obtain the solution. A pre-set integration scheme is provided, which should produce reasonably accurate results, however there may be some cases where the integration scheme needs to be altered. In this case the user needs to enter the appropriate integration scheme by trial-and-error method to get reasonable results.

Isotropy: Select "Isotropic" if material is isotropic, select "Anisotropic" if material is cross-anisotropic. For isotropic material the Young's modulus and Poisson's ratio only is required, while for cross-anisotropic material, two elastic moduli, two Poisson's ratios and a shear modulus are required.

G3.2.2 Loads

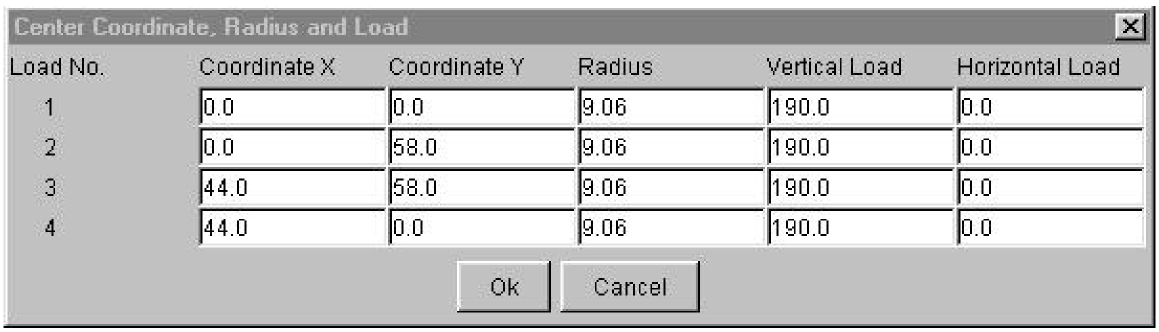
Center Coordinate, Radius and Load

Load No.	Coordinate X	Coordinate Y	Radius	Vertical Load	Horizontal Load
1	0.0	0.0	9.06	190.0	0.0
2	0.0	58.0	9.06	190.0	0.0
3	44.0	58.0	9.06	190.0	0.0
4	44.0	0.0	9.06	190.0	0.0

Ok Cancel

The data entered in the dialog box for load configuration is:

Coordinate X: The x-coordinate of the center of the circular loading.

Coordinate Y: The y-coordinate of the center of the circular loading.

Radius: The radius of the circular loading.

Vertical load: Vertical uniform pressure distributed over the circular area.

Horizontal load: Horizontal uniform pressure distributed over the circular area.

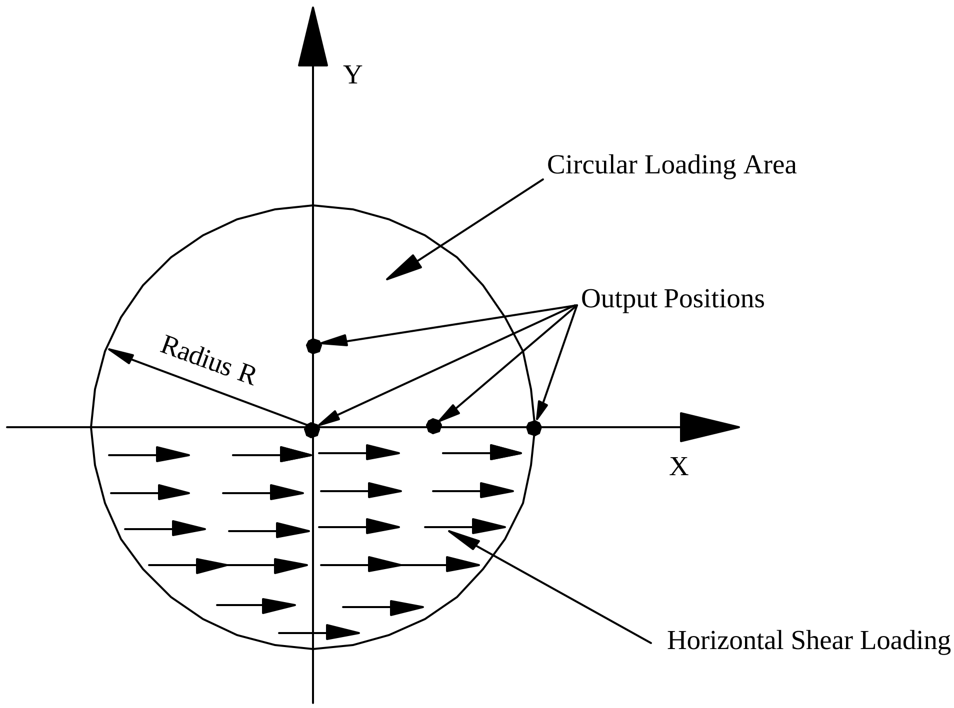

Figure G1. Surface loading shape

G3.2.3 Layer Properties

If in General Information dialog box "Isotropic" is selected, the following dialog box will pop out when clicking Layer Properties menu item.

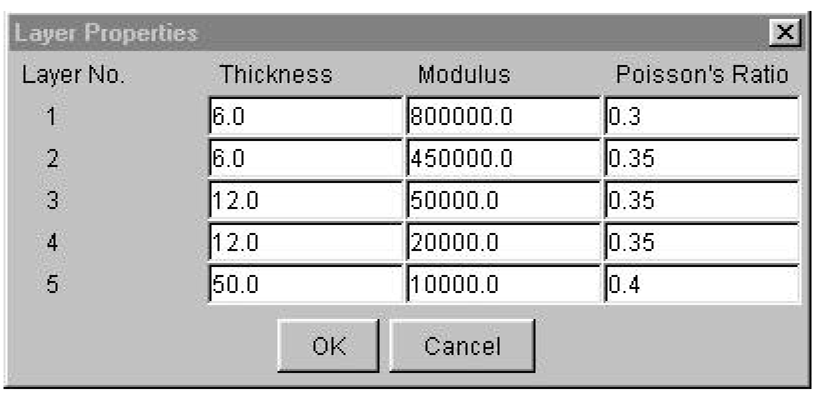
Layer Properties

Layer No.	Thickness	Modulus	Poisson's Ratio
1	6.0	800000.0	0.3
2	6.0	450000.0	0.35
3	12.0	50000.0	0.35
4	12.0	20000.0	0.35
5	50.0	10000.0	0.4

OK Cancel

In this dialog box, three values are entered by the user. They are:

Thickness: The thickness of each layer.

Modulus: The Young's modulus *E* of each layer.

Poisson's Ratio: The Poisson's ratio v of each layer.

If in General Information dialog box "Anisotropic" is selected, which means that the material is cross-anisotropic, the following dialog box will show up when clicking Layer Properties menu item.

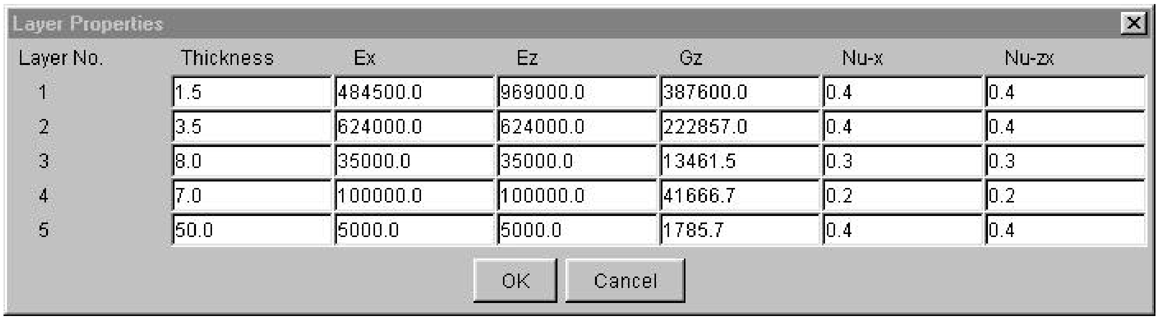

Layer No.	Thickness	Ex	Ez	Gz	Nu-x	Nu-zx
1	1.5	484500.0	969000.0	387600.0	0.4	0.4
2	3.5	624000.0	624000.0	222857.0	0.4	0.4
3	8.0	35000.0	35000.0	13461.5	0.3	0.3
4	7.0	100000.0	100000.0	41666.7	0.2	0.2
5	50.0	5000.0	5000.0	1785.7	0.4	0.4

Values required to be entered are:

Thickness: The thickness of each layer.

Ex: The modulus of elasticity in the horizontal direction E_h. Here the horizontal direction is the x-y plane.

Ez: The modulus of elasticity in the vertical direction E_v.

Nu-x: Poisson's ratio ν_h giving the effect of horizontal strain on complimentary horizontal strain.

Nu-zx: Poisson's ratio ν_{vh} giving the effect of vertical strain on horizontal strain.

Gz: Shear modulus as defined by the equation $\tau = G_v \gamma_{hv}$.

Please note that the following relationship exists:

$$\frac{E_h}{E_v} = \frac{\nu_{hv}}{\nu_{vh}}$$

ν_{hv} is the Poisson's ratio giving the effect of horizontal strain on vertical strain.

The cross-anisotropic properties so selected must satisfy condition as

$$1 - \nu_h - 2\nu_{hv}\nu_{vh} > 0$$

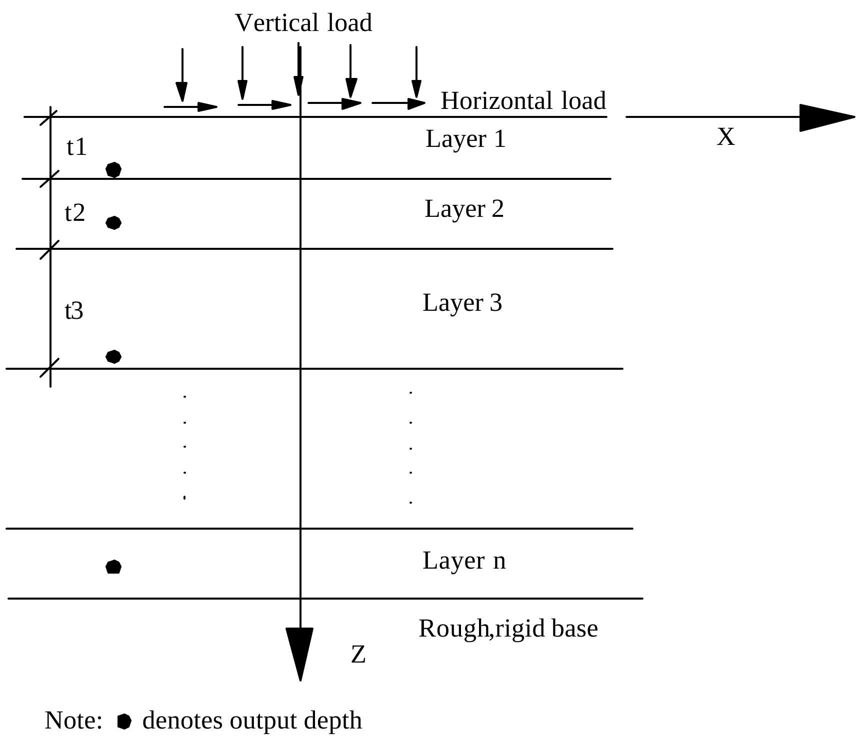

Figure G2. Horizontally layered system

G3.2.4 Output Positions

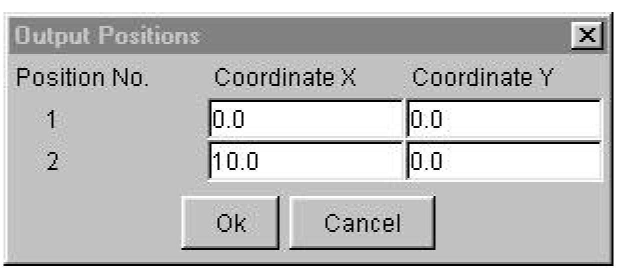

The two input variables are:

Coordinate X: The x-coordinate of the output point on the x-y plane.

Coordinate Y: The y-coordinate of the output point on the x-y plane.

If the user wants to get the general stress-strain-displacement distribution along x-axis (or y-axis) at certain depth, more than two points on x-axis (or y-axis) should be input. The coordinates of the points should be given in order as they will be plotted in the order that they are given.

G3.2.5 Depths

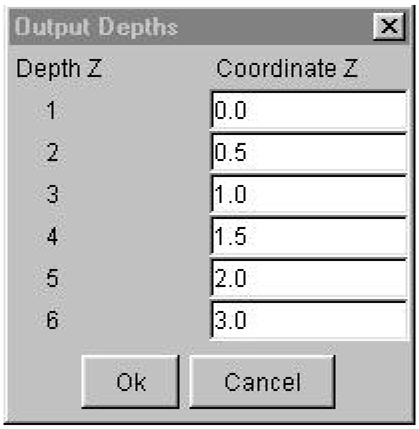

The one input variable is:

Coordinate Z: Enter the z-coordinates at which results are to be calculated.

Please note that it is necessary to input the coordinates in increasing order.

G3.2.6 Specify Integration

If in *General Information* dialog box "Specify integration" is selected, Specify Integration menu item will be activated. The following dialog box will pop out when clicking it.

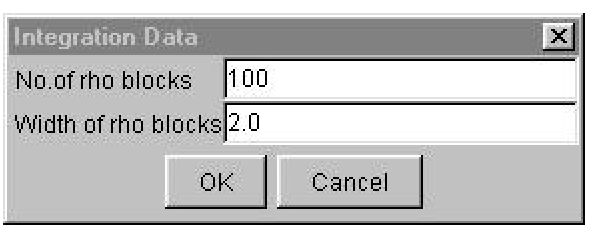

The values entered in the dialog box are:

No. of rho blocks: Total number of blocks divided.

Width of rho blocks: The width of each block, namely DRHO in the following figure.

In the program, integration like

$$g(r) = \int_0^\infty G(r r) dr$$

is used. The infinite integral in the above equation is approximated by making the integration range large enough. Gaussian quadrature is then used to numerically evaluate the integral. Integration is carried out in blocks. For instance to integrate the function $G(r, r)$, we would evaluate the area within each block using Gaussian quadrature, and sum the area so computed.

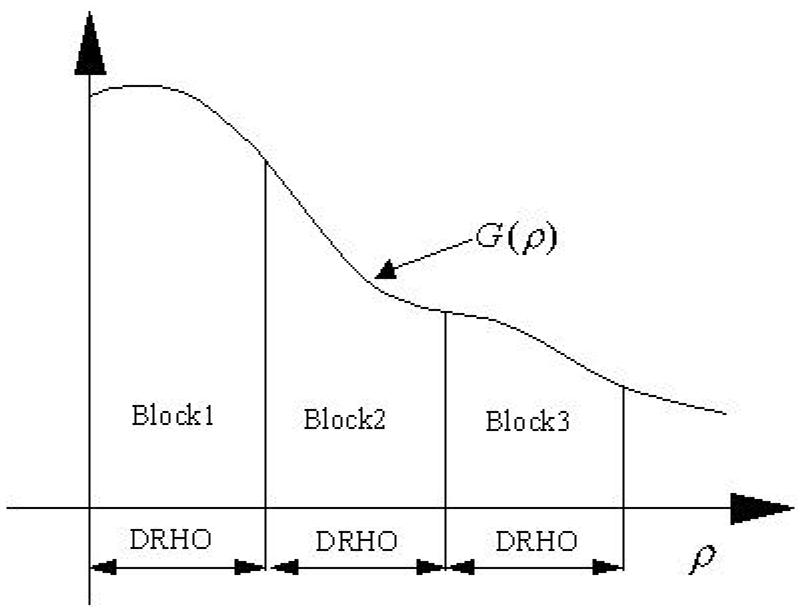

Figure G3. Numerical integration scheme

G3.3 COMPUTATION MENU

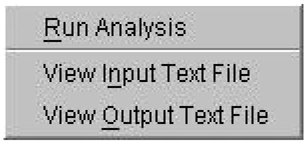

In the Computation Menu pull-down menu, the options used to run the analytical computations after all data are entered and saved are found. After successfully performing the analysis, commands used to view the plain-text input data and the computed result are activated. Menu choices are shown above and are briefly described below.

G3.3.1 Run Analysis

An existing input file, after preparation or modification, will be automatically saved to disk when selecting the Computation-Run Analysis menu item, and computation is performed next. For input data without being saved, it is required to save it into a file before running analysis.

When saving data to disk, an extension of the type *.dat is automatically added to the name of the input file.

The computation automatically creates an output file under the same directory and with the same name as the input file and with the extension *.res. Once a successful run is produced, the users may proceed to the next items for observation of results.

G3.3.2 View Input Text File

This menu option is used to view the input data file in plain-text mode using the inbuilt text editor. This command becomes enabled after computation is finished successfully.

This command is helpful for experienced users who may want to change one or two parameters quickly using the text editor, or for those users wishing to observe the prepared input data in text mode. However, it is recommended that users use the Windows features to edit data files in order to eliminate easily preventable errors.

G3.3.3 View Output Text File

This menu option is used to view the output text file that is automatically produced during each analytical run. This command becomes active after computation successfully executed.

The menu automatically invokes the text editor provided by Sun Microsystem. Output files are automatically saved to disk with the same file name as the input data file but with the extension *.res.

Information usually contained in the output files consists of the following items, listed in order of appearance:

1. Echo-print of input data. Users are strongly recommended to check the echo-print of their input data to check for mistakes.
2. Results about stresses, strains and displacements at each depth under each output position.

G3.4 GRAPHICS MENU

The Graphics Menu is used to generate and observe plots of the results of a successful analysis. Some options may be disabled because the type of output depends on the input data.

G3.4.1 Layout of Loads & Output Positions

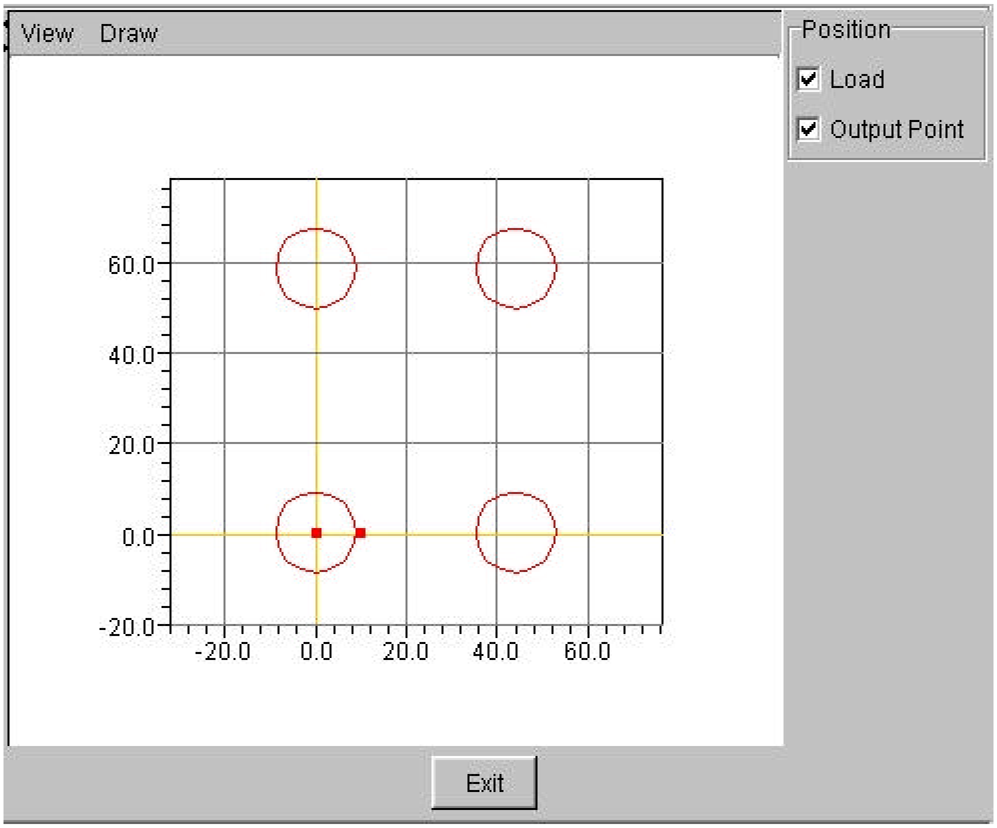

This command is used to display the geometric layout of the circular loading and the output positions. In the above figure, circle denotes the loading and the small solid red square denotes output position.

G3.4.2 Vertical Section

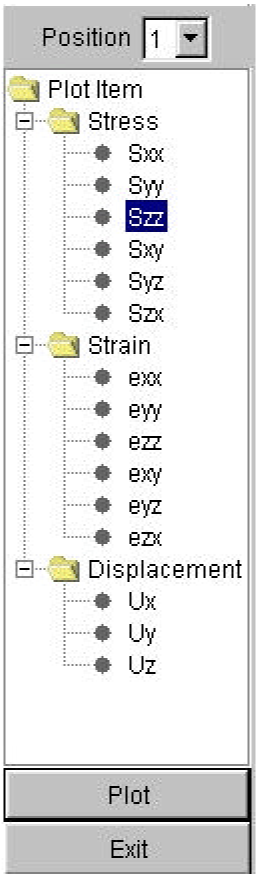

This option helps to plot the stress, strain and displacement distributions along the vertical line beneath any output position. Select output position number of interest, click on the expandable tree structure of the Plot Item and select the component of stress, strain or displacement, then click Plot button, the plot will appear in the drawing panel.

On the upper left part of the drawing panel, there are two menus. One is View Menu, which provides some means to present the results. The plot can be printed by the Print command of the other menu Draw.

Please note that Vertical Section menu item would be disabled when there is only one output depth.

G3.4.3 Horizontal Section

This submenu helps to show the results on the horizontal section. It has two options: Line Parallel to X Axis and Line Parallel to Y Axis. Only one appears at a given time, which depends on where the output positions are on a line parallel to x-axis or y-axis. If none of the above conditions exists, then this Horizontal Section submenu is disabled.

To plot the horizontal distributions of stress, strain and displacement at certain depth, select the corresponding depth number. The procedure is the same as that with Vertical Section.

Please note that if there is only one output position, the Horizontal Section would be disabled.

G3.5 HELP MENU

The user can get online help by clicking the command in this menu.

G4 Examples

G4.1 EXAMPLE 1

An example problem is stated as in the following figure:

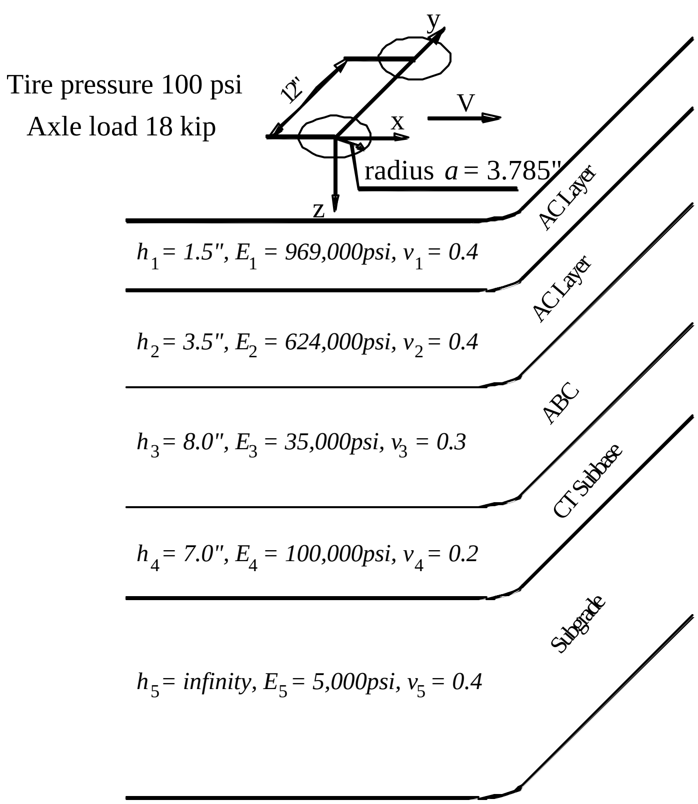

Two circular loads with center-to-center distance 12", vertical pressure 100 psi and radius 3.785" for each load.

Five layers, thickness, elastic modulus *E* and Poisson's ratio *v* for each layer are listed in the figure.

X, Y coordinates of the output point: (0, 0)

Use the user specified integration scheme.

The stress distribution versus depth below the output point (0, 0) is of interest.

The input file is stored in the directory "\Destination_Directory\examples\example1.dat", in which "Destination_Directory" is where the program is installed by the user. To see how the program works, the user just needs to open the file “example1.dat” and run analysis and then see the results.

G4.2 EXAMPLE 2

This problem is about a two-layered system subjected to a horizontal circular shear loading on the surface.

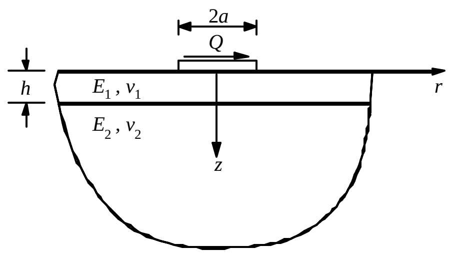

a = 2", h = 1"

E_1 = 10000 psi, E_2 = 5000 psi

One circular shear loading: radius a = 2" and uniform shear loading 100 psi.

Layer thicknesses, 1" (upper), infinity (lower).

Two different material types: E_1=10000 psi, v_1=0.5; E_2=5000 psi, v_2=0.5.

Use the user specified integration scheme.

The shear stress at the layer interface (Z = 1”) is of interest.

The input file is stored in the directory “\Destination_Directory\examples\example2.dat”, in which “Destination_Directory” is where the program is installed by the user. To see how the program works, the user just needs to open the file “example2.dat” and run analysis and then see the results.